DOI: 10.1070/RCR4606

Titanates, zirconates, aluminates and ferrites as waste forms for actinide immobilization

Sergey V. Stefanovsky,[a] Sergey V. Yudintsev [b]

[a] *A.N.Frumkin Institute of Physical Chemistry and Electrochemistry of the Russian Academy of Sciences Leninsky prosp. 31, kor. 4, 119071 Moscow, Russian Federation*
[b] *Institute of Geology of Ore Deposits, Petrography, Mineralogy and Geochemistry, Russian Academy of Sciences Staromonetnyi per. 35, 119017 Moscow, Russian Federation*

Titanate, zirconate, mixed titanate zirconate phases with fluorite and fluorite-related structures, and aluminate and ferrite phases with perovskite and garnet structures are surveyed. These phases are promising hosts for immobilization of actinides and their lanthanide analogues present in nuclear wastes. The data on the chemical stability and radiation resistance of the ceramics based on the above-mentioned phases demonstrating reliability of long-term storage of ceramized actinide wastes are presented. Methods for the synthesis of ceramics using sintering and melting stages are considered. The cold crucible inductive melting is shown to be one of the most promising techniques.
The bibliography includes 423 references.

Contents

I. Introduction 962
II. Key requirements to actinide host phases 963
III. Host phases for actinides 966
IV. Synthesis of high-level waste forms and problems of their manufacturing processes 983
V. Conclusion 986

I. Introduction

The crystalline phases of actinide titanates, zirconates, aluminates, ferrites and phosphates are of interest for analysis of fundamental properties of these elements in solids such as their valence species, short- and long-range order in the phase structure, in particular, the coordination environment, and spectral characteristics. Studies of the phase diagrams for systems containing actinide oxides is important for uranium and thorium geochemistry, elucidation of the actinide behaviour in the environment (in particular, in case of radiation accidents) and development of nuclear power engineering. A highly challenging issue of nuclear power engineering is handling of radioactive waste (RW), first of all, liquid high-level waste (HLW), which is formed upon processing of spent nuclear fuel from nuclear reactors used for various purposes after the extraction recovery of uranium and plutonium (Purex process). This waste contains uranium fission products and corrosion products of reactor materials as well as residual (uranium, plutonium) and minor (neptunium, americium and curium) actinides and process reagents. Actinides (especially plutonium) are the most hazardous components of HLW because they have long half-lives and high radiative and chemical toxicities (Table 1).[1]

Liquid HLW or slurries are stored in special water-cooled stainless-steel tanks. A failure to maintain the storage conditions can cause accidents, like the one that occurred in 1957 at the Mayak production association; therefore, liquid HLW must be converted to stable solid forms such as glass or ceramics. Currently, HLW vitrification is carried out in electric direct-heated furnaces (in Russia, USA, Germany, Japan, India and South Korea) or in induction-heated metallic melters (in France and UK) and gives aluminophosphate- (in Russia) or borosilicate- (in other countries) based glasses. The melter product is poured into canisters and this high-level glass is routed to long-term storage.[2]

Glass is a thermodynamically unstable material and cannot be expected to survive for periods of up to hundreds

S.V.Stefanovsky. Doctor of Chemical Sciences, Professor, Head of the Laboratory of Radiological and Radiation Problems at the IPCE RAS. Telephone: +7(495)335–2030, e-mail: serge.stefanovsky@yandex.ru
S.V.Yudintsev. Corresponding Member of the RAS, Doctor of Geological and Mineralogical Sciences, Head of the Laboratory of Radiogeology and Radiogeoecology at the IGEM RAS.
Telephone: +7(495)953–5562, e-mail: syud@igem.ru
Current research interests of the authors: physical geochemistry and geochemistry of mined elements, radiochemistry, materials science, crystal chemistry, analysis of mineral composition and properties, handling of radioactive wastes.

Received 18 October 2015
Translation: Z.P.Svitanko

© 2016 Russian Academy of Sciences and Turpion Ltd.

Table 1. Actinide half-lives ($T_{1/2}$) and concentrations in the spent nuclear fuel of power reactors (gram per tonne of fuel).[1]

Nuclide	$T_{1/2}$/year	Reactor		
		PWR-440	PWR-1000	LWGR-1000
^{235}U	7.0×10^8	12700	12300	2940
^{236}U	2.3×10^7	4280	5730	2610
^{238}U	4.9×10^9	942 000	929 000	962 000
^{238}Pu	87.8	75.6	126	68.6
^{239}Pu	2.41×10^4	5490	5530	2630
^{241}Am	432.5	517	616	293
^{243}Am	7375	69.3	120	73.8
^{244}Cm	18.1	14.8	31.7	5.66

of thousand years needed for actinide isotopes to decay down to the natural radiation background level. Research is carried out for improvement of extraction processing of spent nuclear fuel with recovery of particular fractions of short- and long-lived components: caesium/strontium, zirconium/molybdenum, technetium, transition metals/TR,† TR/An (An are actinides), actinides, neptunium or separately americium and curium.[3] In this case, short-lived or relatively low-level HLW fractions can be vitrified and some of their components can be used to make ionizing radiation sources (Cs, Sr) or in medicine (Tc), while actinides can be incorporated into persistent, chemically stable and radiation resistant crystalline matrices. Possible alternatives are the americium and neptunium transmutation and temporary curium storage for decay and the accumulation of radiogenic plutonium for repeated use.[4, 5]

Quite a few uranium and thorium minerals as well as minerals containing uranium and thorium as isomorphous impurities occur in nature. There are specimens up to 1 billion years old that have accumulated high concentrations of decay products and have received irradiation doses of $10^{25}-10^{26}$ (α-decays) m^{-3}. Many of them are metamicted to one or another extent, up to transition to the amorphous (disordered or metamict) state, but still demonstrate high degrees of retention of both the parent uranium and thorium and the decay products. These minerals include zirconolite ($CaZrTi_2O_7$), pyrochlore/betafite [$(Ca,U)(Ti,Nb,Ta)_2O_{7-x}$)], tazheranite [$(Ca,U,Ti,Zr)O_2$], perovskite ($CaTiO_3$), zircon ($ZrSiO_4$), brannerite/thorutite [$(U,Th)Ti_2O_6$], apatite [$(Ca_5(PO_4)_3(F,Cl,O,OH)$], britholite [$(Ca,TR)(PO_4)(SiO_4)O$] and monazite ($CePO_4$).[6–13] In some cases, minerals encountered in nature do not contain uranium or thorium,[14, 15] but there are synthetic phases of the same structure that do contain actinides. An example is murataite, which possesses high chemical stability in aqueous solutions.[16, 17] (U,Th)-containing minerals have been found in the natural fission reactor at the Gabon uranium deposit (Africa) and in the Chernobyl 'lava' — the melting product of the reactor core (Ukraine).[18, 19] Studies of the natural, man-made and artificial actinide compounds make it possible to choose materials that are most appropriate for actinide waste immobilization and subsequent disposal in deep geologic repositories.

† TR is a designation for rare earth elements (abbreviated Latin Terra Rare); we will also use the abbreviation REE.

The works dealing with the incorporation of actinides into synthetic phases have been in progress since the 1970s.[20–22] They are based on geological and mineralogical data[5–13, 20, 21] and analysis of the phase diagrams of actinide oxide systems.[23, 24] Chemically stable and radiation-resistant phases of fluorite (tazheranite/phianite) or fluorite-related structure (pyrochlore, murataite, zirconolite) are formed in titanate, zirconate and titanate zirconate systems. In aluminate and ferrite systems, perovskite type compounds are formed, and in phosphate and silicophosphate systems, monazite and apatite/britholite type structures appear. The objectives of the studies are, first of all, to elucidate the capacity of prospective phases as regards immobilization of actinides, to find new phases, to determine their properties, including chemical stability and radiation resistance, the structures and valence states of actinides and rare earth elements and to develop efficient methods for the synthesis of ceramics consisting of these phases. The structures and properties of host phases for immobilization of actinides are the subjects of a number of monographs and reviews.[25–37]

Currently, the only process that has been brought to commercialization is vitrification. Among other reasons (*e.g.*, chemical flexibility of the structural lattice of glass), this is caused by simple process equipment and flow diagrams as compared with ceramic processing, which includes moulding and annealing, cold pressing and sintering or hot pressing. Therefore, in our opinion, most promising is the manufacture of actinide waste forms by melting and crystallization from the melt.

This review presents analysis of publications dealing with actinide compounds and oxide solid solutions that are considered as possible phases for immobilization of actinides and the manufacture of ceramics based on these phases by melting and crystallization from melts, mainly, by cold crucible induction melting. Therefore, only congruently melting phases are considered. Primary attention is devoted to the studies of the last 15 years.

II. Key requirements to actinide host phases

Quite a number of crystalline phases potentially suitable for immobilization of actinides, including transuranium elements (Pu, Am, Cm, Np) and their rare earth analogues, have been studied to date. Titanate-, zirconate-, titanate zirconate-, aluminate-, ferrite-, phosphate- and silicophosphate-based phases have been considered.[4, 20–22, 25–29, 31–37] Initially, the host phases were developed for immobilization and long-term storage of actinides; therefore, chemical stability and radiation resistance were the key suitability criteria. For crystalline phases, these criteria imply stability against amorphization and maintenance of the chemical stability (ability to retain actinides within the phase upon interaction with underground water) under high irradiation doses. Other important parameters are the waste loading, mechanical strength, chemical flexibility, compatibility with the enclosing rock of the storage and some other properties, for example, processing parameters, which are not considered here.

II.1. Chemical stability

Mathematically, leaching is described by the sum of two exponents

$$W = A_1 \exp(-B_1 t) + A_2 \exp(-B_2 t) \quad (1)$$

where W is the leaching rate, A_1, A_2, B_1, B_2 are empirical coefficients, t is the leaching time. The first term of the equation describes the initial stage of dissolution of the easily leachable metastable phase, which is completely dissolved in the first 24 h. The second term describes leaching of the major phase from the sample surface, which is rate-limited by diffusion from the sample bulk towards the surface. At $B_2 \to 0$, the coefficient $A_2 \approx$ const; hence, the second term is represented only by coefficient A_2, which is defined as the 'equilibrium' leaching rate. In the opinion of the authors of monographs,[32, 36] the second term of the equation should have the form

$$W = \Delta \left(\frac{D}{\pi t} \right)^{1/2} \quad (2)$$

where Δ is the density of the matrix and D is the effective diffusion coefficient.

In the initial period of interaction of ceramics with solutions, elements from non-equilibrium (impurity) phases and from interfaces are predominantly leached owing to the migration of leached ions along pore and grain boundaries. Generally, three main mechanisms controlling RW leaching from ceramic forms are considered:

— autocatalytic hydrolysis of main lattice elements;
— diffusion-controlled ion exchange;
— deposition with layer formation.

The chemical stability of vitrified and ceramized RW is determined using special procedures (tests) developed by the Materials Characterization Center (MCC-1 – MCC-5).[38] The MCC-1 procedure includes leaching from a monolithic sample in a Teflon container under static conditions at a constant surface area to volume ratio (0.01 mm^{-1}) and temperatures of 40, 70 or 90 °C in deionized water, silicate – bicarbonate solution or brine. The test according to the MCC-2 procedure is also performed under static conditions but at higher temperature (110, 150 or 190 °C) using Teflon-lined steel capsules. The MCC-3 procedure (and similar PCT procedure [39]) resembles MCC-1 but uses powdered samples with particle size of 149 – 175 μm or <45 μm, and stirring is conducted at a constant ratio of the leaching agent volume to the sample weight (10 ± 1 ml g^{-1}) and temperatures of 40, 90, 110, 150 and 190 °C for specified periods of time. The MCC-4 test, which is similar to the single-pass flow-through test (SPFT), is carried out in a dedicated setup in which the leaching agent is passed through a bed of the sample (usually, powdered) with a known surface area for 28 or 364 days at temperatures of 40, 70 or 90 °C and flow rates of 0.1, 0.01 or 0.001 ml min^{-1}. The MCC-5 test is performed in the Soxhlet apparatus for 3 or 14 days in a flow of doubly distilled water at a boiling point. The leaching rate is calculated in all cases by the relation

$$(LR)_i = \frac{A_i W_0}{A_0 S t} \quad (3)$$

Here $(LR)_i$ is the normalized leaching rate of the ith component, g cm^{-2} day^{-1}; A_i is the weight (g) of component i leached in time t; A_0 is the initial weight (g) of component i in the sample; W_0 is the initial weight (g) of the sample; S is the sample surface area, cm^2; t is the leaching time, days.

Most often, testing is performed by the MCC-1 procedure, according to which a sample with a known surface area is kept in deionized water at 90 °C for several days, water being replaced every day. Leaching in acid or salt solutions simulating ground waters or brines is performed in a similar way.‡

II.2. Radiation resistance

The theoretical grounds of radiation effects in solids have been developed rather comprehensively and considered in many monographs and reviews (see, for example, Refs 40 – 44). When a solid is exposed to radiation, three types of effects are observed:

— effects of interaction of radiation with element nuclei;
— electronic effects (ionization and excitation) upon the interaction of radiation with the electron shells of atoms;
— effects of atom or ion displacements from their normal positions in the lattice points.

Electron beams or γ-rays induce excitation and ionization. The key types of ionization processes include the photoelectric effect, Compton scattering and formation of electron – positron pairs. As a result of ionization, electrons and holes appear in the solid and migrate over the lattice until they recombine, being captured by other electrons or holes, atoms, ions or structural defects. This can give rise to defects of various nature, including paramagnetic ones. Because of their low mass, electrons can execute only single displacements (formation of Frenkel pairs), while most part of their energy is dissipated *via* Coulomb interactions during ionization. For the waste forms in which radiolysis is significant, ionization effects of β-particles become the major source of damage. In addition, β-decay serves as the main source of heat in solidified RW during the first 500 years of storage.

Under the action of γ-quanta, atoms can be displaced, chemical bonds can break and compounds (mainly with covalent bonds) can even become amorphous. Nuclear reactions induced by γ-rays and electrons proceed only at very high energies, which are absent in RW forms, but this can be used in the studies of their radiation resistance, for example, by the photonuclear reaction method.

Heavy charged particles (α-particles, fission fragments, recoil nuclei) cause both displacement and ionization effects. The ionization density depends on the linear energy transfer (LET) value. Heavier particles have larger LET values (Table 2). High concentrations of free radicals, ions and radical ions in tracks increase the probability of recombination and the yields of molecular products of radiolysis. For low-LET particles (γ-quanta, electrons, protons), the concentration of radical products is lower and the yield of molecular products is minor. The largest number of displacements per decay event is induced by fission fragments. The recoil nuclei in α-decay cause approximately an order of magnitude less displacements. The β-particles (electrons) are least active in this respect.

The schematic diagram of development of radiation damage in ceramics is presented in Fig. 1. The first stage [$< 3 \times 10^{18}$ (α-decays) g^{-1}] is characterized by sharp Bragg diffraction peaks with minor contributions of diffusely scattered components. The damage is determined by accumulation of isolated point defects, which increase the unit

‡ In Russia, there is the relevant State Standard GOST R52126-2003.

Table 2. Initial LET values for iron sulfate and cerium sulfate solutions under various types of radiation.[40]

Radiation type	LET /eV nm^{-1}	Radiation type	LET /eV nm^{-1}
^{60}Co	0.2	α-Particles /MeV	
Electrons, 2 MeV	0.2	38	22
X-rays /kV		12	50
250	1.0	5.3 (^{210}Po)	88
8	2.8	3.4	120
Protons /MeV		Fission products,	~7000
2.0	17	65 MeV (average	
0.8	30	mass, 138 a.m.u.)	

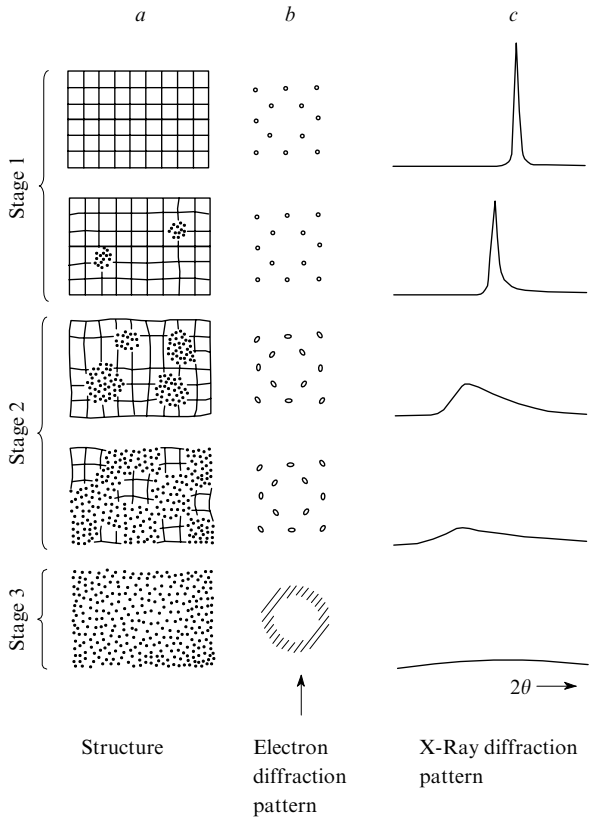


Figure 1. Schematic diagram of the change in the structure (*a*) and electron (*b*) and X-ray diffraction patterns (*c*) of a crystalline substance transforming to amorphous state with increasing α-dose exemplified by zircon.[45]

cell volume and cause distortions that account for the density decrease. These defects can be partly annealed over geological periods of time (hundreds of thousand years and more).

The second stage [$(3-8)\times10^{18}$ (α-decays) g^{-1}] is characterized by a substantial decrease in the intensity of Bragg diffraction peaks, which become asymmetrical owing to the increased contribution of diffusely scattered components. According to high-resolution transmission electron microscopy data, the microstructure comprises areas with a distorted crystal structure and amorphous tracks formed by displacement of α-recoil nuclei. As the α-dose increases, areas with a damaged crystal structure are transformed into aperiodic (amorphous) domains, but no further considerable unit cell expansion is observed in the remaining crystalline areas. In the third stage [$>8\times10^{18}$ (α-decays) g^{-1}], the material becomes fully amorphous.

The radiation resistance of solidified RW is studied using various types of radiation: ^{60}Co γ-radiation, irradiation with electrons and ions on accelerators, neutron irradiation in nuclear reactors, irradiation with α-particles and recoil nuclei from glass- or ceramic-incorporated sources and irradiation with fission fragments upon nuclear reactions. In order to correlate the results of sample irradiation experiments performed by different procedures, a universal radiation dose unit was proposed called dpa (displacements per atom) meaning the number of displacements experienced by each atom throughout the irradiation. This value can be calculated, for example, using the TRIM/SRIM computer software.[46] A correlation between the number of displacements per atom (dpa) and the 'age' (storage time) of conditioned RW was established.

II.2.a. Actinide doping

The α-decay of RW actinides and the daughter products formed results in the radiation damage at the atomic level and comprises two concurrent processes:

— α-particle with a ~5 MeV energy has a range of 10–20 μm and spends most of energy for ionization; at low velocities at the end of the range, it displaces 100–200 atoms giving rise to defects like Frenkel pairs;

— recoil nucleus with a ~0.1 MeV energy produces 1000–2000 atom displacements over the range equal to ~10 nm, thus forming tracks of disordered material.

In order to simulate the radiation damage in An-containing RW, the most appropriate method is the incorporation of short-lived α-emitters such as ^{238}Pu ($T_{1/2}$ = 87.7 years) and ^{244}Cm ($T_{1/2}$ = 18.1 years) into glass or ceramic.[26,42–44] More rarely, ^{242}Cm ($T_{1/2}$ = 163 days),[47] ^{241}Am ($T_{1/2}$ = 432.6 years)[48–50] and ^{210}Po ($T_{1/2}$ = 138.4 days)[51] are employed. This procedure is able to simulate the damage during storage of vitrified and crystalline RW forms for a period of 10^3-10^6 years with accumulation of radiation dose of up to $10^{24}-10^{25}$ (α-decays) m^{-3}.

II.2.b. Study of the natural analogues

One of the methods to assess the radiation damage during the long-term storage of solidified HLW and actinide wastes is to study natural minerals containing ^{238}U, ^{235}U and ^{232}Th and their daughter decay products. The concentration of UO_2 in some minerals reaches tens of mass percent (in pyrochlores, up to ~30 mass %) and the cumulative doses are ~10^{20} (α-decays) g^{-1}, or 5 10^{26} (α-decays) m^{-3}. Even minerals containing trace amounts of uranium, for example, zircon can accumulate a dose of up to ~10^{19} (α-decays) g^{-1} throughout the time of existence of ~10^9 years.[26,28]

For studying minerals with different concentrations of radioactive elements and different geologic age, it is possible to assess the radiation damage as a function of the radiation dose from artificially incorporated α-emitters. Minerals containing high concentrations of α-emitters and large geologic age (millions of years) are, most often, metamict. Usually, the α-dose leading to amorphization of synthetic minerals and the α-dose of the mitamict natural minerals are in good agreement with each other. Among the minerals

considered as host phases for actinides, zirconolite and pyrochlore are most stable [up to $\sim 10^{19}$ (α-decays) g^{-1}, or $\sim 0.8-1.0$ dpa], and perovskite, zircon, apatite, monazite and sphene are less stable ($\sim 0.20-0.55$ dpa).

II.2.c. Charged particle irradiation

A convenient procedure for evaluating the radiation damage is irradiation with accelerated charged particles, especially when α-particle (or inert gas ions) irradiation is combined with lead ion irradiation, which allows simulation of the action of both α-particles and recoil nuclei. Practically, various accelerated particles are used — electrons, protons, α-particles, inert gas ions (Ne, Ar, Kr, Xe) and lead ions; more rarely, other particles. Using this procedure, it is possible to reach high doses over very short periods of time.[26, 42–44] Difficulties arise in the subsequent analysis of irradiated samples, as the damages are formed in a very thin layer (up to hundreds of nanometres).

A drawback of this procedure is that the damages are homogeneously distributed and do not mimic the heterogeneous radiation effects that can arise in the case of non-uniform distribution of actinides or fission products in the materials. Some ceramic phases may incorporate no actinides, for example, hollandite in the Synroc ceramic. Upon ion irradiation, they are exposed to the same doses as actinide-containing phases, which is not the case for real storage conditions. Nevertheless, this procedure is fast and, hence, one of most popular.

II.2.d. Neutron irradiation

The radiation damage brought about by α-particles and recoil nuclei in crystalline compounds can be simulated by fast neutron irradiation (this mimics, most of all, the action of recoil nuclei as a result of elastic displacement of atoms)[52] or thermal neutron irradiation of a ^{235}U-doped material to induce the nuclear fission.[53] Fast neutrons dissipate the energy *via* elastic collisions, resulting in numerous atom displacements. If the sample contains nuclei with a rather large neutron capture cross-section, then the sample acquires induced radioactivity. Fast neutron irradiation acts similarly to recoil nuclei; however, because of the absence of α-particles, it is impossible to simulate the effect of helium formation. Thermal neutron irradiation of a ^{235}U-containing material gives rise to a large number of fission fragments, which produce extensive atom displacement areas (fission fragment tracks). This does not occur in real HLW; therefore, this procedure is less adequate than other procedures.

III. Host phases for actinides

III.1. Fluorite and fluorite-related structure phases

Since the mid-1970s, zirconolite, pyrochlore and later murataite (derived from fluorite) structure phases have been considered as promising host phases for actinides and REE[25] owing to their broad isomorphism and high radiation resistance and chemical stability. This group includes phases with the elementary fluorite unit cell (1C), two-fold (pyrochlore, 2C) and three-fold fluorite unit cell (murataite, 3C), polysomatic series of pyrochlore–murataite phases composed of alternating pyrochlore (2C) and murataite (3C) blocks (modules): 2C + 3C + 2C (7C), 2C + 3C (5C) and 3C + 2C + 3C (8C), and also zirconolite phases: 2T and 4T (tetragonal), 3O (orthorhombic), 2M and 6M (monoclinic), which are also derived from the fluorite structure.[17, 54–60]

III.1.a. Fluorite type cubic zirconia and zirconates

The fluorite structure (space group *Fm*3*m*) is inherent in the cubic ZrO_2 modification stable at temperatures above ~ 2300 °C. The Zr^{4+} ion positions correspond to the cubic close packing sites, while O^{2-} positions correspond to all tetrahedral voids. Each Zr^{4+} ion is surrounded by eight O^{2-} ions located at a distance of 2.20 Å. In the 1100–2300 °C temperature range, a tetragonal polymorph exists, while the phase stable below 1100 °C is monoclinic (baddeleyite).[61]

The cubic phase of ZrO_2 can be stabilized by introducing other quadruply charged ions (Ce^{4+}, Hf^{4+}, U^{4+}, Pu^{4+}, Am^{4+}) or Ca^{2+} and TR^{3+} ions. Some of the Zr^{4+} ions are replaced by other quadruply or lower charged ions (in this case, oxygen deficiency arises to maintain the charge balance). For practical purposes, Y_2O_3 is used most often (for jewelry, with addition of other REE oxides). In the $ZrO_2-Y_2O_3$ system, there exists an extensive region of fluorite type cubic solid solutions.[23]

The Nd, Sm, Eu, Gd and Tb oxide systems comprise wide fluorite type cubic solid solution fields,[23, 24] while UO_2, PuO_2 and AmO_2 systems form a continuous solid solution. At 1200 °C, two solid solution homogeneity regions exist in the $ZrO_2-Am_2O_3$ system: one tetragonal (0 mol.%–3 mol.% Am_2O_3) and one cubic ($\sim$1mol.%–38 mol.% Am_2O_3).[23] In the vicinity of $(TR,An)_2Zr_2O_7$ composition, the fluorite structure becomes defective with lowering the temperature and then transforms into the pyrochlore structure.[62, 63] The order–disorder transition temperature (the dot in Fig. 2) depends on the composition.[23, 24, 62–65]

Zirconia-based phases with the fluorite, defective fluorite and pyrochlore structures are radiation resistant and chemically stable. Therefore, they were proposed as promising hosts for immobilization of long-lived actinides of Pu-

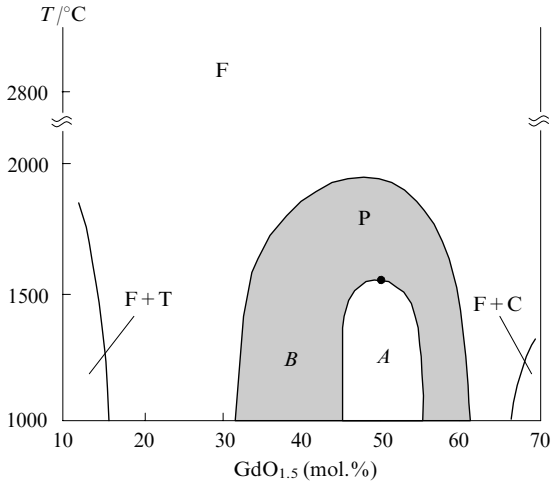


Figure 2. Part of the phase diagram of the $ZrO_2-GdO_{1.5}$ system.[62, 63]
A and *B* are the stability regions for the pyrochlore and defective fluorite type phases; F is fluorite type cubic solid solution; P is pyrochlore type solid solution; C is cubic solid solution with a Tl_2O_3 type structure; T is a tetragonal solid solution; the dot marks the order–disorder transition for the pyrochlore phase.

and Am/Cm-containing wastes.[66–69] The $Gd_2Ti_{2-x}Zr_xO_7$ phases with $x \geqslant 1.8$ are not amorphized upon irradiation with accelerated ions even at 25 K and doses of up to 5 dpa.[70] The I^+ and Sr^+ irradiation of Y-stabilized ZrO_2 with up to 300 dpa doses resulted in the formation of a defective fluorite structure but not in amorphization. The latter was achieved upon Cs^+ ion irradiation at room temperature only at a fluence of 10^{21} ion m^{-2}, or 330 dpa.[71] The irradiation of Y-stabilized ZrO_2 (9.5 mol.% Y_2O_3) with He^+ ions (100 keV) up to 11.65 dpa gave rise to numerous helium bubbles and cracks in the sample but did not induce amorphization.[72]

Y-Stabilized ZrO_2 is considered as an inert matrix fuel. This material demonstrated a high degree of retention of implanted Cs^+ ions *via* the formation of Cs_2ZrO_3.[73] The $Er_{0.05}Y_{0.10}Th_{0.10}Zr_{0.75}O_{1.925}$ samples irradiated with xenon ions (60 keV) using ion accelerators and the $(Er,Y,Pu,Zr)O_{2-x}$ samples irradiated in a reactor maintained a crystalline structure.[74] After irradiation in a reactor, $(Pu,Er,Y,Hf,Am)ZrO_{2-x}$ (0.8 mass % Am) demonstrated a (10^9 times) higher stability in groundwater than glass and several orders of magnitude higher stability than UO_2 under oxidizing conditions.[75]

High radiation resistance was found for stabilized pyrochlore type ZrO_2 and zirconate samples after self-irradiation with ^{238}Pu and ^{241}Am they incorporated.[49, 50, 76–79] Depending on the irradiation dose, abnormal behaviour of the phase is observed, being induced by two opposite processes — accumulation of radiation defects and defect recombination restoring the structure. For an ^{241}Am-based sample, this is manifested as a broadening and decrease in the intensity of X-ray reflections at low doses (up to $\sim$0.11 dpa) and the subsequent narrowing down and intensity increase of the reflections as the dose increases to $\sim$0.78 dpa.[49, 50]

Single crystals of cubic zirconia stabilized by 9.4 mol.% Y_2O_3 showed a high stability to the action of simulated Canadian Shield brine both at 25 and at 85 °C. The Nb and Hf normalized leaching rates at these temperatures were 1.4×10^{-12} and 7.0×10^{-12} kg m^{-2} s^{-1}, or 1.2×10^{-8} and 6.0×10^{-8} g cm^{-2} day^{-1}, respectively.[66]

In nitric acid (pH 1) at 150 °C, CeO_2- and Nd_2O_3-doped $Zr_{0.86}Y_{0.14}O_{1.93}$ samples showed leaching rates of about 10^{-5} g m^{-2} day^{-1} for Ce and $\sim 10^{-4}$ g m^{-2} day^{-1} for Ce, Nd and Y present simultaneously.[80] The Np leaching rate from the $(Zr,Np,Y)O_{2-x}$ ceramic containing 20 mol.% to 40 mol.% NpO_2 was less than 10^{-5} g m^{-2} day^{-1} (according to a 84-day MCC-2 test at 150 °C in distilled water).[81] In a series of experiments involving $Gd_2Ti_{2-x}Zr_xO_7$ pyrochlores, the minimum gadolinium leaching rate (according to SPFT data, pH 2, $T = 90$ °C) determined for the sample with $x = 1.75$ was 1.33×10^{-4} g m^{-2} day^{-1}. For a pure fluorite gadolinium zirconate, the Gd leaching rate was somewhat higher, but the sample turned out to be not quite homogeneous. The Au^{2+} ion (2 MeV) irradiation up to a fluence of 5 ion nm^{-2} did not change the rates of leaching from zirconate samples based on a fluorite type phase.[82]

The ZrO_2–Cm_2O_3 system (Fig. 3) has been studied over the range from ZrO_2 to the $CmZrO_{3.5}$ ($Cm_2Zr_2O_7$) composition corresponding to the pyrochlore.[83–86] The existence of two fluorite and pyrochlore type cubic phases was ascertained. Zirconia-based phases have high capacity for isomorphous substitution towards triply charged actinide

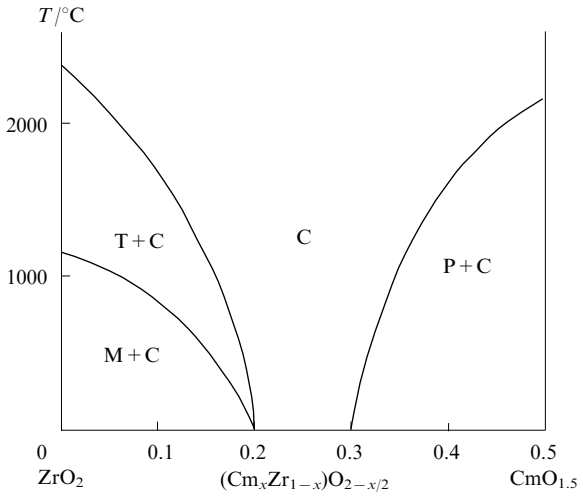


Figure 3. Phase diagram of the $CmO_{1.5}$–ZrO_2 system.[83] Structures: C is fluorite (cubic), solid solution; M is monoclinic, solid solution; T is tetragonal, solid solution; P is pyrochlore.

ions. For example, there exist compounds $Am_2Zr_2O_7$ and $Cm_2Zr_2O_7$; in the latter, the $^{244}Cm_2O_3$ content can be as high as $\sim$81 mass %.

A key issue in the synthesis of zirconate ceramics is the necessity of thorough preparation of the feed formulation and the use of very high temperature and pressure. For manufacturing REE–zirconate oxide ceramic, sintering is conducted at 1500–1600 °C for $\sim$50 h and is followed by grinding and one more sintering.[87] Even the synthesis from a sol–gel precursor requires sintering at 1200 °C for 12 h, repeated sintering of the pellets, sintering at 1500 °C for 30 h and hot pressing at 1600 °C under a 200 MPa pressure for 2 h; however, in this case, too, foreign phase impurities are detected.[82, 88] The solid-phase reactions are markedly accelerated by mechanical pretreatment of the feed formulation. The duration of sintering at 1500 °C decreases in this case to 3–6 h and the product is virtually a single phase.[89, 90]

III.1.b. Pyrochlore structure phases

Pyrochlore $A_2B_2O_6X$ (X = O^{2-}, OH^-, F^-, vacancy) has a cubic crystal lattice (space group $Fd3m$, $Z = 8$). Its structure is a derivative of the fluorite structure in which the unit cell is doubled, 1/8 of oxygen atoms are absent and anion vacancies are ordered.[91] Owing to the missing anion, the cubic environment of the B site is transformed into an octahedral one.[49] The oxygen anions are located at octahedron vertices and occupy six out of the eight vertices of the cube. The other two vertices are occupied by X anions. The compounds $(A^{3+})_2(B^{4+})_2O_7$ have a pyrochlore structure at $1.46 < R_A/R_B < 1.80$ (R_A and R_B are the radii of A and B ions, respectively).[49, 54, 55, 61] The pyrochlore structure can be represented as two interpenetrating networks of BO_6 octahedra and A_2X chains (Fig. 4).

Currently, more than 500 pyrochlore type compounds are known, some of them containing actinides. The pyrochlore structure is inherent in $Cm_2Ti_2O_7$, $CaThTi_2O_7$, $CaUTi_2O_7$, $CaNpTi_2O_7$ and $CaPuTi_2O_7$.[13, 83–86] Zirconates and hafnates can have either pyrochlore or fluorite structure (Table 3).[24, 54, 55, 92] The pyrochlore structure is retained

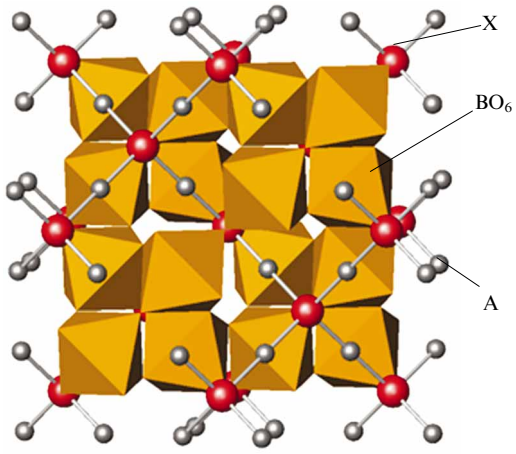


Figure 4. Pyrochlore structure (http://www.chemtube3d.com/solidstate/SS-Pyrochlore.htm).

Table 3. Pyrochlore type REE and actinide phases $A_2B_2O_7$.[92]

A cation	B cation			
	Ti^{4+} (0.061)	Sn^{4+} (0.069)	Hf^{4+} (0.071)	Zr^{4+} (0.072)
A *is a rare earth element*				
La^{3+} (0.116)	–	+	+	+
Ce^{3+} (0.114)	–	+	+	+
Pr^{3+} (0.113)	–	+	+	+
Nd^{3+} (0.111)	–	+	+	+
Pm^{3+} (0.109)	–	+	+	+
Sm^{3+} (0.108)	+	+	+	±
Eu^{3+} (0.107)	+	+	+	±
Gd^{3+} (0.105)	+	+	+	±
Tb^{3+} (0.104)	+	+	+	–
Dy^{3+} (0.103)	+	+	–	–
Y^{3+} (0.102)	+	+	–	–
Ho^{3+} (0.102)	+	+	–	–
Er^{3+} (0.100)	+	+	–	–
Tm^{3+} (0.099)	+	+	–	–
Yb^{3+} (0.099)	+	+	–	–
Lu^{3+} (0.098)	+	–	–	–
A *is actinide or* $Ca^{2+} + An^{4+}$, $Ca^{2+} + Ce^{4+}$				
Pu^{3+} (0.110)	–	+	+	+
Am^{3+} (0.109)	–	+	+	+
$Ca^{2+} + Th^{4+}$ (0.1085) [a]	+	+	+	±
Cm^{3+} (0.108)	+	+	+	±
$Ca^{2+} + U^{4+}$ (0.106) [a]	+	+	+	±
$Ca^{2+} + Np^{4+}$ (0.105) [a]	+	+	+	±
$Ca^{2+} + Ce^{4+}$ (0.1045) [a]	+	+	+	–
$Ca^{2+} + Pu^{4+}$ (0.104) [a]	+	+	+	–

Note. The following designations are used: plus — the structure is stable, minus — the structure is unstable; plus or minus — a structural modification of the pyrochlore and fluorite structures is possible; the numbers in parentheses are ion radii (nm).
[a] Mean ion radius.

over the whole range of compositions for $(Gd_{1-x}Nd_x)_2Zr_2O_7$ (Ref. 93), $(Gd_{1-x}Ce_x)_2Zr_2O_7$ (Ref. 94) and $(Nd_{1-x}Ce_x)_2Zr_2O_{7-y}$.[95]

Actinide titanates were synthesized and studied earlier than zirconates or hafnates but most studies were carried out for samples containing < 10 mass % PuO_2 and even lower percentages of americium and curium oxides. The reasons are both the difficulty of handling highly radioactive materials and consideration of the critical mass limit. With regard to the problem of disposal of surplus weapons-grade plutonium, studies of radiation resistance of $^{239}PuO_2$-doped (up to ~12 mass %) pyrochlore phases were undertaken.[96–103] In most of these studies, plutonium was mimicked by cerium or uranium, and the products were almost never single phases (usually, zirconolite, perovskite, brannerite or rutile were present as impurity phases).

The radiation resistance of pyrochlore ceramics was studied by analyzing damage in natural samples,[104] actinide doping, in particular, with the ^{244}Cm isotope, and ion irradiation.[26–29,33,44] The effect of α-decay on the ^{244}Cm-doped pyrochlore $Gd_2Ti_2O_7$ phase was studied in most detail.[105–108] At low doses of $\sim 0.6 \times 10^{18}$ (α-decays) g^{-1}, the material exhibited a clear point electron diffraction pattern and clearly discernable single defects and fragment tracks. With increasing dose, the density of radiation-induced defects increased until the clusters of single defects became poorly discernable and a diffuse ring appeared in the electron diffraction pattern, indicative of the presence of amorphous material. At higher doses, the material became almost completely amorphous with some residual crystallinity. After 3.1×10^{18} (α-decays) g^{-1}, the material was amorphous without remaining crystallinity and the electron diffraction pattern displayed only diffuse rings typical of amorphous state.

An increase in the α-dose was found [106] to entail exponential increase in the volume and a ~2.5-fold increase in the integrated dissolution rate of ^{244}Cm-doped pyrochlore ceramic.[26,107] However, the rates of transition of curium and plutonium ions into solution can also increase 20–50-fold because of incongruent melting. With increasing the α-dose, the fracture toughness passes through a broad maximum at $\sim 1.4 \times 10^{18}$ (α-decays) g^{-1} (Ref. 108). After the isochronal annealing of completely amorphized $Gd_2Ti_2O_7$ for 12 h, linear density recovery was observed before the temperature of the onset of recrystallization (700 °C). The complete density recovery and recrystallization of the initial pyrochlore structure occured at 850 °C. The $Gd_{1.935}{}^{244}Cm_{0.065}TiZrO_7$ sample transformed into the metamict state at a 4.6×10^{18} (α-decays) g^{-1} (0.60 dpa) dose. The perovskite and baddeleyite impurity phases became amorphous at $\sim 2 \times 10^{18}$ (α-decays) g^{-1} (0.26 dpa), *i.e.*, they have also incorporated some curium.[109]

In connection with the problem of disposal of surplus weapons-grade plutonium, the radiation resistance of pyrochlore type phases doped with 8.7 mass % (Refs 110, 111) and ~11.9 mass % $^{238}PuO_2$ (Refs 112, 113) was studied. According to X-ray powder diffraction data, pyrochlore was the major phase in the samples obtained by cold pressing and sintering, while impurity phases included brannerite (formally described as UTi_2O_6), rutile and a fluorite type phase, presumably $(Pu,U)O_2$. On keeping the samples, the pyrochlore unit cell parameter increased — the relative volume gain was 1.2%–1.6 % in six months, and sample amorphization became clear-cut at

$5 \times 10^{16} - 2.5 \times 10^{17}$ (α-decays) g^{-1}, while at 8.8×10^{17} (α-decays) g^{-1}, the diffraction pattern became substantially blurred and most of X-ray reflections disappeared.[110] A study of hydrolytic stability by the MCC-1 procedure demonstrated that sample stability decreases considerably after the metamict transformation: the normalized Pu and U weight losses after a 28-day leaching increased 30- and 6-fold, respectively. By the 28th day, the leaching rates (V_{28}) from the freshly prepared (*I*) and amorphized (*II*) samples at a cumulative dose of 1.68×10^{25} (α-decays) m^{-3} were as follows:

Element	Gd	U	Pu
V_{28} /g m^{-2} day^{-1}			
I	1.1×10^{-2}	7×10^{-3}	3.3×10^{-4}
II	3.3×10^{-3}	4.6×10^{-2}	8.9×10^{-3}

The radiation damage in a ceramic of a similar composition, obtained also by cold pressing and sintering at 1350 °C, but under argon, was studied in the USA. The samples consisted of the major phase (pyrochlore) and some additional phases (Hf-rutile, zirconolite and brannerite). Pyrochlore became amorphous at a dose of 3.7×10^{18} (α-decays) g^{-1}. The hydrolytic stability testing by the SPFT procedure showed leaching rates of 1.3×10^{-3} and 7.2×10^{-4} g m^{-2} day^{-1} after and before amorphization, respectively, for samples consisting mainly from pyrochlore and containing additional phases apart from pyrochlore. Despite the amorphization, the samples retained the integrity and hydrolytic stability.[112, 113]

The conclusion of Russian researchers[111] stating that pyrochlore is not the host of choice for immobilization of plutonium does not take away the fact that the gadolinium leaching rate decreases after the sample amorphization; therefore, pyrochlore can be quite an appropriate host for trivalent actinides.

Systematic studies of natural pyrochlore group minerals have been reported in a number of publications.[9, 96, 114–116] These are usual accessory minerals encountered in various rocks — carbonatites and nepheline-syenite and granite pegmatites. Actinides can be located in the A sites and their content can be quite large (up to 30 mass % U). The charge balance is provided by cation deficiency in the A sites and substitutions in the B sites. Natural pyrochlores are classified in terms of the principal cations in the octahedral site: microlite (Ta > Nb, Ti < 33 mol.%), pyrochlore (Nb ⩾ Ta, Ti < 33 mol.%), betafite (Ti ⩾ 33 mol.%).[114] The radiation damages in microlite, which contained up to 30 mass % and 5 mass % UO_2 and ThO_2, were studied in most detail. Depending on the sample age, the calculated cumulative dose reached 80 dpa. With increasing dose, the intensity of diffraction peaks decreased and the peaks were broadened but not so fast as in the case of the synthetic actinide-doped material. The diffraction peaks did not shift towards smaller 2θ angles because the unit cell expansion resulting from dose increase and defect accumulation was counterbalanced by the replacement of calcium and sodium by uranium. Evidently, the unit cell compression upon chemical substitution compensates for its expansion caused by radiation damage. High-resolution transmission electron microscopy data support the interpretation based on X-ray diffraction.[9]

Changes in the first and second coordination spheres can be monitored by spectroscopic methods, of which most efficient are X-ray absorption near edge (XANES) and extended X-ray absorption (EXAFS) fine structure investigation methods.[117–125] These results were used to propose a model for the metamict state comprising the following effects:[126]

— slight distortion of the nearest coordination polyhedra;

— decrease in the coordination number and bond length in the primary coordination polyhedron;

— some increase in the mean distance to the second nearest neighbouring polyhedron;

— loss of periodicity relative to the second nearest neighbouring polyhedron.

Hogarth[127] noted the following: if the analyzed pyrochlore specimens are from the same locality, the calculated dose needed for transition from the crystalline to metamict state increases with the mineral age. This is an obvious proof for healing of damages caused by α-recoil nuclei throughout a geological period. The relationship between the critical amorphization dose (D_c) and geological age was modelled with the assumption of the disappearance of α-recoil tracks, similarly to the disappearance of fission fragment tracks. The critical parameters include the α-decay dose, specimen age, thermal prehistory and the average α-recoil track lifetime. The dose variation as a function of age for natural pyrochlores can be corrected by taking into account the annealing of the recoil track. The annealing under the existing conditions for a long period of time gives a higher apparent amorphization dose. The real time dependences of the dose can be obtained using an exponential equation and considering annealing in terms of half-life of recoil tracks in the material.[127] The average track lifetime (τ_a) is assumed to be 100 million years. This type of data analysis for zircon and zirconolite gave average track lifetimes of 400 and 700 million years, respectively. This does not correspond to the track lifetimes estimated by the differential etching procedure, which was used to determine the lifetimes of the damaged sites in monazite, metamict betafite, thorite and metamict samarskite.[128–132] For the phases that retain the crystallinity despite high α-doses (> 10 dpa), the α-recoil track lifetime was about 10^4 years. Thus, natural samples provide clear evidence for the annealing taking place over geological periods of time. The final state of the mineral — either crystalline or metamict — depends on the average lifetime of the α-recoil track, which, in turn, depends on the type (composition and structure) of actinide-containing material or mineral.

A number of investigations of the radiation resistance of pyrochlore type phases using noble gas ion (Ne^+, Kr^+, Xe^+)[133–147] irradiation have been reported.[133–147] Smith *et al.*[133] irradiated the pyrochlore $(Ca_{0.87}U_{0.62})_{1.49}(Ti_{1.76}.Zr_{0.24})_{2.00}O_{6.72}$ with Kr^+ ions ($E = 1.5$ MeV) and found that $D_c = (4.1 \pm 0.3) \times 10^{18}$ ion m^{-2}; this was comparable with the D_c value for zirconolite, which was considered in the same study. Wang *et al.*[134] irradiated hot-pressed $Gd_2Ti_2O_7$ samples with Xe^+ ($E = 1.5$ MeV), Kr^+ ($E = 1.0$ MeV) and Ar^+ ions ($E = 0.6$ MeV) in the temperature range from 20 to 1073 K. For these cases, the critical amorphization temperatures (T_c) found by extrapolation were 1300, 1100 and 950 K, respectively. Transmission electron microscopy examination demonstrated that in early irradiation stages, the pyrochlore was transformed into a defective fluorite phase. A study of the radiation resistance of the pyrochlore

$Gd_2(Zr_xTi_{1-x})_2O_7$ upon Kr^+ ion (1 MeV) irradiation demonstrated [135] that with increasing content of zirconium in the samples, the radiation resistance increases: this is reflected as increasing D_c and decreasing T_c values. Pyrochlores containing $\geqslant 1.8$ formula units of zirconium did not amorphize even at 25 K.

Wang *et al.*[136] compared the radiation resistance of $Gd_2Ti_2O_7$, $Sm_2Ti_2O_7$, $Eu_2Ti_2O_7$ and $Y_2Ti_2O_7$ phases obtained by cold pressing and sintering in the temperature range of 20–1023 K upon Kr^+ ion irradiation ($E = 1$ MeV). The amorphization of all of these phases involved the intermediate formation of a fluorite substructure. A high-resolution transmission electron microscopy examination showed damage sites as isolated cascades and the cation disorder. Pyrochlores containing REE transformed into amorphous state more readily and had higher critical amorphization temperature than the yttrium pyrochlore. The differences between the susceptibility to amorphization of these pyrochlores are attributable to different sizes of displacement cascades induced by cations of different mass. Further detailing of the mechanism of amorphization induced by ion irradiation showed [137] that single displacement cascades are followed by the stage of cascade overlap and that complete amorphization occurs if these amorphous domains occupy the whole sample bulk. Hence, the ion-induced amorphization can be analyzed using the vitrification model at the nanometre level. Quenching of the melt formed in the displacement cascade results in recrystallization of the shell, the central part of the track being amorphous.

Lumpkin *et al.*,[138] who studied the pyrochlore amorphization mechanism, exposed synthetic single crystals of the $Cd_2Nb_2O_7$ pyrochlore to Ne^+ and Xe^+ ion irradiation. The material turned amorphous under the action of Ne^+ and Xe^+ ions at temperatures below 480 and 620 K, respectively. The amorphization of $Cd_2Nb_2O_7$ at room temperature required a 36 times greater fluence of Ne^+ ions with 280 keV energy than Xe^+ ions with 1200 keV energy. The calcium and niobium atom disordering over all possible cationic sites took place at medium ion doses before amorphization.

Generally, for all pyrochlore type compounds, the mechanism of radiation damage is the same. The radiation resistance and chemical stability are enhanced as titanium atoms are replaced by zirconium atoms but the temperature and duration of synthesis increase.

III.1.c. Murataite phases with fluorite cell multiplicity of > 2

In the muliphase ceramics obtained by cold pressing and sintering [148–152] and in the Synroc-C type material containing 20 mass % of one sort of HLW from the Mayak production association,[16, 153, 154] a cubic phase classified as murataite was detected (Table 4 and Fig. 5). This phase, which occupied ~5% of the sample volume, accumulated

Table 4. Compositions of murataite phases (mass %) in the hosts with simulated HLW.[16]

Sample	Al_2O_3	CaO	TiO_2	MnO	FeO	Ce_2O_3	ZrO_2	UO_2
Waste from the Mayak production association (Russia) [a]								
sample centre	0.8	15.8	55.7	3.7	–	6.1	5.8	12.1
sample periphery	2.8	16.1	66.6	5.7	–	3.7	4.3	0.8
Waste from Savannah River plant (USA) [b]	9.5	8.0	32.8	8.0	23.9	1.0 [c]	13.5	3.3

[a] The sample contained also SiO_2, K_2O, Cr_2O_3 and NiO. [b] The sample contained Na_2O. [c] Sum of lanthanides without separation.

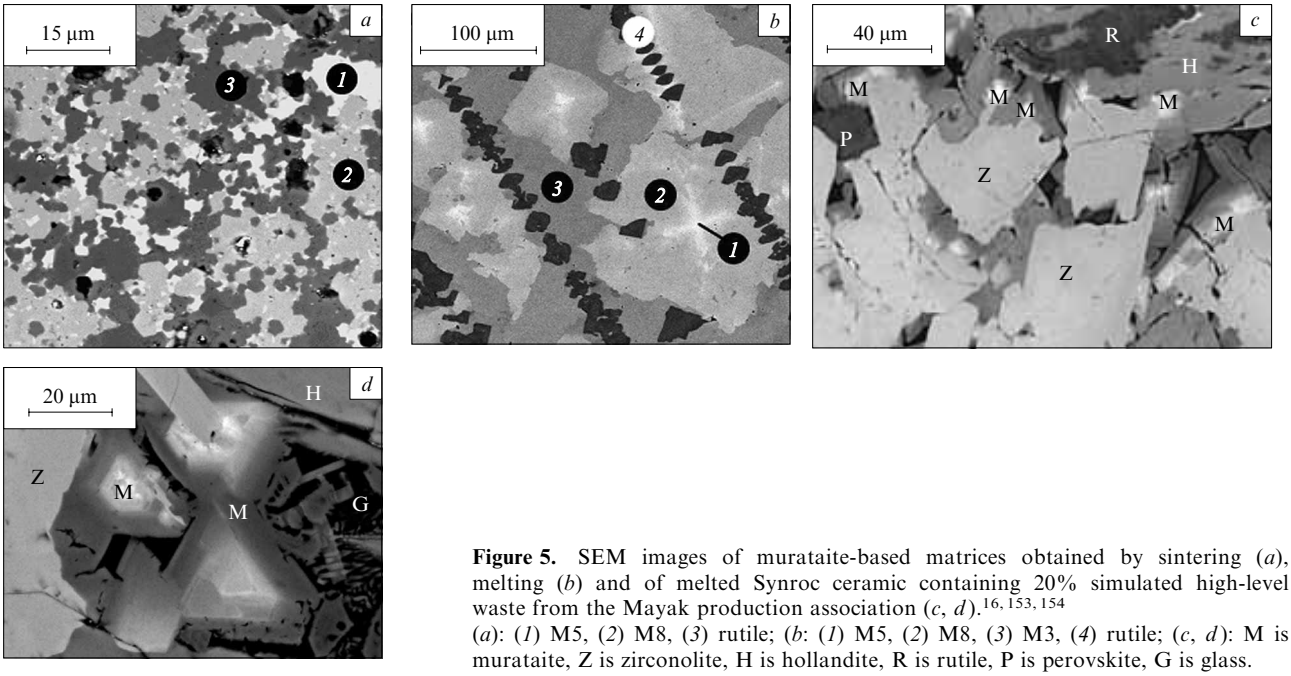


Figure 5. SEM images of murataite-based matrices obtained by sintering (*a*), melting (*b*) and of melted Synroc ceramic containing 20% simulated high-level waste from the Mayak production association (*c*, *d*).[16, 153, 154]
(*a*): (*1*) M5, (*2*) M8, (*3*) rutile; (*b*: (*1*) M5, (*2*) M8, (*3*) M3, (*4*) rutile; (*c*, *d*): M is murataite, Z is zirconolite, H is hollandite, R is rutile, P is perovskite, G is glass.

up to 40% of uranium weight present in the sample. A clear-cut zonal structure of grains was noted: uranium concentration in the grain central part was 10 – 20 times higher than at the periphery, which created an additional barrier against leaching.

Synthetic muratatite is a cubic phase ($F\bar{4}3m$) with a tripled fluorite unit cell (a = 14.86 Å) and the ideal formula $^{VIII}A_3{}^{V}B_2{}^{VI}C_6O_{20-22}$, where A = Ca, Mn, TR, An; B = Mn, Ti, Zr, U; C = Ti, Al, Fe; here and below, the Roman numerals in the left superscript designate the coordination numbers (C.N.). The stoichiometric composition of the natural phase is $A_4B_3C_6O_{18}(F,OH)_4$, where A = Na, TR, Ca; B = Zn, Fe; C = Ti, Fe, Nb.[14 – 16, 155, 156] Unlike synthetic analogues, it is devoid of uranium but contains sodium, zinc, niobium and fluorine and other (yttrium) REE composition. The key isomorphous substitution patterns are the following:

— replacement of the A atom: $Ca^{2+} \rightarrow Mn^{2+}$ (synthetic), $2\,Ca^{2+} \rightarrow Na^{+} + TR^{3+}$ (natural);

— replacement of the B atom: $Ti^{4+} \rightarrow Zr^{4+} \rightarrow U^{4+}$ (synthetic), $Zn^{2+} \rightarrow Fe^{2+}$ (natural);

— replacement of the C atom: $2\,Ti^{4+} \rightarrow (Al,Fe)^{3+} + Nb^{5+}$ (natural);

— simultaneous replacement of the A and C atoms: $Ca^{2+} + Ti^{4+} \rightarrow Na^{+} + Nb^{5+}$ (natural).

Below we briefly summarize the main research data on the structure, composition variations and chemical stability and radiation resistance of muratatite ceramics.[16, 17, 57, 58, 157 – 205]

Evidently, the ability of muratatite to incorporate large amounts of HLW components is attributable to the presence of several structural sites (Table 5) providing for accommodation of cations with charges from +1 to +5 and radii from 0.5 – 0.6 (Al^{3+}, Nb^{5+}) to 1.0 – 1.2 Å (Na^{+}, Ca^{2+}, TR^{3+}, $An^{3+,4+}$). The total content of REE – actinide fraction of HLW in synthetic muratatite reaches 20 mass %;[16, 156] the possibility of incorporation of up to 10 mass % plutonium was demonstrated.[157]

For synthetic samples it was found that the highest content of muratatite is achieved in ceramics of the following composition:

Oxide	TiO_2	MnO	CaO	Al_2O_3	Fe_2O_3	ZrO_2	See §
Content (mass %)	55	10	10	5	5	5	10

Subsequently this composition was considered as basic. A transmission electron microscopic examination revealed structure types with motif periodicity of 3, 5, 7 and 8 relative to the fluorite unit cell, which were designated as M3, M5, M7 and M8, respectively. The main reflections in the X-ray diffraction patterns are in the following ranges of interplanar spacing /Å: 2.86 – 2.79, 2.47 – 2.43, 1.75 – 1.72 and 1.50 – 1.42. In these ranges, several closely located or overlapping reflections from different muratatite type phases are observed. In ceramics produced by sintering, muratatite phases form isolated homogeneous grains (see Fig. 5 *a*). In contrast, the matrices obtained by crystallization from a melt are composed of muratatite grains of zonal structure with variable composition of fragments (see Fig. 5 *b* – *d* and Tables 4 and 6). The centre of these grains is composed of zirconolite or M5 structure, while the periphery consists of M8 and/or M3 structures. The close association of zirconolite and muratatite, which was also noted for a host phase incorporating simulated waste from the Mayak production association,[153, 154] is obviously caused by structural similarity of these two phases.

§ Actinide or REE oxides.

Table 5. Crystallographic parameters and cation site numbers for synthetic muratatites M3, M5 and M8.[195]

Parameter	M3	M5	M8
Crystallographic parameters			
Space group	$F\bar{4}3m$	$F\bar{4}3m$	$F\bar{4}3m$
a /Å	14.676(15)	24.564(7)	39.105(12)
V /Å^3	3161.3(6)	14822(7)	59799(32)
R_1	0.063	0.074	0.156
Numbers of cation sites in the crystal structure			
Structure with C.N.			
4	1	–	2
5	1	2	7
6	1	5	15
7	–	1	6
8	2	6	10
Total	5	14	40

The TEM images reveal a superstructure, which is a typical feature of all synthetic phases. Strong reflections correspond to the cubic face-centred sublattice, the size of which is close to the size of fluorite unit cell; weak reflections determine the true unit cell parameters. In the electron diffraction patterns of pyrochlore (see Fig. 6 *a*), one can see unit cell doubling relative to the fluorite pseudo-cell. The muratatite periodicity is convenient to correlate with the same pseudo-cell. Depending on the supercell size, the following muratatite varieties are distinguished: M3 (see Fig. 6 *b*), M5 (see Fig. 6 *c*), M7 and M8 (see Fig. 6 *d*). In terms of this system, the natural mineral corresponds to the M3 structure of synthetic phases.

Apart from the above-indicated differences in the reflection intensities, the electron diffraction patterns of muratatites along the [110] direction display one more specific feature. Among the weak superstructure reflections, those with $hkl = 5n \pm 2$ and $hkl = 5n \pm 3$ for the muratatite M5 and $hkl = 8n \pm 3$ and $hkl = 8n \pm 5$ for M8 prove to be systematically enhanced. For each muratatite variety, both sets of reflections can be considered to be first- and second-order satellites. In the case of M5, the first-order satellite is located at a 2/5 distance from the main reflection, while the less intense second-order satellite is at a 3/5 distance from the same main reflection. Whereas for a unit cell with the parameter 5a and the main reflection of hkl = 555, the reflections 222 and 333 are enhanced, in the direct space, this corresponds to planes that cut off 3/5 and 2/5 parts, respectively, along the diagonal of the large (true) unit cell orthogonally to the [111] direction. In the same way, the large unit cell in M8 is split into subcells in 3 : 5 ratio along the [111] diagonal. The high-resolution TEM images (see Fig. 6) show clear-cut splitting of atomic layers into two groups in 2 : 3 (M5) and 3 : 5 (M8) ratios.

The synthetic types of muratatites can be regarded as phases with commensurately and non-commensurately modulated structure. However, the proportion of non-

Table 6. Phase compositions (mass %) in murataite ceramics containing lanthanides.[179]

Oxide	Sample with 10 mass % La_2O_3					Sample with 10 mass % Gd_2O_3				
	Z (M5)	M8	P	C	T	M5	M8	M3	C	T
Al_2O_3	3.8	8.4	1.4	5.3	N.f.	1.6	3.7	7.3	4.6	0.6
CaO	6.6	6.7	22.6	2.7	0.3	7.6	9.4	9.4	5.1	0.6
TiO_2	47.2	50.9	48.6	65.5	51.9	46.8	54.3	56.9	75.2	53.0
MnO	12.8	15.2	1.5	9.3	29.1	6.5	8.5	11.1	7.4	25.4
Fe_2O_3	4.8	7.1	0.6	6.1	18.1 [a]	2.0	2.6	6.6	6.9	20.4 [a]
ZrO_2	22.9	8.5	N.f.	4.6	0.6	17.0	8.5	3.3	0.8	N.f.
La_2O_3	1.9	3.2	25.3	6.5	N.f.	–	–	–	–	–
Gd_2O_3	–	–	–	–	–	18.5	13.0	5.4	N.f.	N.f.

Note. The following designations are used: *Z* is zirconolite (?), M8 is murataite, P is perovskite, C is crichtonite, T is pyrophanite, N.f. is not found.
[a] In relation to FeO.

commensurately modulated microcrystals is at least an order of magnitude lower than that of commensurate ones. The substitution modulation and a shift modulation with a period equal to one-third of the body diagonal length were found. This conclusion can be drawn taking into account the presence of satellites of the primary beam and the intensity ratio of the satellites located on both sides of strong reflections (nearer and farther relative to the primary electron beam).

According to an X-ray diffraction study,[152] the crystal structure of a natural murataite sample with the idealized formula $R_6(M')_{12}(M'')_4TX_{43}$ (R = Y, Na, Ca, Mn; M′ = Ti, Fe; M″ = Fe, Ti; T = Zn; X = O, F) is cubic (space group $F\bar{4}3m$, a = 14.89 Å, Z = 4) and contains four cationic sites: an eight-vertex polyhedron $R^{[8]}$, octahedron $M'^{[6]}$, five-vertex polyhedron (trigonal bipyramid) $M''^{[5]}$ and regular tetrahedron $T^{[4]}$. Three octahedra M′ are linked via edges to form compact groups $(M')_3X_{13}$, four of which share vertices to form the polyanion $[(M')_{12}TX_{40}]^{n-}$ shaped like a truncated (Laves) tetrahedron (with the small zinc-containing tetrahedron T at the centre). This polyanion, known as a Keggin complex, is considered as the key building block of the murataite crystal structure. The $M''^{[5]}$ sites, the number of which is three times less than the number of M′ sites, do not play a structure-forming role but only 'clamp' the six-membered rings of the M′ octahedra.

One more genetic line of the synthetic murataite structure was studied immediately after discovery.[148, 206] For the $(Ca,Mn)_2Zr(Fe,Al)_4Ti_3O_{16}$ phase, it was represented as a fluorite oxide structure with a tripled ratio of the cubic unit cell parameters: a (murataite) ≈ 3a (fluorite). The structures of numerous inorganic compounds and minerals containing Zr, Ti, Ca, Mn, Mg, REE and other elements are derived from the fluorite structure of simple MO_2 oxides (M = Zr, Hf, Tb, Ce, U, T, *etc*., a = 5.07–5.47 Å, space group $Fm3m$). For example, zirconium oxides 'stabilized' by minor components (Ti, Ca, Mn, Mg) have fluorite unit cell parameters in the range of

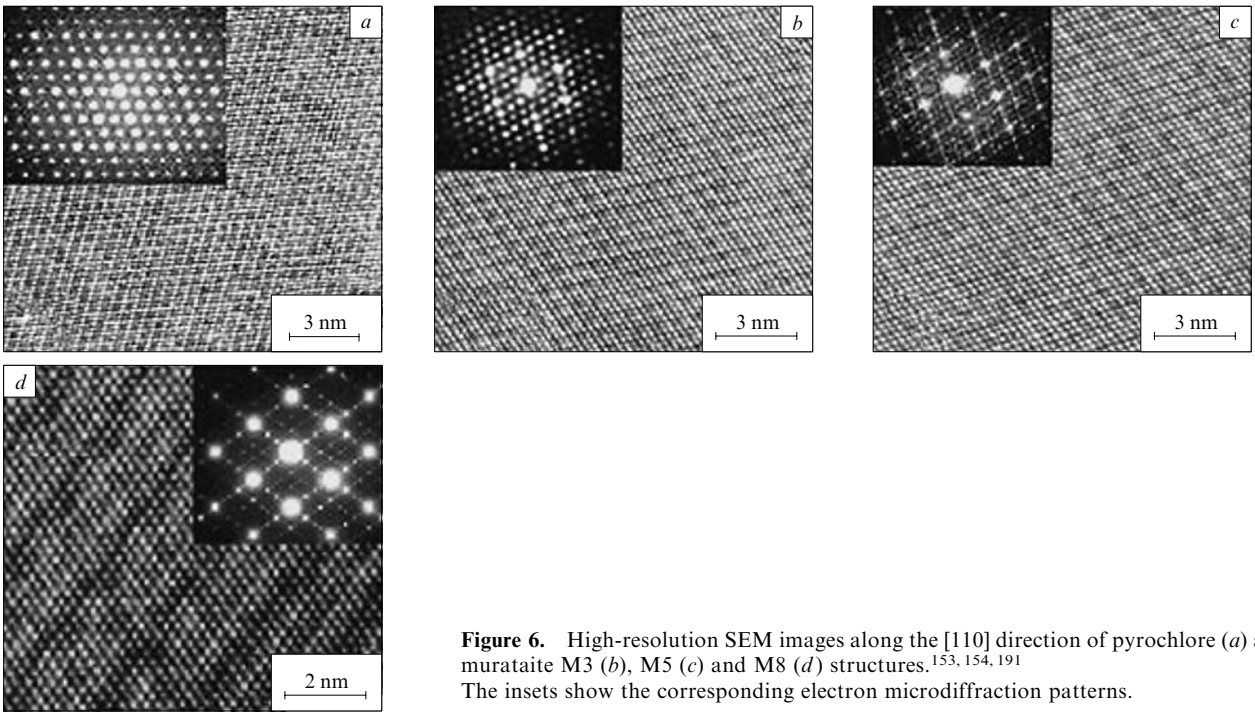


Figure 6. High-resolution SEM images along the [110] direction of pyrochlore (*a*) and murataite M3 (*b*), M5 (*c*) and M8 (*d*) structures.[153, 154, 191]
The insets show the corresponding electron microdiffraction patterns.

4.9 – 5.1 Å; in the case of the mineral tazheranite (Zr, Ca, Ti)O_{2-x}, a is 5.11 Å.[207] A common feature of the compounds is the formation of derivatives with vacancies in the anionic (oxygen) sublattice upon replacement of a quadruply charged cation that forms the cubic close-packed structure by cations with a lower charge (no matter, in the ordered or disordered manner). The simplest formulae of ordered derivatives can be written as A_nO_{2n-k}, where n and k are simple integers, $k \leqslant n/2$,[207] and the polyhedra A are cubes that are either intact or truncated at one (seven-vertex polyhedra) or two (octahedra) vertices and occupy cation sites in the cubic close-packed structure.

Urusov *et al.*[57] substantiated the assumption that the group of synthetic murataites is a polysomatic series of compounds with the pyrochlore and murataite mineral structures as the terminal members. This hypothesis provides an explanation for the details of reflection intensity distribution in the microdiffraction patterns and characteristic features of high-resolution patterns. According to the hypothesis, the synthetic murataite structures can be assembled from two types of modules representing the initial murataite M3 and pyrochlore P structures. The M5 structure is assembled from one M3 and one P modules, while M8 is composed of two M3 and one P modules.

In this model, it was assumed that the pyrochlore and murataite modules are two-dimensional layers and their alternation can produce the whole diversity of murataite types. In the designation of close packings, the fluorite motif is given by alternation of three layers with the same composition and polyhedral topology ... ABC ... , differing in the relative packing of neighbours. According to this approach, pyrochlore is a six-layer packing, ... A(1)B(2)C(1)A(2)B(1)C(2) ... . The A(1) and A(2) layers differ from each other in the polyhedral topology and composition; the B(1) and B(2) layers differ from each other in the same way. The A(1) and B(1) or A(2) and B(2) layers have the same compositions, but different topologies, as they have different local environments. High-resolution transmission electron microscopy and microdiffraction studies of pyrochlore showed the presence of two layers. In this case, the M5 structure can be represented as alternation of M3 and P modules and its layer-by-layer structure along the [111] diagonal can be described as

$$\begin{aligned} &\ldots \mathrm{A(1)B(2)\,|\,C(3)A(4)B(5)\,|\,C(1)A(2),\,|\,B(3)C(4)A(5)\,|} \\ &\quad \mathrm{|\,B(1)C(2)\,|\,A(3)B(4)C(5)} \ldots \end{aligned} \qquad (4)$$

In this set of close-packed cationic layers, vertical lines separate the pyrochlore (layers 1 and 2) and murataite (layers 3, 4 and 5) modules of the 'assembled' M5. From the same standpoint, the M8 structure can be interpreted as being assembled from one P and two M3 modules. The assembly of intricate structures from two basic modules provides a consistent explanation for the electron diffraction patterns and high-resolution electron microscopy images of these compounds. This hypothesis accounts for the absence of M4 structure, because it is degenerated to the 2P structure, and the probable absence of M6, because it should be degenerated to mere doubling of M3. However, the assembly of two P and one M3 modules may give rise to the M7 structure, which was detected in some samples.[162 – 164, 170, 171, 177, 183] Thus, the modular layered model for various murataite structures provided an understanding for the structural diversity of this intriguing and practically valuable class of complex oxides. Although it was not exactly confirmed in the subsequent X-ray diffraction studies, it can be claimed that the general nature of 'murataite' structures (particularly, the assembly of pyrochlore and murataite blocks) has already been established in the first stage of investigation.

Relying on the results of crystal structure solution, the formula $(Y,Na)_6(Zn,Fe)_5Ti_{12}O_{29}(O,F)_{10}F_4$ was proposed for natural murataite.[155] Krivovichev and co-workers[17] ascertained the following: if murataite is considered as a fluorite structure derivative with the tripled cubic unit cell, the complete set of cation and anion sites in the ideal structure (without vacancies) should correspond to the formula $3^3 \times MX_2 = M_{27}X_{54}$, where M and X are the cation and anion sites, respectively. The gross formula of natural murataite corresponds to $M_{23}X_{43}$, which is indicative of the presence of vacancies in the anion and cation sites. The structure of the synthetic M3 is given as $[Ca_{3.24}Mn_{2.66}.$ $.Ti_{1.90}Tb_{1.20}Fe_{0.76}\square_{0.24}](Al_{0.71}Fe_{0.29})(Ti_{3.92}Al_{0.08})(Ti_{9.96}Zr_{2.04})O_{42}$ or $Ca_{3.24}(Mn_{2.66}Fe_{1.06})_{\Sigma\,=\,3.72}Ti_{15.78}Tb_{1.20}Al_{0.79}Zr_{2.04}O_{42}$, which is fairly similar to the stoichiometry $Ca_{3.27}(Mn_{2.96}Fe_{0.83})_{\Sigma\,=\,3.79}Ti_{15.90}Tb_{1.18}Al_{2.14}Zr_{1.04}O_{42}$ according to elemental analysis. Unlike natural murataite, the synthetic M3 structure has fewer vacancies in the cation sublattice. According to structural studies, M3 has five cation sites rather than four, as present in natural murataite, and the additional cation site has eight-fold coordination formed by Ca^{2+} and Tb^{3+} cations. The structure-chemical difference between the synthetic and natural murataites is that the latter contains a substantial amount of fluorine, which makes up for the absence of the additional cation site.[17]

Structure solution for synthetic murataite M5 has been reported.[17, 190] According to microprobe analysis, the crystal composition was $Ca_{3.17}Mn_{1.39}U_{0.92}Zr_{0.79}Ti_{8.57}Fe_{0.30}Al_{0.34}O_{26.09}$. The M5 structure has 14 cation sites, five of them being octahedral; the bond lengths are in the range of 1.797 – 2.246 Å. Considering the bond lengths and scattering ability, these sites were classified as titanium sites. However, the scattering factors for the Ti(1), Ti(2), Ti(4) and Ti(5) sites were somewhat higher than that for titanium; therefore, the refinement for the mixed occupancy of these sites was performed with the assumption that they accommodate zirconium atoms. Like M3, the M5 structure has five-coordinate sites with a trigonal bipyramidal geometry, which are mainly occupied by manganese [Mn(1) and Mn(2)]. The sites of large cations in M5 can be divided into two groups: seven eight-coordinate and one seven-coordinate sites. Note that no sites with C.N. of 7 are present in M3. Due to the complex composition, a large number of atom sites and, as a consequence, the presence of diverse short-range ordering mechanisms, unambiguous positioning of cations among the structural sites appears quite problematic and can be made only roughly. Also, it may be exactly the partial local ordering that gives rise to the modulation waves detected as diffuse scattering and to weak satellite reflections.

Like pyrochlore and M3, the M5 structure can be represented as a combination of an octahedral framework and a metal oxide substructure formed by 'non-octahedral' cations. The octahedral framework has a unique feature: it is formed by whole pyrochlore unit cells arranged according to the face-centred cubic (or 3D staggered) pattern as

building modules. These modules of ~1.8 nm size can be reasonably called pyrochlore nanoclusters. The composition of the octahedral framework is rather intricate and can be represented as $[(Ti,Zr)_{29}O_{86}]^{56-}$. The framework negative charge is counterbalanced by the cationic metal – oxygen sub-framework formed by 'non-octahedral' cations. The cation sub-framework composed of oxo-centred $O'A_4$ tetrahedra is described as $[O_{39}A_{67}]$ and is a deficient analogue of the fluorite tetrahedral framework.

Considering the compositions of the octahedral modular framework and cation–oxygen substructure, the M5 structure can be generally represented as $Mn_8M_{59}O_{39}[(Ti,Zr)_{29}O_{86}]_2$. The exact crystal chemical formula calculated from the determined site occupancy factors is $Ca_{24.47}Mn_{21.97}U_{7.71}Al_{2.46}Ti_{59.84}Zr_{8.56}O_{172}$; this is generally in line with microprobe analysis data. Note that the empirical and structural formulae calculated in relation to 172 oxygen atoms give approximately equal numbers of cations — 125.19 and 125.00, respectively. It is also noteworthy that in some cases, conversion of the chemical analysis data for M5 samples to 172 oxygen atoms resulted in <125 cations. This attests to the possible formation of vacancies in the cation sites, which is typical of pyrochlore complex oxides.

The M8 structure was studied for a zonal crystal with the following composition of the M8 zone:[190]

Oxide	Al_2O_3	CaO	TiO_2	MnO	Fe_2O_3	ZrO_2	Ho_2O_3
Content (mass %)	2.84	7.30	55.95	8.05	2.80	6.34	23.91

The structure contains 40 cation sites, which is an order of magnitude greater than this number in M3. Two sites are tetrahedral and are centres of Keggin complexes, seven sites are trigonal-bipyramidal and are located at the central part of 3^46^4 truncated tetrahedra, fifteen sites are in the octahedral coordination and form the octahedral framework. The large cation sites are divided into two group, eight-coordinate (10 sites) and seven-coordinate (6 sites) ones (see Table 5).

Unlike M5, the M8 structure incorporates α-Keggin complexes, which share vertices to form murataite nanoclusters, which are actually cubic unit cells of M3. The nanocluster size is 2.5 nm. These modules are located at the vertices and centres of faces of the face-centred cubic unit cell [the coordinates of the centre of gravity of the 'zero' module are (0 0 0)]. The pyrochlore modules (like in M5, they are the pyrochlore unit cells) are located between the murataite nanoclusters. These modules also form a face-centred cubic unit cell shifted by the vector (0 0 1/2) with respect to the murataite substructure. The M8 structure is based on staggered alternation of the murataite and pyrochlore nanoclusters, representing the unit cells of the parent structures.

Taking into account all cation and anion sites in the M8 structure, their ratio can be represented by the formula $M_{512}X_{823}$. The total number of sites in the octuple fluorite structure corresponds to the formula $8^3 \times MX_2 = M_{512}X_{1024}$. From this, one can conclude that in the M8 structure, cations occupy all fluorite cation sites, while a considerable part of anion sites are vacant.

The calculation of the formula of the M8 phase considering 823 oxygen atoms gives the following composition: $Al_{23.02}Ca_{52.85}Ti_{284.10}Mn_{54.31}Fe_{17.59}Zr_{14.83}Ho_{38.04}O_{823}$. Proceeding from the data on site occupancy, one can propose the $Al_{14.86}Ca_{53.00}Ti_{285.46}Mn_{58.76}Fe_{29.54}Zr_{16.64}Ho_{31.95}O_{823}$ formula, which is consistent with the empirical formula with allowance made for the error caused by composition non-uniformity of the zonal crystal, affecting both the structure refinement and the results of analysis.

The M3, M5 and M8 phases contain altogether 3, 12 and 31, respectively, sites with C.N. of six and more, which allows placement of large actinide cations, including Am, $Cm^{3+/4+}$ and REE. As a rule, $(TR)^{3+/4+}$ and $An^{3+/4+}$ as well as Ca^{2+} and Na^+ cations should occupy sites with C.N. = 8, while the C.N. = 6 sites would be occupied by Ti^{4+}, Fe^{3+} and Al^{3+}.

Depending on the gross composition, in particular, the content of actinide and analogous REE oxides, ceramics obtained by cold pressing and sintering are usually single phases (M3, M5, M8). During preparation by crystallization from the melt, several (at least two) phases, growing over each other, are usually formed. In the multiphase titanate ceramic such as Synroc-C, murataite grains grow over zirconolite (see Fig. 5).[16, 153, 154] In a ceramic, with the murataite gross composition, the first phase to be isolated during crystallization of a melt was zirconolite (in a system with increased zirconium content) or the phase with the highest content of actinides, their REE analogues and zirconium and the highest proportion of pyrochlore modules (M5 or M8 depending on the composition), *i.e.*, the usual phase segregation sequence is the following: Z(M5)–M8–M3. The last-mentioned phase is depleted in actinides, REE and calcium and enriched in titanium, aluminium and iron. At the end, the residual crichtonite phase (nominally $AB_{21}O_{38}$) devoid of actinides crystallizes and the interstitial glassy phase is often present (because of melt contamination with silica from the refractory lining of the cold 'crucible').

A specific feature of REE ceramics is the frequent presence of perovskite $(Ca,TR)(Ti,Al,Fe)O_3$. X-Ray diffraction patterns of melted ceramics with 10 mass % REE oxides are similar to the X-ray diffraction patterns of actinide-containing samples; the proportion of the perovskite phase decreases in the series from La to Gd. A perovskite content higher than expected is found in the Eu-containing sample, apparently, because of the formation of the $(Ca,Eu^{2+})TiO_3$ phase. As the time for which the melt is kept increases to three hours, the perovskite reflection intensity decreases, because Eu^{II} to Eu^{III} oxidation is likely to take place, Eu^{II} being incorporated in the murataite phases.[158, 178, 179] The Pu-containing ceramics, especially those prepared in a reducing atmosphere, also contain a perovskite phase of the $PuAlO_3$ or $(Ca,Pu)(Ti,Al)O_3$ type.[157, 161, 174] By analogy with Pu- and REE-containing ceramics, the formation of a perovskite phase (such as $AmAlO_3$ and $CmAlO_3$) is also expected for Am- and Cm-containing samples.

Murataite ceramics incorporating real actinides (Th, U, Np, Pu, Am, Cm) and their REE analogues (lanthanum and lanthanides) were obtained both by sintering and by melting. Samples of the basic composition containing each 10 mass % ThO_2, UO_2, NpO_2 or PuO_2 were synthesized and also three curium-containing samples were prepared, containing (mass %): 3.8 Al_2O_3; 10.5 CaO; 54.0 TiO_2; 10.6 MnO; 6.0 Fe_2O_3; 4.6 ZrO_2; 8.1 ThO_2; and 2.4 Cm_2O_3 (including 1.8 mass % $^{244}Cm_2O_3$), one by cold pressing and sintering at 1250 °C and the other two by melting at 1325

and 1350 °C.[157, 158, 168, 169, 174–176, 180–182, 187, 191, 195] The samples with Th, U, Np and Pu obtained by melting in air (oxidizing atmosphere) at ~1400 °C consisted mainly (85 vol.%–90 vol.%) of murataite structures with 5-, 8- and 3-fold fluorite unit cells (see Tables 6 and 7). The impurity phases were perovskite (in Th-containing sample), crichtonite, rutile and a cubic fluorite type oxide (only in Pu-containing sample). The Pu-containing sample prepared in a reducing atmosphere contained a noticeable amount of the perovskite phase, probably, as a result of reduction of some Pu^{IV} to Pu^{III}. The curium sample obtained by cold pressing and sintering contained trace amounts of oxides from the feed formulation, as phase formation was not completed, whereas melted and crystallized materials were mainly homogeneous, although they also contained some additional phases.[157–159, 174–176, 180–182]

In the MCC-3 (PCT) testing at 95 °C, the uranium leaching rate was $\sim 10^{-6}$ g m^{-2} day^{-1} in the first 24 h of contact with water and decreased by almost two orders of magnitude by the 28th day of the contact. The same value was obtained by the same procedure for the plutonium leaching rate on the seventh day of contact with water.[158] The actinide leaching rates (Th, U, Np, Pu) determined by the MCC-1 procedure at 90 °C (seven-day test) were 10^{-6} g m^{-2} day^{-1} in the first to third day and 10^{-7} g m^{-2} day^{-1} on the seventh day.[168] Even under drastic conditions of the dynamic MCC-4 test (SPFT) at 90 °C, the rates of uranium and thorium leaching from murataite ceramics were low: 2.4×10^{-5} and 1.1×10^{-7} g m^{-2} day^{-1} (Ref. 175).

The radiation resistance of murataite ceramics was determined by irradiation with accelerated krypton ions (1 MeV)[196–203] and incorporation of ^{244}Cm isotopes.[186, 204, 205] In both cases, increasing the fluence (cumulative dose) induced gradual disordering of the crystal lattice. At a fluence of ~4.4 10^{17} m^{-2}, undamaged areas retaining the long-range order and amorphous domains could be distinguished; an amorphous halo appeared in the electron diffraction patterns, its intensity increasing with increasing fluence. When the fluence was $\sim 9.4 \times 10^{17}$ m^{-2}, the structure was amorphized to a considerable extent, and at $\sim 1.6 \times 10^{18}$ m^{-2}, the material was almost completely metamict. The critical doses for amorphization of M5 and M8 were 1.85×10^{18} and 1.75×10^{18} m^{-2}, respectively (~0.2 dpa). The lattice disorder involved the following stages: M8–M5–M3–P–dP (diffuse pyrochlore)–A (metamict state).

For the ^{244}Cm-doped sample, an increase in the cumulative radiation dose resulted in the decrease in intensity with simultaneous broadening of M5 phase reflections in the diffraction patterns of the sintered sample. The M5 phase turned X-ray amorphous at 2.73×10^{18} (α-decays) g^{-1} (0.21 dpa). The splitting of the major murataite peak with separation of the 2.819 Å component after exposure to a dose of up to 1.23×10^{18} (α-decays) g^{-1} (0.095 dpa) can be attributed to the formation of the M8 phase; at a dose of 1.97×10^{18} (α-decays) g^{-1} (0.152 dpa), the main reflection of this phase shifted to 2.847 Å due to lattice 'swelling'.[186, 204, 205]

The reflection at ~2.803 Å in murataite ceramics is usually attributed to the M3 structure,[14, 15, 155, 158] which contains a minimum amount of actinides. Apparently, that is why this phase in sintered ceramics virtually does not amorphize, although increase in the cumulative dose entails peak broadening due to some disorder of the positions of atoms in the crystal lattice of this variety.

In ceramics obtained by melting at 1325 and 1350 °C, the M5 and M8 murataite phases become virtually fully X-ray amorphous at similar doses of 2.46×10^{18} and 2.53×10^{18} (α-decays) g^{-1}, respectively, which do not differ much from those for sintered ceramics [2.73×10^{18} (α-decays) g^{-1}, or 0.21 dpa].[186, 204, 205]

In melted ceramics, the M5 phase with the highest actinide content always forms the central part of the grain, which is enveloped by zones of the M8 and M3 phases. A higher content of the ^{244}Cm isotope in M5 compared with its content in other varieties accounts for early amorphization of M5 at a lower dose. In sintered ceramics, the major murataite phase is depleted in curium, which is incorporated in other minor phases (pyrochlore, perovskite). This increases the time and the dose required for amorphization. The difference between these values for melted and sintered ceramics are insignificant (do not exceed 10%). If the results are averaged, the value $D_c = 0.20$ dpa may be taken as a real dose needed for transition to X-ray amorphous state for murataite ceramic as a whole without assignment to a particular structural variety. This value is somewhat higher than the D_c values of murataite polytypes (0.14–0.15 dpa) subjected to ion bombardment.[196–203]

As the dose is accumulated, the other phases also amorphize. The reflection at 2.940 Å, presumably, from the minor pyrochlore phase disappears at a cumulative dose of 1.23×10^{18} (α-decays) g^{-1} (0.095 dpa), which is approximately half that for pyrochlore containing ^{238}Pu or ^{244}Cm.[26, 110, 112, 113] A possible reason is a high curium concentration in pyrochlore and a high rate of dose accumulation, which results in fast amorphization.

At a dose of 2.73×10^{18} (α-decays) g^{-1} (0.21 dpa), the crichtonite remainders are present in the X-ray diffraction

Table 7. Phase compositions (mass %) in murataite ceramic samples with 10 mass % UO_2 obtained by various processes.[181]

Oxide	Sintering at 1300 °C			Melting at 1600 °C–crystallization			
	M8	M3	rutile	M5	M8	M3	rutile
Al_2O_3	1.3	2.9	0.2	2.1	4.5	7.1	0.5
CaO	13.2	11.8	0.3	13.8	12.6	11.4	0.2
TiO_2	50.7	51.1	92.6	48.6	52.7	52.5	90.3
MnO	7.3	9.2	0.6	7.3	9.6	10.8	0.5
Fe_2O_3	1.8	3.7	0.8	3.6	4.6	6.5	0.8
ZrO_2	7.2	9.1	2.9	10.4	6.0	3.3	5.0
UO_2	18.5	12.2	2.6	14.1	10.1	8.4	2.7

pattern of the sintered ceramics, but its unit cell parameter increases by ~1.2%. Crichtonite transforms to X-ray amorphous state at a cumulative dose of 2.80×10^{18} (α-decays) g^{-1} (0.215 dpa). The perovskite and pseudobrookite phases are less prone to amorphization. When the sample is exposed to a dose of 1.70×10^{18} (α-decays) g^{-1} (0.13 dpa), the unit cell parameters slightly increase, but no peak broadening was noted to within the measurement error. Apparently, these phases, like M3, contain only a minor admixture of curium.

In order to restore the destroyed structure, the amorphized sintered ceramic sample was heated for 5 h at 1250 °C in air. The calcined ceramics had virtually the same phase composition as the sample before amorphization. Differences were in the intensity of some reflections and a smaller number of weak peaks corresponding to minor phases.

The effect of amorphization on the stability of murataite ceramics was assessed by conducting leaching experiments in distilled water at 90 °C.[186, 204, 205] Three experiments were carried out for the same sample, first, immediately after the synthesis, second, when the amorphized pellet had been kept after the synthesis under argon; and third, for the same pellet after grinding away of 0.01 mm from its surface. Grinding was meant to remove the surface layer, from which elements had been leached in the first and second experiments.

The leaching rates of most elements (Ca, Fe, Mn and Cm) from the initial sample were much higher than from the amorphized sample (Table 8); this is at variance with the usual situation where amorphization results in higher actinide leaching rates.[26, 110, 112, 113] Probably, this is caused by the fact that mineral formation reactions in the sintered murataite sample had not proceeded to completion, and phases with low stability in solution remained in the pellet. In addition, when the murataite ceramic is obtained by sintering rather than by melting and crystallization, no zonal grains with the highest actinide concentration at the centre and the lowest one at the periphery are formed (this would have prevented curium from leaching). The curium leaching rate from the same ceramic after grinding (and removal of the layer depleted in these phases) increased 2–4-fold. In general, the sintered murataite-containing ceramic obtained by the procedure used in this work is similar in the corrosion stability to pyrochlore and zirconolite host phases.[26]

III.1.d. Zirconolite

Zirconolite with the nominal formula $CaZrTi_2O_7$ is among the first phases proposed for the incorporation of actinides into Synroc ceramics.[21, 22, 25] The mineral species 'zirconolite' combines various minerals with monoclinic (pristine zirconolite and zirconolite-2M), trigonal (zirkelite, zirconolite-3T) or orthorhombic (polymignite, zirconolite-3O) symmetry[208–210] and the zirconolite-4M (Ref. 211) and zirconolite-6T (Ref. 212) structures discovered later. They are adjoined by the mineral pyrochlore with cubic symmetry.[54–56] All these phases were also found in the synthesized ceramic hosts for RW immobilization. The three first-mentioned phases are, in some cases, encountered in nature as intergrowth with one another or with pyrochlore. The minerals have an anion-deficient fluorite-like structure. It differs from the fluorite structure by cation ordering in the planes perpendicular to the *c* axis of the unit cell. The ideal crystal chemical formula of the minerals corresponds to $A_2B_2O_7$. The A sites are occupied by calcium and zirconium atoms as well as by alkali and alkaline earth elements, REE and actinides, which are capable of isomorphous substitution for the principal atoms owing to similar sizes and ion charges. The B sites are mainly occupied by titanium atoms; as secondary components isomorphous with titanium, Nb,

Table 8. Leaching rates from the starting and amorphized samples of ^{244}Cm-doped murataite ceramic.[186, 204, 205]

Element	Leaching period /days	Leaching rate /g cm^{-2} day^{-1}		
		starting sample	sample after amorphization without surface grinding	sample after amorphization and surface grinding
Cm	3	1.4×10^{-5}	1.0×10^{-7}	3.7×10^{-7}
	7	7.8×10^{-5}	9.0×10^{-8}	3.9×10^{-7}
	14	5.4×10^{-6}	7.8×10^{-7}	5.7×10^{-7}
Ca	3	8.9×10^{-5}	3.7×10^{-6}	1.1×10^{-5}
	7	4.1×10^{-5}	3.1×10^{-6}	6.8×10^{-6}
	14	2.1×10^{-5}	2.3×10^{-6}	5.4×10^{-6}
Mn	3	1.6×10^{-5}	2.7×10^{-7}	7.0×10^{-7}
	7	5.0×10^{-5}	2.3×10^{-7}	6.0×10^{-7}
	14	5.1×10^{-5}	1.7×10^{-7}	5.1×10^{-7}
Zr	3	3.3×10^{-6}	9.6×10^{-6}	7.6×10^{-6}
	7	5.7×10^{-6}	8.3×10^{-6}	6.5×10^{-6}
	14	5.0×10^{-6}	6.2×10^{-6}	4.9×10^{-6}
Ti	3	1.0×10^{-7}	3.4×10^{-7}	2.6×10^{-7}
	7	9.0×10^{-8}	2.9×10^{-7}	2.2×10^{-7}
	14	6.7×10^{-8}	2.2×10^{-7}	1.6×10^{-7}
Fe	3	3.2×10^{-5}	7.1×10^{-6}	1.1×10^{-5}
	7	2.2×10^{-5}	6.1×10^{-6}	7.6×10^{-6}
	14	1.6×10^{-5}	4.6×10^{-6}	9.1×10^{-6}
Al	3	1.5×10^{-5}	5.3×10^{-5}	3.6×10^{-5}
	7	7.2×10^{-6}	4.5×10^{-5}	3.3×10^{-5}
	14	3.8×10^{-6}	3.4×10^{-5}	3.0×10^{-5}

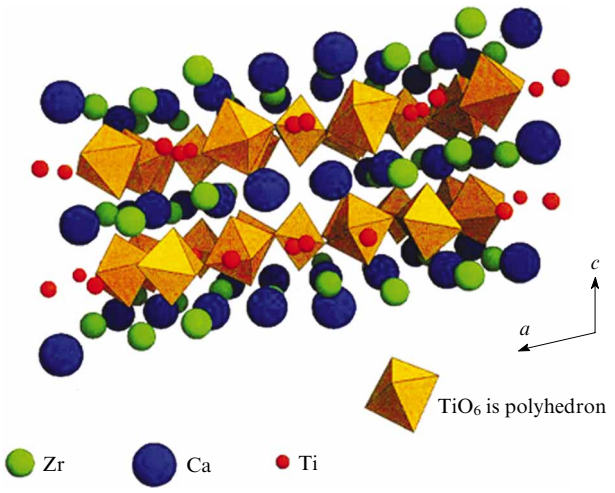


Figure 7. Structure of the most frequently occurring variety of zirconolite-2M.[60]

Ta, Al, Mg, iron group metals and chromium can be present.

According to a number of studies,[25, 60, 213 – 217] the zirconolite group minerals are composed of hexagonal and trigonal rings connected to one another; at the centres of the rings, there are titanium atoms surrounded by six oxygen atoms (Fig. 7). Some of the titanium atoms are surrounded by five oxygen atoms forming trigonal bipyramids. The indicated sites are matched by three types of lattice titanium atoms, namely, Ti(1) and Ti(3) with C.N. = 6 and Ti(2) with C.N. = 5; the numbers of these atoms in the unit cell are 8, 4 and 4, respectively. The large calcium cations with C.N. = 8 are located between two networks of TiO_6 octahedra in the interstices of a distorted cube. Zirconium atoms surrounded by seven oxygen atoms according to the hexagonal pyramidal geometry are located in the same positions. With allowance for the different C.N. values of atoms, the crystal chemical formula of the zirconolite group minerals is properly represented as $^{VIII}Ca_2{}^{VII}Zr_2{}^{VI}Ti_3{}^{V}TiO_{14}$.

Every two layers of TiO_6 octahedron networks, together with interlayer cations, compose a unit structural module. Zirconolite has the simplest two-module lattice in which the adjacent modules are shifted relative to each other. The shift of adjacent modules accompanied by simultaneous rotation through a multiple of 120° angle makes the lattice more intricate. This gives rise to a three-module unit cell typical of zirconolites-3T (zirkelite) and -3O (polymignite). The unit cell parameters of the minerals are summarized in Table 9. The two- and three-module zirconolite and zirkelite motifs can alternate in the lattice, which results in fine twinning and intergrowth of these phases in mineral grains, which can be detected only by electron probe X-ray microanalysis.

The composition ranges of natural and synthetic zirconolite group minerals are quite similar, the following typical patterns of isomorphous component exchange being observed in the crystal lattice:

$$Ca^{2+} \rightarrow \quad (5)$$

$$\rightarrow Na^{+}, K^{+}, Mn^{2+}, Sr^{2+}, Ba^{2+}, Y^{3+}, TR^{2+(3+)}, Th^{4+}, U^{4+}$$

$$Zr^{4+} \rightarrow TR^{3+}, Hf^{4+}, Th^{4+}, U^{4+}, Ti^{4+} \quad (6)$$

$$Ti^{4+} \rightarrow \quad (7)$$

$$\rightarrow (Mg, Fe, Co, Ni)^{2+}, (Al, Cr, Ti, Fe)^{3+}, Si^{4+}, (Nb, Ta)^{5+}$$

The key isomorphous substitution patterns that are of interest for immobilization of HLW components, first of all, REE and actinides, are the following:

— isovalent

$$Ca^{2+} \rightarrow M^{2+}, Zr^{4+} \rightarrow M^{4+}, Ti^{4+} \rightarrow M^{4+} \quad (8)$$

where M^{n+} are ions that meet the Goldschmidt's rules of substitution;

— heterovalent

$$Ca^{2+} + Ti^{4+} \rightarrow M_1^{3+} + M_2^{3+}; M_1 = TR^{3+}, An^{3+}; \quad (9)$$

$$M_2 = Al^{3+}, Fe^{3+}$$

$$Ca^{2+} + Zr^{4+} \rightarrow 2\,M^{3+}; M^{3+} = TR^{3+}, An^{3+} \quad (10)$$

$$Zr^{4+} + Ti^{4+} \rightarrow M^{3+} + M^{5+}; M^{3+} = TR^{3+}, An^{3+}; \quad (11)$$

$$M^{5+} = Nb^{5+}, Ta^{5+}$$

The highest concentrations of additional components corresponding to the isomorphous mineral capacity are similar for the natural and synthetic samples, being 20 mass % – 25 mass % for actinides, ~15 mass % – 18 mass % in total for niobium and tantalum, 10 mass % – 12 mass % for the REE sum, about 8 mass % for the sum of iron and magnesium family elements, ~4 mass % – 6 mass % for aluminium, 2 mass % for silicon and ~1 mass % for sodium, potassium, strontium and chromium. As can be seen from the isomorphous substitution patterns, An^{3+} ions (An = Pu, Am, Cm) should replace the Ca^{2+} ions (Scheme 9) and, at higher concentrations, also Zr^{4+} ions (Scheme 10); as this takes place, the mineral structure is transformed to the pyrochlore structure ($An_2Ti_2O_7$). If the An^{4+} ions replace Zr^{4+} (Scheme 6) to give $CaAn^{4+}Ti_2O_7$, the structure is also transformed to pyrochlore.

Table 9. Unit cell parameters of synthetic zirconolite group phases.[25]

Mineral	Symmetry	Parameter /Å			Angle /deg		
		a	*b*	*c*	α	β	γ
Zirconolite (zirconolite-2M)	Monoclinic	12.61	7.31	11.44	90	100.52	90
Zirkelite (zirconolite-3T)	Trigonal	7.29	7.29	16.89	90	90	120
Polymignite (zirconolite-3O)	Orthorhombic	10.15	14.15	7.28	90	90	90
Pyrochlore	Cubic	10.30	10.30	10.30	90	90	90

According to experimental data,[25, 218–221] the following oxides can be isomorphously incorporated into a synthetic zirconolite solid solution:

Oxide	Content (mass %)	Oxide	Content (mass %)
UO_2	27	Nb_2O_5	14
PuO_2 or NpO_2	24	Al_2O_3	7
ThO_2	20	MnO	5
Sum of REE oxides (mainly light and medium Nd_2O_3, Sm_2O_3)	29	FeO	4
		MgO	5
		SrO, Na_2O	up to 1

Here by zirconolite are meant all structural types — monoclinic, orthorhombic, trigonal and cubic (pyrochlore). If only the monoclinic phase is considered, then the limiting content of the additional components that does not disrupt the crystal system is much lower, for example, for PuO_2 it is about 11 mass % – 12 mass %.[218, 220] At a higher plutonium content, a cubic pyrochlore phase with a PuO_2 content of ~20 mass % appears together with the monoclinic lattice. Additional components occupy particular structural sites in the mineral, according to the charge and radius of their ions. The following types of iso- and heterovalent exchange were found:

$$(Nb, Al, Mg, Fe) \rightleftarrows Ti \quad (12)$$

$$(Th, TR, Mn, Sr, Na) \rightleftarrows Ca \quad (13)$$

$$(U, TR) \rightleftarrows Zr \quad (14)$$

$$U + (Al, Mg, Fe) \rightleftarrows Ca + Ti \quad (15)$$

The atoms with sizes close to the size of tetravalent titanium, for example, Mg and Fe, occupy predominantly the Ti(1) and Ti(3) sites of the crystal lattice. The smallest cations (niobium, aluminium and iron) are concentrated in Ti(2) sites.

Studies of synthetic samples also showed[213, 217] that at relatively low concentrations of additional elements, a zirconolite type monoclinic structure is stable. Upon simultaneous incorporation of actinides (REE) and Al, Mg or Fe atoms, a zirkelite (trigonal, 3T) or polymignite (orthorhombic, 3O) type structure becomes stable. The formation of a trigonal structure is facilitated by incorporation of a considerable amount (15 at.% – 40 at.%) of quadruply charged cations, first of all, thorium into sites with C.N. = 8 that are initially occupied by calcium. An orthorhombic structure is formed if calcium atoms are replaced by REE. The electroneutrality is maintained owing to the simultaneous replacement of some of titanium atoms by doubly or triply charged cations. High concentrations of REE and actinides stabilize the pyrochlore cubic structure.[25, 217–222] As shown in a study of isomorphism involving actinide and REE cations in zirconolites, the percentage of Ce^{4+} and Pu^{4+} decreases from 70% – 100% for the synthesis in air down to almost zero for the synthesis in a reducing or inert atmosphere (H_2/N_2, Ar). Neptunium is usually present as Np^{IV} (Refs 220 and 221). As regards americium and curium, to our knowledge, no data were reported.

Zirconolite is stable to amorphization under self-irradiation by incorporated ^{238}Pu and ^{244}Cm isotopes as well as in nature: for minerals differing in the synthetic phase composition and absolute age, the critical amorphization dose is in the range from 0.5 to 6 dpa.[25, 26, 43, 45, 53, 56, 105–108, 124, 126, 133, 136] In Synroc ceramics, zirconolite is chemically the most stable phase.[25] The leaching rates (V) measured in MCC-1 and MCC-2 tests for a number of elements were found to be [220, 221]

Element	V/g m^{-2} day^{-1}	Element	V/g m^{-2} day^{-1}
Ca	10^{-1}–10^{-2}	Al	~10^{-2}
Ba	10^{-2}–10^{-3}	Ti	10^{-6}
Nd	10^{-3}–10^{-4}	Zr	10^{-7}
U	10^{-4}–10^{-5}	Pu	~10^{-4}–10^{-5}

Zirconolite is stable in alkaline and acidic solutions at temperatures of up to 250°C and pressures of up to 50 MPa.[220]

III.2. Perovskite type titanates, aluminates and ferrites

The perovskite structure is inherent in compounds ABO_3 when the ratio of cation radii obeys the condition

$$0.73 \leqslant \frac{r_A + r_O}{\sqrt{2}(r_B + r_O)} \leqslant 1.0 \quad (16)$$

In the perovskite structure (Fig. 8), the vertex-sharing BO_6 octahedra form a three-dimensional framework with large cavities, which accommodate the A cations with coordina-

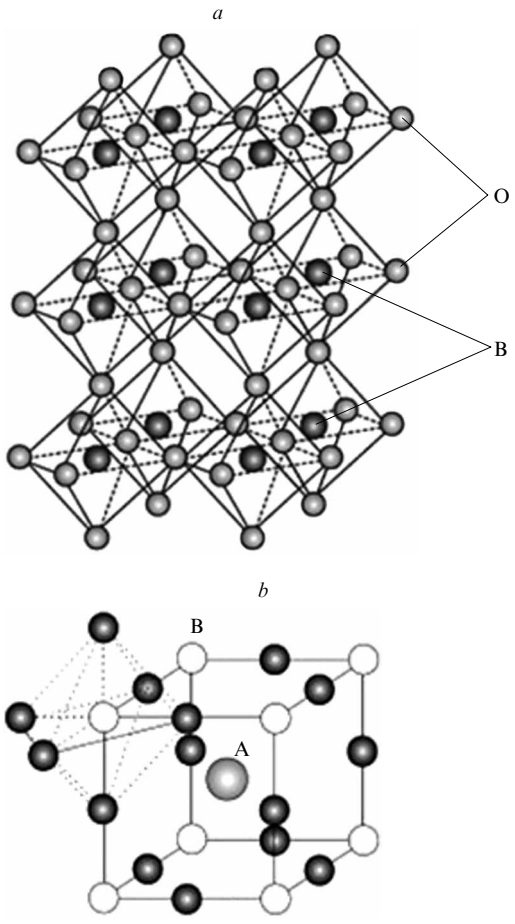


Figure 8. Framework of the cubic perovskite formed by vertex-sharing octahedra (*a*) and positions of cations with C.N. = 6 (B) and 12 (A) in the structure (*b*).[91]

Table 10. Compounds of the perovskite structural type.[4,25]

Formula	Symmetry	Space group
$CaTiO_3$	Orthorhombic	*Pnma*
$SrTiO_3$	Cubic	*Pm3m*
$La_{0.67}TiO_3$	Orthorhombic	*Cmmm* (?)
$Ce_{0.67}TiO_3$	Cubic	*Pm3m*
$Pr_{0.67}TiO_3$	Orthorhombic	*I4mmm*
$Nd_{0.67}TiO_3$	Orthorhombic and/or cubic	*I4mmm*
$Eu^{2+}TiO_3$	Cubic	*P3m*
$(Pr, \ldots, Gd)^{3+}Ti^{3+}O_3$	Orthorhombic	*Pnma*
$(La, \ldots, Nd)AlO_3$	Rhombohedral	*R3m*, $R\bar{3}c$
$(Sm, \ldots, Lu, Y)AlO_3$	Orthorhombic	*Pnma, Pbnm, Pbn*
$Pu^{3+}AlO_3$	"	*Amm2*
$Am^{3+}AlO_3$	Hexagonal or rhombohedral	*R3m*
$Cm^{3+}AlO_3$	Cubic, rhombohedral	?, *Pbnm*
$BaCm^{4+}O_3$	Cubic	?
$(La \ldots Gd)FeO_3$	Orthorhombic	*Pna*$2\bar{1}$, *Pbnm, Pnma*
$Cm^{3+}Fe^{3+}O_3$	"	*Pbnm*
$Ba_x(TR)_yTiO_3$	"	*Pbam, Pba2*
$CaZrO_3$	"	*Pnma, Pcmn*
$Ca_{0.5}U_{0.5}Ti^{3+}O_3$	Orthorhombic (?)	*Pnma*
$Na_{0.5}(TR)_{0.5}Ti^{4+}O_3$	Cubic	*Pm3m*
$NaNbO_3$	"	*Pm3m*

tion number of 12 with respect to oxygen. The perovskites $A^{2+}B^{4+}O_3$ may crystallize in the orthorhombic or cubic system, while $A^{3+}B^{3+}O_3$ structures are orthorhombic or rhombohedral (Table 10). Orthorhombic compounds form continuous solid solutions with $CaTiO_3$; the solid solutions are also orthorhombic; however, in the presence of $CaTiO_3$ solid solution with perovskite type compounds with a different symmetry, structural rearrangement may take place. Perovskites represented by the $A^{2+}B^{4+}O_3$, $A^{+}B^{5+}O_3$ and $A^{3+}B^{3+}O_3$ solid solutions frequently occur as accessory minerals in many silica-undersaturated rocks, both igneous and metamorphic. It was found that natural perovskites possess a high capacity for retaining uranium, thorium and products of their decay;[223] therefore, these perovskites are promising for actinide immobilization. The principal isomorphous substitutions in perovskites are the following:

$$Ca^{2+} \rightarrow Sr^{2+} \quad (17)$$

$$Ca^{2+} + Ti^{4+} \rightarrow (TR)^{3+} + Al^{3+}(Ti^{3+}, Fe^{3+}) \quad (18)$$

$$Ca^{2+} \rightarrow An^{4+} + \square(\text{vacancy}) \quad (19)$$

Perovskite is the basic phase for immobilization of strontium, light and medium REE, trivalent actinides and sodium.[25] In zirconolite–perovskite systems, REE are mainly incorporated into perovskite, the distribution coefficient in favour of perovskite decreases from ~12 for Ce^{3+} to ~2 for Gd^{3+} (Refs 224–226). The actinide cations (Pu^{3+}, Am^{3+} and Cm^{3+}) have radii close to those of light REE (Ce, Nd, Sm)$^{3+}$ and are expected to show a similar crystal chemical behaviour.

Among the known compounds of the perovskite family, of most interest are $PuAlO_3$, $AmAlO_3$, $CmAlO_3$, $CmFeO_3$ and $BaCmO_3$. A structural analogue of $GdFeO_3$ is $CmFeO_3$,[24] but little is known about its properties. More is known about $CmAlO_3$: it becomes amorphous after a dose of 1.4×10^{18} (α-decays) g^{-1} (Ref. 227). The structure is restored after annealing at 1000 °C for 30 min. Leaching of calcium and curium from perovskite ceramic, according to MCC-1 test data, followed an intricate dependence on the α-dose and duration. The highest leaching rates observed after 25 days were 5–8 g m^{-2} day^{-1} for curium and 8–10 g m^{-2} day^{-1} for calcium at doses of $(1.6–4.0) \times 10^{17}$ (α-decays) g^{-1} (Ref. 228).

Numerous studies have been devoted to natural and actinide-doped perovskites and perovskite ceramics. In natural perovskites that have accumulated 2.6×10^{18} (α-decays) g^{-1}, no signs of transition to amorphous state were detected.[229,230]

The $Nd_{0.5}Sm_{0.4592}{}^{244}Cm_{0.0285}Cm_{0.0032}Am_{0.0002}Pu_{0.0067}AlO_3$, synthetic perovskite, containing 3 mass % ^{244}Cm transformed to the metamict state. The curium leaching rate (MCC-1 test) was 6.8×10^{-3} g m^{-2} day^{-1} for the initial sample and increased to 1.7×10^{-1} g m^{-2} day^{-1}, *i.e.*, 25-fold, after amorphization; the leaching rates of Nd, Sm and Al increased to a lesser extent — approximately by an order of magnitude.[231]

The perovskite samples obtained by cold pressing and sintering were irradiated with fast neutrons in a reactor.[52,232] At a maximum dose of 2.6×10^{24} n m^{-2} (or 0.7 dpa), which corresponds to 8×10^{18} (α-decays) g^{-1}, the volume has increased by 6% and, according to X-ray powder diffraction data, no amorphization has taken place. Analogous results were obtained[233] for ^{238}Pu-doped $CaTiO_3$. Subsequently, it was found[234] for $CaTiO_3$ irradiated with fast neutrons that at a fluence of 2.2×10^{24} n m^{-2}, the perovskite remained largely crystalline. In a study of several natural perovskite samples, the degree of their radiation damage depended on the thorium and uranium oxide contents. The perovskite grains containing 1.4 mass %–3.1 mass % ThO_2 that accumulated $(0.3–0.6) \times 10^{19}$ (α-decays) g^{-1} were slightly damaged, while grains containing 6 mass % ThO_2 after a dose of $(0.8–1.2) \times 10^{19}$ (α-decays) g^{-1} were already substantially amorphous. The D_c value was estimated as $(3–6) \times 10^{19}$ (α-decays) g^{-1} (Ref. 235).

According to Karioris *et al.*,[236] $CaTiO_3$ readily amorphizes upon irradiation with Ar^+ ions (3 MeV). Some other publications[237,238] are devoted to the dependence of perovskite D_c on the chemical composition and the presence of cation vacancies. Smith *et al.*[237] found that on irradiation with Kr^+ ions (800 keV), the D_c value decreases in the series

$$SrTiO_3 > CaTiO_3 > BaTiO_3 > KNbO_3 > KTaO_3 \quad (20)$$

and that transition from the cubic to tetragonal structure affects D_c only slightly. The perovskites $CaTiO_3$, $(Na,TR,Ca)TiO_3$ (a natural perovskite called loparite), $NaNbO_3$, $Sr_{0.7}La_{0.2}TiO_3$, $Sr_{0.4}La_{0.4}TiO_3$, $Sr_{0.1}La_{0.6}TiO_3$ and $La_{0.67}TiO_3$ were irradiated with Kr^+ ions (1.5 MeV). As the sodium concentration increased, the critical dose decreased from $\sim 9.2 \times 10^{18}$ to $\sim 3.4 \times 10^{18}$ ions m^{-2}; with increasing the number of cation vacancies, D_c decreased from $> 170 \times 10^{18}$ ions m^{-2} for $Sr_{0.7}La_{0.2}TiO_3$ to 2.4×10^{18} ions m^{-2} for $La_{0.67}TiO_3$. A comparison of the radiation resistances of lanthanum titanates La_2TiO_5 or $La_{0.67}TiO_3$ with the perovskite structure and monoclinic $La_2Ti_2O_7$ showed that disordered systems are more stable than the ordered ones, owing to higher recombination rate

of defects. In terms of the radiation resistance, the perovskite $La_{0.67}TiO_3$ (T_c = 852 K) occupies an intermediate position between La_2TiO_5 (T_c = 840 K) and $La_2Ti_2O_7$ (T_c = 1027 K).[238,239] A number of publications consider the chemical stability of the perovskite ceramics based on $LnAlO_3$ and $LnFeO_3$ doped with ^{90}Sr, ^{147}Pm, ^{238}U, ^{238}Pu and ^{241}Am.[224,226,240,241] The ^{90}Sr, ^{147}Pm, ^{238}Pu and ^{241}Am leaching rates measured in a Soxhlet apparatus at 95 °C were $\sim 10^{-4}$ g m^{-2} day^{-1}, while the leaching rate of uranium was two orders of magnitude higher. Probably, uranium occurred in the tetravalent state and was not incorporated in the perovskite structure, unlike divalent strontium and trivalent promethium, plutonium and americium.

III.3. Garnet structure aluminates and ferrites

The garnet structure $^{VIII}A_3{}^{VI}B_2[TO_4]_3$ (space group *Ia3d*, Z = 8) is composed of alternating TO_4 tetrahedra and BO_6 octahedra connected into a 3D framework by sharing vertices.[3,242,243] The cavities accommodate eight-coordinate cations (Fig. 9). The garnet structure can be inherent in silicates, aluminates, ferrites, germanates and vanadates. The A sites are occupied by divalent (Ca, Mn, Fe) and trivalent (REE) elements. The rare earth elements can be completely or partly replaced by actinides. The B sites may be occupied by di- and trivalent (Fe, Al, Ga, Cr, Mn, In, Sc, Co), tetravalent (Zr, Ti, Sn, Ru) and pentavalent (Sb, V, Nb, Ta, Pa,) elements; and the T sites accommodate tetravalent (Si, Ge, Sn), trivalent (Al, Ga, Fe) and pentavalent (P, V, As) elements. Garnet type solid solutions containing REE are formed in the following series:

— $(TR,M^{III})_3(M^{III})_5O_{12}$;
— $(TR,M^{II})_3(M^{III}M^{IV})_5O_{12}$;
— $(TR,M^{II})_3(M^{I}M^{III}M^{IV})_5O_{12}$.

The natural garnets — silicates — usually contain less than 3 mass % REE and less than 1 mass % actinides[242] (however, recently, a specimen with 27 mass % U was found[244]). The TR–Al–Ga garnets capable of incorporating up to 4 mass % – 6 mass % UO_2 and PuO_2 were synthesized.[245–247] From crystal chemical considerations, for inserting tri- and tetravalent actinides into the A site of a garnet, it is necessary to place larger ions with lower charge into the B and T sites. The largest triply charged cation able to occupy these sites is Fe^{3+}. The garnets $(Ca_2Ce)(ZrFe)Fe_3O_{12}$, $(Ca_2Th)(ZrFe)Fe_3O_{12}$ and $(Ca_2Ce)Zr_2Fe_3O_{12}$ were synthesized and tested by the MCC-2 procedure. The leaching rates in water were $\sim 3\times10^{-5}$ g m^{-2} day^{-1} for Gd and $\sim 10^{-6}$ g m^{-2} day^{-1} for Ce and Th, while in an acidic solution (0.01 M HCl), the values were $\sim 10^{-3}$ g m^{-2} day^{-1} for Gd and Th and $\sim 2\times10^{-1}$ g m^{-2} day^{-1} for Ce.[248] The true incorporation of uranium, plutonium and neptunium into garnets was confirmed by *ab initio* calculations of the electronic structure using density functional theory.[249–251]

The radiation resistance of the garnets $Y_{2.88}Cm_{0.12}Al_5O_{12}$ and $(Ca_{1.5}Gd_{0.91}Cm_{0.09}Th_{0.5})ZrFe_4O_{12}$ was determined using Kr^+ ion (1 MeV) irradiation and incorporation of ^{244}Cm.[201,252–255] For ion irradiated garnets, the dose needed for amorphization was D_c = 0.15–0.20 dpa and the critical temperature T_c = 550 °C. The ^{244}Cm-doped ferrite garnet became amorphous at a dose of 0.15–0.17 dpa; the aluminate garnet was fully amorphous at a dose of 0.4 dpa.[255] In terms of the radiation resistance, aluminate garnets are not inferior to zirconolite and are superior to the titanate pyrochlore. High stability of garnets towards aqueous solutions makes them suitable as hosts for actinides.

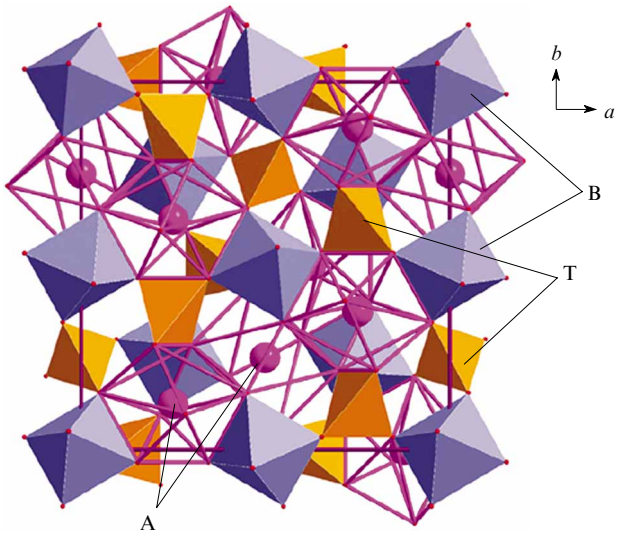


Figure 9. Garnet structure $^{VIII}A_3{}^{VI}B_2[TO_4]_3$ (Ref. 243). The TO_4 tetrahedra, the BO_6 octahedra and cations with C.N. = 8 are designated by letters T, B and A, respectively.

III.4. Ceramics based on other congruently melting phases

Among the phases, potentially suitable for immobilization of actinides that can be obtained by melt crystallization, noteworthy are some titanates (brannerite), titanosilicates (sphene, perrierite–chevkinite), silicates and silicophosphates (britholite, nagelschmidtite).

Brannerite (the ideal formula is $^{VI}A^{VI}B_2O_6$) is a complex oxide, mainly uranium and titanium oxide, with a monoclinic lattice (space group *C*2/*m*, *Z* = 2) and the unit cell parameters: *a* = 9.8123(15), *b* = 3.7697(6), *c* = 6.9253(9) Å, β = 118.957(6)° (Ref. 256). The brannerite structure is composed of layers connected by edges of titanium octahedra linked by columns of uranium octahedra (Fig. 10).[138] The octahedral oxygen environment is typical of Ti^{4+} with the radius of 0.605 Å,[257] whereas the larger U^{4+} cation (^{VIII}r = 1.00 Å) usually has C.N. ⩾ 8 and is less prone to form the octahedral environment (^{VI}r = 0.89 Å). This implies that in brannerite, uranium occurs in higher oxidation states, as was confirmed experimentally.[258–264] Uranium in +6 (^{VI}r = 0.73 Å) and +5 (^{VI}r = 0.76 Å) oxidation states tends to form the octahedral environment. The structures of Ce^{4+} (^{VI}r = 0.87 Å) and Pu^{4+} (^{VI}r = 0.86 Å) titanates are similar. These details determine the high role of exchange in the brannerite structures involving doubly and triply charged alkali, alkaline earth, transition and rare earth cations and quadruply charged cerium and thorium cations (^{VI}r = 0.94 Å) in natural minerals and plutonium in synthetic samples.

Although brannerite has often been found as a minor phase in various titanates,[265–272] it has not been considered in the literature as a host phase for immobilization of actinides (except for one publication[28]), although it differs little in its characteristics from other candidate actinide phases. In particular, the leaching rate of uranium from the brannerite ceramic at 90 °C and pH 8

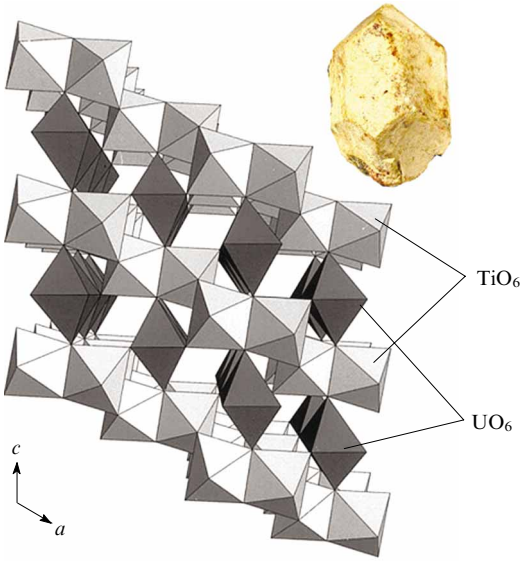


Figure 10. Brannerite structure; view along the [0$\bar{1}$0] direction.[138] Layers of the TiO_6 octahedra are connected by columns of UO_6 octahedra. The image in the upper right corner is a photograph of the 61 × 42 × 37 mm brannerite crystal from pegmatites.

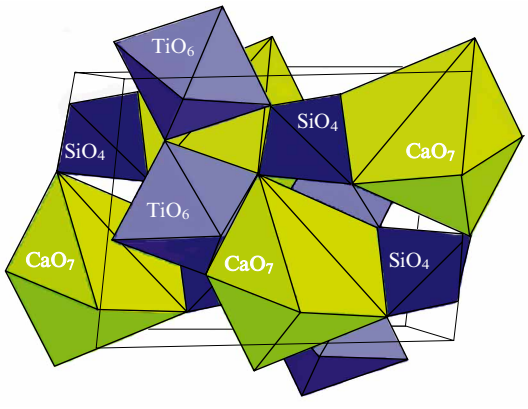


Figure 11. Sphene (titanite) structure (http://cryst.geol.msu.ru/courses/crchem/titanit.pdf). The SiO_4 tetrahedra are connected by monocapped CaO_7 octahedra and TiO_6 octahedra.

($<10^{-4}$ g m^{-2} day^{-1}) is approximately an order of magnitude higher than that from pyrochlore and zirconolite ceramics and three order of magnitude lower than that from glasses.[273] Under leaching experiment conditions (20–50 °C and pH 2–12), the brannerite dissolution rate was 10^{-3}–10^{-5} g m^{-2} day^{-1} (Ref. 274). The relatively high chemical stability of brannerite towards acidic and alkaline aqueous solutions has been demonstrated in a number of papers.[12, 275–282]

The radiation resistance of brannerite is somewhat lower than that of a number of other titanate phases (zirconolite, pyrochlore, murataite); most of samples occurring in nature are completely or partly metamict.[28, 283] Upon irradiation with accelerated krypton ions (1–1.5 MeV), the critical dose for amorphization at room temperature was ~0.1 dpa for cerium- and thorium-containing brannerite and ~0.15 dpa for uranium-containing brannerite.[284, 285] In ceramics for plutonium immobilization doped with 10 mass % $^{238}PuO_2$, brannerite also showed the lowest radiation resistance among other titanate phases (zirconolite, pyrochlore).[113, 286]

The crystal structure of sphene (titanite) of the ideal composition of $CaTiSiO_5$ belongs to space group $C2/c$ with the following unit cell parameters: $a = 6.56$, $b = 8.72$, $c = 7.44$ Å, $\beta = 119°43'$. Sphene is frequently encountered as an accessory mineral in intrusive rocks (syenite, feldspathoid syenites, monzonites, tonalites, granodiorites), pegmatites (as a rule, granitic and nepheline-syenites), extrusive rocks (especially in phonolites), metamorphic rocks (marble, skarn, granite gneiss, slates and amphibolites), Alpine veins (with adular, smoky quartz, chlorite and apatite) and heavy sand and sandstone fractions.[287, 288] The sphene structure is shown in Fig. 11.

In natural sphene, isomorphous substitutions of Na^+, Ce^{3+}, La^{3+}, Y^{3+}, Th^{4+} for calcium, Fe^{3+}, Al^{3+}, Nb^{5+} for titanium, and HO^- and F^- for oxygen are possible. The presence of small amounts of Fe^{2+}, Mn^{2+}, Mg^{2+}, Cr^{3+}, Sn^{2+} and traces of Zr^{4+}, Pb^{2+}, Sr^{2+}, V^{5+}, Cu^{2+}, Ga^{3+}, Ta^{5+} and Ba^{2+} is also possible. The content of ThO_2 can reach 0.28 mass % (Refs 289–292). Therefore, it was to be expected that, apart from alkali, alkaline earth and iron group elements, synthetic sphene would incorporate trivalent REE and actinides and some portion of tetravalent actinides. The measured isomorphous capacity of synthetic sphene towards U^{4+}, Pu^{4+}, Pu^{3+}, Hf^{4+} and Gd^{3+} [in atoms per formula units (afu)] is 0.02–0.05 (Ref. 215); or 0.07 (Ref. 290); 0.02, 0.05, 0.5 and 0.3 (Ref. 215); or 0.25 (Ref. 290), respectively. From this, it follows that sphene can be considered as a host phase for actinides and REE only when they are present in RW in relatively low concentrations; the preferred material for this purpose is glass ceramics consisting of sphene in an aluminosilicate matrix.

It was shown[291] that the sphene crystal phase is formed within the following ranges (Δ) of oxide contents:

Oxide	Na_2O	Al_2O_3	CaO	TiO_2	SiO_2
Δ (mol.%)	4.6–9.5	3.1–7.1	10.7–20.7	10.7–22.1	49.6–63.9

Relying on the investigation data, the following composition was chosen as the basic one

Oxide	Na_2O	Al_2O_3	CaO	TiO_2	SiO_2
Content (mol.%)	6.6	5.1	16.5	14.8	57.0

At 1300–1400 °C, this is a liquid melt that forms liquating glass on cooling, while on subsequent heating in the range of 950–1050 °C for 1 h, it crystallizes to give glass ceramics containing ~40 vol.% sphene (the only crystalline phase).[291]

By special investigations on doping of the basic composition with ions simulating REE and actinides present in RW, it was shown that with increasing the concentration of the additional oxides from 0 mol.% to 4 mol.%, the composition of the crystalline component becomes more complicated: at low contents of REE oxides (1 mol.%–2 mol.%), perovskite [(Ca,Na,TR)TiO_3], apatite [$Ca(TR)_8(SiO_4)_6O_{2-x}$], pyrochlore [$(TR,Ca,Ce^{4+})_2Ti_2O_{7-x}$] and fluorite ($TRO_{2-x}$) phases appear apart from sphene, and at higher concentrations of these oxides (3 mol.%–4 mol.%), sphene may not crystal-

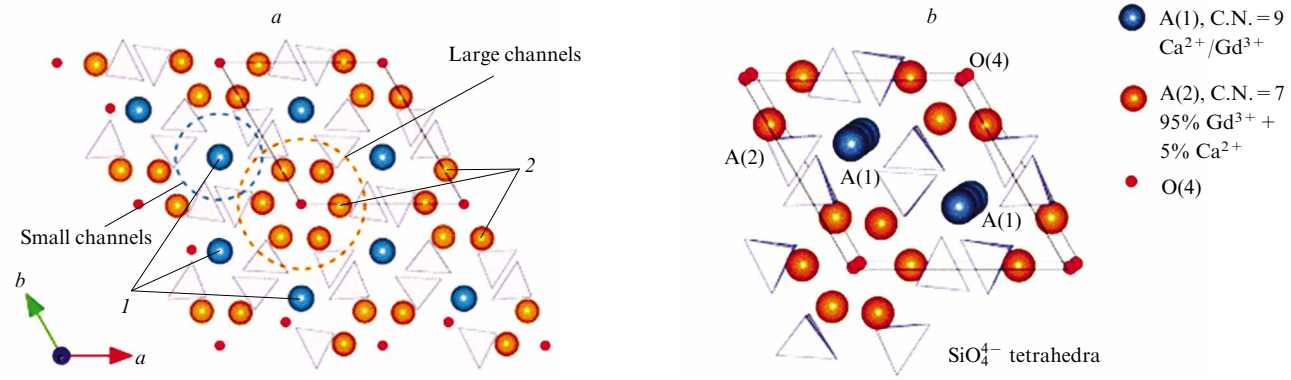


Figure 12. Crystal structure of stoichiometric REE apatites $(Ca,TR)_{10}(SiO_4)_6O_2$ (Refs 91, 302).
(*a*) View along the [001] direction; (*1*) A cations [$(TR)^{3+}$, Ca^{2+} or cation vacancies]; (*2*) oxygen anions; vacancies and interstitial oxygen ions are not shown; (*b*) positions of two types of cation [A(1) and A(2)] and oxygen [O(4)] sites.

lize at all, only the above-listed new phases being isolated.[292] All these phases are also able to accumulate actinides.

A study of the distribution of RW component ions between the sphene and residual glass phases showed that REE and Ni^{2+} ions are mainly concentrated in sphene (the distribution coefficients range from 2 to 10), whereas U^{6+} and Cs^+ ions are mainly accumulated in the glass phase (especially Cs^+; the distribution coefficient in favour of glass is ~40). The Sr^{2+} ions are distributed between sphene and the glass phase in approximately equal amounts. The leaching rates of RW elements from the sphene glass ceramic are lower than those from borosilicate glasses and slightly higher than those from the Synroc ceramic.[291]

Although sphene is inferior to titanate phases in the radiation resistance, in view of low actinide content, sphene can be regarded as an acceptable host phase for immobilizing actinides in glass ceramics. The natural samples that have accumulated $>5\times10^{18}$ (α-decays) g^{-1} were metamict.[293, 294] This is approximately equal to the critical dose of amorphization upon irradiation with argon ions (3 MeV). The rate of sphene dissolution after metamict transformation increased not more than 5-fold with respect to that for the initial samples.[295] Upon irradiation with accelerated electrons with energy of 200 keV, sphene remained in the crystalline state at a fluence of $>2\times10^{27}$ e m^{-2} (Ref. 296). After irradiation with bismuth ions with energy of 280 keV up to a fluence of 6×10^{11} m^{-2}, the thickness of the metamict layer did not exceed 100 nm.[297]

In some cases, in particular, on cold crucible induction melting of sphene glass ceramics, a monoclinic phase with $a = 13.58$, $b = 5.79$, $c = 22.4$ Å, $\beta = 102°$ crystallized from the solution.[298–300] These parameters correspond to the unit cell dimensions of natural perrierite (chevkinite) group minerals with the ideal formula $Fe_2(La,Ce)_4Ti_3[Si_2O_7]_2O_8$, monoclinic symmetry, space group $C2/m$, $Z = 2$ and lattice parameters $a = 13.61$, $b = 5.63$, $c = 13.63$ Å, $\beta = 113°28'$ for perrierite and $a = 13.56$, $b = 5.82$, $c = 11.21$ Å, $\beta = 100°45'$ for chevkinite. According to Ito,[301] the general formula of sphene group minerals is $A_4(BC)_5Si_4O_{22}$; the A sites are occupied by large cations — Na^+, Ca^{2+}, Sr^{2+}, $(TR)^{3+}$, Th^{4+} and U^{4+}; the B sites contain Mg^{2+}, Fe^{2+} and Mn^{2+} ions; and the C sites contain Nb^{5+}, Ti^{4+}, Al^{3+} and Fe^{3+}. In conformity with its composition, the formula of the synthetic perrierite-like phase can be written as $[(Ca,Sr,Na)_2Zr_2]_4(Ti,Al)_5(Si,Al)_4O_{22}$. This phase could also incorporate minor amounts of actinide and REE; however, no studies of this type were carried out.

Currently, the interest in titanosilicate phases as actinide hosts is moderate because of their low isomorphous capacity towards actinides and relatively low chemical stability and radiation resistance. Nevertheless, glass ceramics containing these phases can be used for processing actinide-containing intermediate- and low-level wastes.¶

Apatite has the general formula $^{IX-VII}A_{10}{}^{IV}B_6O_{24}X_2$ (space group $P6_3/m$, $Z = 1$), A = Ca, TR, Th, Al, Fe, Mn, Mg, Na or K; B = Si, P, B, F or Al; X = O, OH or F.[302] The structure of the apatite $Ca_{10}(PO_4)_6O$ or its rare earth analogue — britholite $(Ca,TR)_{10}(SiO_4)_6O_2$ — is composed of PO_4 and/or SiO_4 tetrahedra linking single or triple columns of the Ca^{2+} ions, which are seven- or nine-coordinate with respect to oxygen (Fig. 12).[91, 302] Extensive isomorphous substitutions are possible both in the cationic and anionic sublattices:

$$Ca^{2+} \rightarrow M^{2+} \quad (21)$$

$$Ca^{2+} + P^{5+} \rightarrow (TR,An)^{3+} + Si^{4+} \quad (22)$$

$$2\,(OH,F,Cl)^- \rightarrow O^{2-}, CO_3^{2-}, SO_4^{2-} \quad (23)$$

Usually, researchers deal with the solid solutions $Ca_{4-x}(TR)_{6-x}SiO_4)_{6-y}(PO_4)_yO_2$.[24, 28] In natural apatites, the content of actinides, mainly thorium, does not exceed 1% but actinides are incorporated into the lattice of synthetic britholites more easily and the uranium content in them can reach 0.5 afu.

Data on the radiation resistance of phases with the apatite structure published up to 1997 were summarized by Ewing *et al.*[126] and the data published up to 2007 were surveyed by Yudintsev *et al.*[29] Below we consider only some principal results. The solid solution phases $Ca_{4-x}(TR)_{6-x}(SiO_4)_{6-y}(PO_4)_yO_2$ doped with ^{244}Cm were transformed into the amorphous state on exposure to α-radiation. The same was observed for $Ca_{10}(PO_4)_6F_2$ and $Ca_2La_8(SiO_4)_6O_2$ and for britholites of intricate composi-

¶ See, for example, the paper by A S Aloy, Yu A Barbanel', A V Trofimenko *Izv. Vyssh. Uchebn. Zaved., Yadernaya Energetika* (1) 28 (2013).

tion irradiated with Kr^+ ions with energy of 1 and 1.5 MeV and Xe^+ ions with energy of 1.5 MeV. The D_c value at 300 K was ~0.4 dpa for $Ca_2La_8(SiO_4)_6O_2$ and 0.15 dpa for complex britholites. Natural minerals with elevated contents of REE and silica, which proved to be partially or completely metamict, were also found. For these materials, D_c was more than 1 dpa.

For the ^{244}Cm-doped $Ca_2La_8(SiO_4)_6O_2$ phase, amorphization mechanism was found to be the same as for other crystalline phases. The dose required for complete amorphization of $Ca_2La_8(SiO_4)_6O_2$ does not depend on the energy spectrum of recoil nuclei at low temperature (< 15 K) and increases with temperature rise in two stages upon irradiation with both Ne^+ ions (0.8 MeV) and Kr^+ ions (1.5 MeV). The value $D_c = 0.3-0.5$ dpa for heavier Kr^+ ions below room temperature is close to the value of 0.4 dpa, which was determined upon complete amorphization of ^{244}Cm-doped $Ca_2La_8(SiO_4)_6O_2$ at room temperature. Utsonomiya *et al.*[303] determined the critical amorphization temperatures for two synthetic britholite samples irradiated with accelerated Kr^+ and Xe^+ ions (1–1.5 MeV), which were 880–1010 K. The subsequent electron irradiation at a dose rate of 1.07×10^{25} m^{-2} s^{-1} up to absorbed dose of 6.2×10^{13} Gy induced recrystallization, similarly to what was observed in phosphate apatites.

The compounds $Cm_{9.33}\square_{0.67}(SiO_4)_6O_2$ and $Cm_8(SiO_4)_6$ also belong to the apatite structural type. In the former compound, cation vacancies can be occupied by alkaline earth metal ions. Both compounds crystallize in the hexagonal system and are stable in air at room temperature.[304]

Britholite type phases and nagelschmidtite type silicophosphates are often present in glass ceramics for immobilization of radioactive phosphate slags, in particular, organic and mixed RW incinerator slags.[305–317] The nagelschmidtite $Ca_7(PO_4)_2(SiO_4)_2$ is a β-whitlockite–larnite solid solution phase [$Ca_3(PO_4)_2-Ca_2SiO_4$] with a hexagonal lattice (a = 5.38, c = 7.1 Å). Initially, this mineral was detected in the Thomas slag,[318, 319] and later it was found in nature.[320, 321] The nagelschmidtite structural model proposed by Sugiyama *et al.*[322] implies the presence of calcium ion and Ca–T layers (T are SiO_4 and PO_4 tetrahedra) similar to the layers present in the α-Ca_2SiO_4 structure. The vacant calcium sites are ordered in the Ca–T layers upon SiO_4 and PO_4 substitution. The arrangement of TO_4 units is similar to the arrangement found previously in the structures of Ca_2SiO_4 varieties. Neither synthetic nor known natural samples contain actinides. However, like in apatites, in the nagelschmidtite structure, isomorphous substitution is possible in which Ca^{2+} ions are replaced by other doubly charged ions

$$Ca^{2+} \rightarrow M^{2+} \quad (24)$$

or singly and triply charged ions

$$2\,Ca^{2+} \rightarrow M^{+} + M^{3+} \quad (25)$$

where $M^{3+} = Al^{3+}$, Fe^{3+}, $(TR)^{3+}$, An^{3+}, or

$$2\,Ca^{2+} \rightarrow M^{4+} + \square\ \text{(vacancy)} \quad (26)$$

where $M^{4+} = Ce^{4+}$, Pr^{4+}, An^{4+}. In particular, there is the synthetic orthorhombic phase $Na_2Ca_3Al_2(PO_4)_2(SiO_4)_2$ in which substitution takes place according to the second above-presented pattern [chart (25)].[323] A similar composition was found for the nagelschmidtite crystals that are isolated in slag-containing glass ceramics, but their small size (< 1 μm) precluded determination of the exact composition. The nagelschmidtite structure is also inherent in $Ca_5Na_2(PO_4)_4$ (hexagonal unit cell, space group $P6_3mc$, a = 10.4, c = 21.71 Å, Z = 6).[324]

Back in early studies,[305–308] it was noted that when the nagelschmidtite phase is present in glass ceramics for immobilization of actinide-containing slags, the leaching rate of actinides decreases by at least an order of magnitude compared with the leaching rate from homogeneous glass, presumably, owing to their incorporation into nagelschmidtite. Like sphene and perrierite, nagelschmidtite can hardly be considered as a candidate for actinide immobilization; however, being present in glass ceramics used for immobilization of actinide-containing intermediate- and low-level wastes, it could efficiently concentrate actinides and thus their leaching could be markedly suppressed.

IV. Synthesis of high-level waste forms and problems of their manufacturing processes

IV.1. Processes using sintering

Titanates, zirconates, aluminates and ferrites have, as a rule, high melting points (> 1500 °C);[23, 24] their synthesis by solid-phase sintering also requires high temperature. The traditional method for the manufacture of ceramics by wet ceramic paste moulding and annealing is inapplicable because of both high risk of leakage of radioactive liquids and insufficient quality of the final product. The solid-phase synthesis of actinide and REE refractory phases, including titanates and titanate zirconates, is often carried out by cold pressing and sintering and, more rarely, by hot uniaxial or isostatic pressing. For manufacturing a homogeneous product with completed phase-formation reactions by these methods, a thorough preparation of the feed formulation is required (see, for example, the book by Ringwood *et al.*[25]), the product quality being dependent on the feed particle size and uniformity and on whether or not the particles occur in the reactive form. Special methods are used to provide for a better contact between the particles such as ultrafine grinding using mechanoactivating devices, co-precipitation from solutions or sol–gel process with alkoxides as well as spark plasma sintering. In the cold pressing process, sintering is carried out at temperatures below 1600 °C. The obtained product is ground, pressed again into pellets and sintered. The process is repeated for up to three times but even in this case, the most refractory products are not quire homogeneous.[82] In the case of hot uniaxial and isostatic pressing, a higher quality product is formed with a density of up to 98%–99% of the theoretical value.

Generally, the techniques using pressing and sintering (especially under pressure) are of low efficiency: they require long-term heating and accurate implementation of all process operations. Nevertheless, the cold pressing and sintering technique is used most often to prepare samples in the laboratory; hot uniaxial and isostatic pressing are also used, and cold crucible induction melting is used more rarely. The Australian Nuclear Science and Technology Organisation (ANSTO) has a demonstration facility with a hot uniaxial pressing unit for the production of Synroc ceramics.[25] A cold pressing and sintering unit operated at the Lawrence Livermore National Laboratory (USA) for immobilization of surplus weapons-grade plutonium.[325]

Later, the use of hot isostatic pressing for processing of wastes accumulated at the Idaho National Laboratory (USA) was considered.[326] All these units operated on simulated HLW and were not used in industry. The only unit put into industrial operation is the hot isostatic pressing plant for the processing of high- and intermediate-level wastes from ^{99}Mo production in Australia.[327]

The spark plasma sintering technique is based on very fast heating of the sample and the mould by successive millisecond high-power direct-current pulses.[328] The spark plasma sintering serves for the production of engineering ceramics;[329–331] since recently, it has been used to synthesize HLW and actinide waste forms.[332–336] The key advantages of this method include short process time and high (close to theoretical) density of the obtained material.

IV.2. Melting techniques for the manufacture of waste forms for actinides

The techniques that include the formation and subsequent cooling of a primary melt are successfully used for vitrification of high- and intermediate-level wastes both in Russia and abroad — in France, USA, UK, Germany, Japan, India and South Korea.[1] However, the glass melting temperatures, namely, from ~900–1000 °C for the phosphate glass in Russia to ~1100–1200 °C for the borosilicate glass in other countries, is below the temperature needed for melting of titanates, zirconates, aluminates and ferrites. Therefore, to obtain these phases by a melting process, special equipment is required. The following manufacturing processes have been proposed: high-frequency (10^5–10^7 Hz) cold crucible induction melting, microwave melting (10^8–10^9 Hz), plasma melting and self-propagating high-temperature synthesis.

Melting followed by spontaneous or oriented crystallization has been successfully used for the manufacture of glass ceramics of various compositions for immobilization of high- and intermediate-level wastes (see, for example, papers [1, 21, 31, 32, 291, 337]). These glass ceramics incorporated the crystalline phases of silicates and aluminosilicates (nepheline, pyroxene, orthosilicate), titanosilicates (sphene, perrierite, benitoite), silicophosphates (britholite, nagelschmidtite), titanates and titanate zirconates (pyrochlore, zirconolite, perovskite, hollandite, murataite, *etc.*), aluminates and ferrites (garnet, Al-perovskite, *etc.*). The first type of Synroc ceramic (Synroc-A consisting of zirconolite, perovskite, hollandite, kalsilite, leucite and celsian) was prepared by melting at 1300 °C followed by crystallization.[21, 22] Later, Synroc-B and Synroc-C types and other ceramic HLW forms were obtained from melts.[338–340] However, as noted above, most of the congruently melting phases for immobilization of actinides have high melting points (>1500 °C). Substantial progress in the development of melting technologies for the synthesis of these materials was achieved after adapting the cold crucible induction melting technique.[341–380]

IV.3. Cold crucible induction melting

The cold crucible operation principle (Fig. 13) is penetration of the electromagnetic field from an induction coil into the melt through gaps between water-cooled pipes or sections that form the cold crucible.[341–344] The penetration depth (δ) is related to the specific electrical resistance (ρ), relative magnetic permeability of the material (μ) and the current frequency (f) in the following way:

$$\delta = 503\sqrt{\frac{\rho}{\mu f}} \qquad (27)$$

for $\delta \leqslant d/2$, where d is the crucible diameter, $f = 10^5$–10^7 Hz, $\mu = 1$ (for non-magnetic materials).

The feed is non-conductive; therefore, it is heated to form the melt in such a volume starting from which the melting would subsequently be maintained spontaneously upon absorption of RF field energy.

The following advantages of cold crucible should be noted:

— the absence of a contact between the melt and the cold crucible walls: the melt and the walls are separated by a transient layer of partly melted feed (skull), which considerably increases the crucible service life in comparison with the service lives of other types of crucibles;

— the absence of internal electrodes in contact with the melt; this eliminates the issues of electrode replacement;

— active hydrodynamic regime implemented by eddy current stirring of the melt; this provides for high specific throughput;

— the possibility to reach high temperature (up to ~3000 °C);

— small dimensions and weight compared with these parameters of ceramic melters with similar throughputs; this facilitates the assembly, disassembly and removal of the crucible in the case of failure.

Cold crucible melting can be implemented for the formation of a block or for discharge. In the former case, the block is built up in the crucible, which is then disassembled. The latter process implies withdrawal of the melt from the crucible by lowering the crucible or the substrate. In the case of 'discharge' melting, a discharge device is envisaged; the melt is poured into canisters (similarly to vitrification in ceramic or metallic melters with heated walls).

As can be seen from relation (27), the penetration depth of the electromagnetic field into the melt and, hence, the crucible diameter depend on the current frequency. Low-duty and low-capacity laboratory units operate at 5–30 MHz frequencies (the frequencies allowed in Russia considering the radio interferences are 5.28, 13.81 and 27.12 MHz). In experimental units (test stands), the frequency of 1.76 MHz is used most often. For industrial HLW vitrification units considered as an alternative to electrical bath furnaces and metallic hot crucibles, <1 MHz frequencies were proposed;[345–347] this would increase the crucible diameter and the throughput (mass velocity of melt output). The most impressive progress along this line was made in France, in particular, owing to the use of additional devices and processes (stirrers, gas bubbling).[345, 346] For increasing the specific throughput, a frequency decrease is not very useful.[345] To solidify actinide HLW, high-output crucibles are not required, and a throughput of up to 10 kg h^{-1} is sufficient. Units operating at 1.76 MHz have been developed;[348–354] however, they are to be adjusted to radiochemical plant conditions.

An important feature of fluorite (tazheranite/phianite) or fluorite-related (pyrochlore, murataite, zirconolite) cubic phases is congruent melting and, hence, they can be synthesized by melt crystallization. This may give both a ceramic material, similar to cast stone materials, with a composition close to the nominal composition for these phases, and various glass ceramics based on them (this technique has

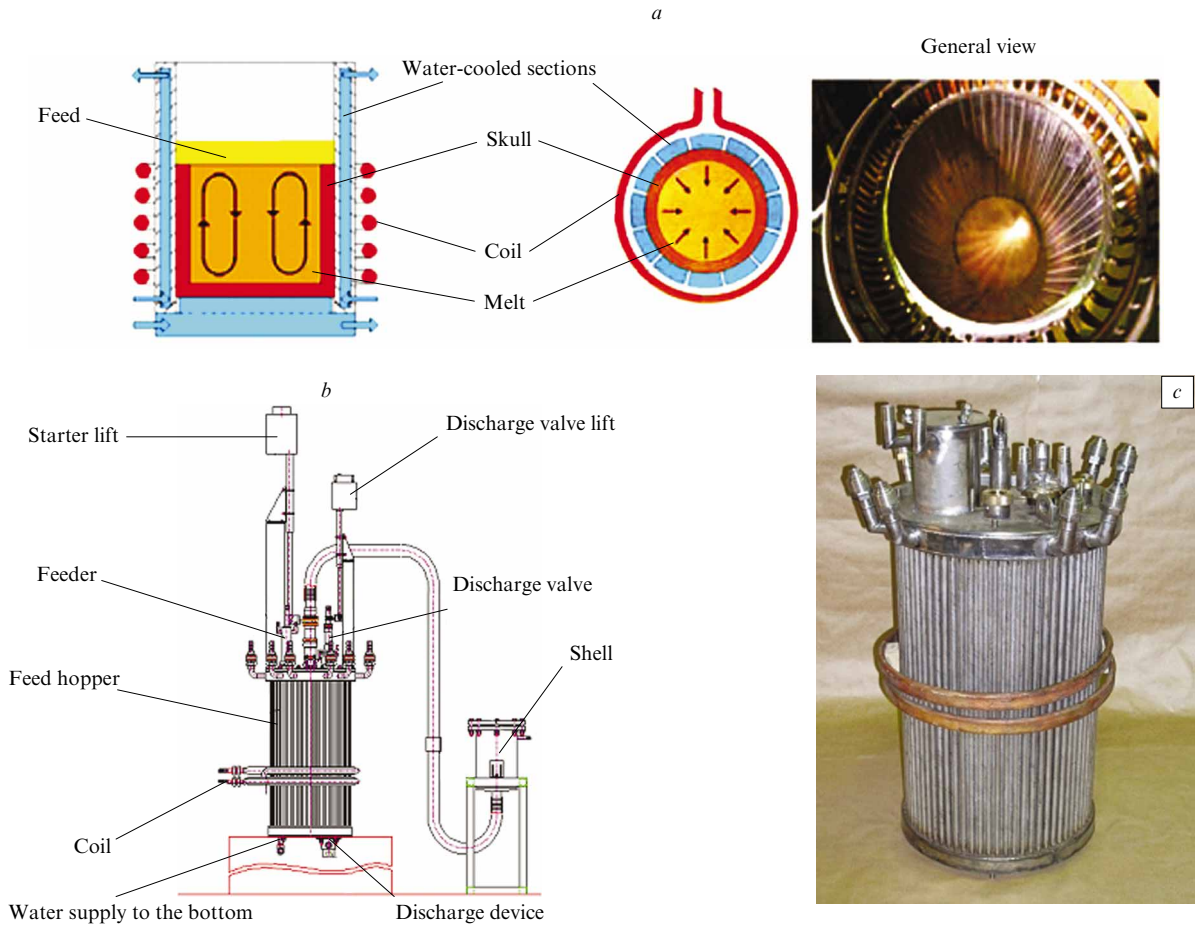


Figure 13. Diagram illustrating the operation principle (*a*), block diagram (*b*) and general view of a cold crucible with an internal diameter of ~430 mm (*c*) belonging to the Federal State Unitary Enterprise RADON.[348, 353]

found wide use for the production of materials for technology and jewelry [341 – 344, 355] and also ceramic HLW forms).[348 – 354, 356 – 380]

The hydrolytic stability of melted ceramics is approximately at the same level as that of cold-pressed and sintered materials. Exceptions are provided by melted murataite ceramics, from which the leaching rates of actinides, REE and zirconium are one to two orders of magnitude lower than those from the sintered materials owing to the zonal grain structure [27, 29, 158, 159, 163, 167, 169, 172, 173, 175, 187, 188, 273, 374, 376]).

Ceramic materials obtained by melting with subsequent crystallization, in particular, by cold crucible induction melting, have a number of differences from cold-pressed and sintered, hot uniaxially pressed and isostatically pressed ceramics. First, as has been already repeatedly noted, only congruently melting phases can be obtained from the melt.

Second, melting is usually carried out in air, *i.e.*, under oxidizing conditions. It is fairly difficult to arrange indifferent or, the more so, reducing conditions, unlike, for example, hot uniaxial and isostatic pressing techniques, in which the pressing chamber can be filled with any gas and/or a reducing agent can be added to the feed formulation, as in the synthesis of Synroc ceramics, where titanium powder is used.[25] As a result, the phase composition and distribution of some elements (including variable valence ones) between phases in melted ceramics differ from those in pressed samples.[359] The key problems are associated with the transition of some caesium, strontium and molybdenum into a powellite ($CaMoO_4$) type molybdate phase with relatively low chemical stability. There is no such problem with actinides, which are distributed between zirconolite and perovskite, depending on the oxidation state, in the Synroc ceramics.

Third, the cold crucible induction melting is inevitably accompanied by contamination of the melt with the crucible lining material, which is used to prevent the mixture from leaking out. Since the lining is often prepared from liquid glass, silica and sodium and/or potassium oxides can get into the melt, which results in the formation of a glassy phase.

Fourth, in all high-temperature processes, including melting, microwave and plasma melting, there appears a problem associated with component vaporization from the melt surface. In the cold crucible induction melting, this problem can be solved by forming a cold feed formulation cap on the top of the melt, which functions as an absorber; however, because of the active hydrodynamic conditions in the cold crucible, this cap is rather difficult to stabilize. In the synthesis of actinide-containing ceramics, this problem is insignificant, because most of actinide compounds we consider are non-volatile.

Finally, there exist the problem of shrinkage cavity upon the discharge of 'short' melts into containers (canisters). Due to fast formation of a solid crust on top of the melt in the container, the residual gases have no time to be released to the atmosphere and are accumulated under the crust forming cavities, which disrupt the homogeneity and decrease the density of the block.

IV.4. Microwave melting

The possibility of manufacturing glasses, crystalline compounds and multiphase ceramics by microwave heating was considered by researchers in Japan,[381,382] UK,[383–385] Russia,[269,386–390] and the USA.[391] As the key benefits of this way of heating, the following is considered:[386,387] high efficiency of microwave absorption by liquid wastes at different treatment stages (high performance); equipment reliability, simplicity, small size and repairability; the possibility of positioning the energy source outside the working zone; high throughput; and short process stabilization time. There are some bottlenecks preventing the industrial use of the process, namely, difficulty of attaining a uniform high-temperature heating of inhomogeneous feed formulations and coordination of the generator and reaction chamber operation. Most publications on the use of microwave heating are devoted to processing of liquid RW and only one paper[269] describes the synthesis of pyrochlore–brannerite ceramics and gives detailed characterization of the obtained product. Currently, the possibility of using microwave radiation for the synthesis of high-temperature crystalline compounds and multiphase ceramics remains problematic.

IV.5. Plasma melting

The first studies on the vitrification of RW in plasma reactors were accomplished in the early 1980s.[392–394] Subsequently, syntheses of some glassy crystalline and crystalline materials in plasma arc devices were reported.[395] The major effort was concentrated on the design of fully functional systems for the processing of solid RW and toxic wastes.[396–399] The seemingly obvious benefits of plasma heating (high temperature, intense heat and mass exchange) prove to be difficult to implement, as on contact of the plasma plume with the material being treated, heating starts from the surface, and the residence time of the material in flow type reactors is often too short for the phase formation to be completed. The completion of the batch processes and melt homogenization require long time, which sharply decreases the throughput. Apparently, combined techniques such as plasma reactor–cold crucible have better prospects.[400–402]

IV.6. Self-propagating high-temperature synthesis

The method of self-propagating high-temperature synthesis (SHS) is based on the utilization of the heat of exothermic redox reactions. The feed consisting of the major (working) compound, an oxidant and a reducing agent is thoroughly mixed, charged into the reactor and ignited on one end using a special device (igniting torch). The combustion front heated up to 2000–2500 °C moves along the reactor in several seconds and melts the material, which then crystallizes as the front moves along.[403] The short reaction time in the reaction front restricts the component loss *via* vaporization. For consolidation of the final product, the reactor can be equipped with a compacting device.

The first works on this subject date back to the 1960s.[404,405] Later, ceramics were obtained based on zirconolite, pyrochlore, perovskite, sphene, aluminium garnet and so on,[406–417] including those doped with plutonium, americium[411] and technetium,[414] and glassy materials for the immobilization of RW of complex composition, in particular, actinide-containing ones.[418–421]

Uncompacted porous and inhomogeneous SHS products contain the target phases and a metallic alloy. The additional compacting affords final products of acceptable quality; the leaching rate of REE (simulating actinides) from these products determined according to the Russian State Standard GOST R 52126-2003 is 10^{-3} g m^{-2} day^{-1} or lower.

A test SHS unit has now been constructed in a hot cell and is being tested using model solutions containing uranium, americium and other elements simulating HLW.[422] It is noteworthy that, despite the seeming simplicity of the process, the process flow diagram is difficult to implement, especially under conditions of a radiochemical plant; hence, the prospects of industrial use of the SHS are uncertain.

V. Conclusion

Actinide-containing titanates, zirconates, titanate zirconates, aluminates and ferrites that have the fluorite (tazheranite/phianite) and related (pyrochlore, murataite, zirconolite) structures and also the perovskite and garnet structures are promising for immobilization of HLW fractions (minor actinides and plutonium). Ceramics based on these phases have high chemical stability and, in some cases (fluorite and pyrochlore type zirconates and zirconolite), also high radiation resistance, which ensure their preservation for the periods required for the decay of long-lived radioactive elements to the natural background level (hundreds of thousands to millions of years). An important benefit of these phases is congruent melting, which allows them to be synthesized by melt crystallization. Of particular interest are melted ceramics based on murataite, more precisely, phases of the pyrochlore–murataite series. Owing to the zonal structure of grains with actinides being concentrated in the central parts, the leaching rates of actinides from these materials are very low even under dynamic conditions at elevated temperatures.

Nevertheless, some problems are still to be solved.[33] One of them is the stability of actinide solid solutions under self-radiation. As noted above, the metamict transformation proceeds through several stages of crystal lattice disordering. For instance, the pyrochlore lattice is transformed into a disordered pyrochlore lattice, then into fluorite lattice and, finally, the substance is transformed into an amorphous state. It is unknown whether or not a pyrochlore type solid solution would degrade upon transition to the fluorite structure with isolation of actinides as a separate phase and, if yes, how much time this would take. Other concerns are related to the mechanical self-destruction of actinide-containing ceramics and crystals as a result of self-irradiation (with potential formation of colloid particles). There has also been anxiety that the differential and anisotropic swelling of the lattice upon self-irradiation could induce micro- and macrocracking of coarse-grained polycrystalline materials; however, fast neutron bombardment experiments with Synroc-C samples obtained by cold crucible induction melting showed the absence of cracking; apparently, the

presence of pores provides certain relaxation of the differential swelling of the lattice.[423] Sintered ceramic pellets produced from phases of various structural types (pyrochlore, murataite, perovskite, garnet) containing ^{244}Cm also retained the shape and mechanical integrity after amorphization.[109, 186, 205, 252]

The chemical flexibility problem can also substantially affect the physicochemical and isolation properties of RW forms. Upon the radioactive decay of actinides and fission fragments, the daughter products are usually isotopes of the elements that form ions with a charge and radius differing from those of the parent element isotope; this may induce destabilization of the RW form — crystallization, mechanical destruction, change of thermophysical parameters and so on. For example, plutonium isotopes decay to give americium and neptunium, $^{137}Cs^{+}$ decays to $^{137}Ba^{2+}$, and the decay of $^{90}Sr^{2+}$ gives first $^{90}Y^{3+}$ and then $^{90}Zr^{4+}$, which have different radii and charges.

The selection of the optimal technique for ceramization of HLW and actinide wastes is still a pressing problem. In our opinion, the cold crucible induction melting is a promising strategy for the synthesis of such phases and ceramics based on them. The possibility of employing other approaches such as microwave melting, SHS and compaction by spark plasma sintering requires further evaluation.

The review was prepared within the framework of state order with financial support of the Federal Agency of Scientific Organizations (Subject Matter No. 0136-2014-001).

References

1. I N Bekman *Plutonii. Uchebnoe Posobie* (Plutonium. Tutorial) (Moscow: Izd. MGU, 2010)
2. S A Dmitriev, S V Stefanovsky *Obrashchenie s Radioaktivnymi Otkhodami* (Radioactive Waste Handling) (Moscow: Mendeleev University of Chemical Technology of Russia, 2000)
3. L H Baetslé, T Wakabayashi, S Sakurai, in *Proceedings of the GLOBAL 99 Conference. Nuclear Technology — Bridging the Millenia* (Jackson Hole, WY: American Nuclear Society, 1999) P. 354
4. S V Stefanovsky, A A Zherebtsov, S A Dmitriev *Fiz. Khim. Obrabotki Mater.* (2) 56 (2014)
5. S V Stefanovsky, A A Zherebtsov, S A Dmitriev *Fiz. Khim. Obrabotki Mater.* (3) 44 (2014)
6. W Sinclair, A E Ringwood *Geochem. J.* **15** 229 (1981)
7. R C Ewing, T J Headley *J. Nucl. Mater.* **119** 102 (1983)
8. R C Ewing *Catal. Mineral.* **39** 697 (2001)
9. G R Lumpkin, R C Ewing *Phys. Chem. Mineral.* **2** 16 (1988)
10. G R Lumpkin, R C Ewing *Am. Mineral.* **77** 179 (1992)
11. G R Lumpkin, K P Hart, P J McGlinn, T E Payne, R Giere, C T Williams *Radiochim. Acta* **66 – 67** 469 (1994)
12. G R Lumpkin *J. Nucl. Mater.* **289** 136 (2001)
13. N P Laverov, V I Velichkin, B I Omel'yanenko, S V Yudintsev *Geol. Ore Depos.* **45** 1 (2003) [*Geolog. Rudnykh Mestorozhdenii* **45** 3 (2003)]
14. J W Adams, T Botinelly, W N Sharp, K Robinson *Am. Mineral.* **59** 172 (1974)
15. A M Portnov, L S Dubakina, G K Krivokoneva *Dokl. Akad. Nauk. SSSR* **261** 741 (1981)
16. N P Laverov, I A Sobolev, S V Stefanovsky, S V Yudintsev, B I Omel'yanenko, B S Nikonov *Dokl. Earth Sci.* **363** 1104 (1998) [*Dokl. Akad. Nauk* **362** 670 (1998)]
17. A S Pakhomova, S V Krivovichev, S V Yudintsev, S V Stefanovsky *Z. Kristallogr.* **228** 151 (2013)
18. S Sunder, N H Miller, A M Duclos *MRS Proc.* **333** 631 (1994)
19. B E Burakov, E B Anderson, E M Pazukhin *Radiochim. Acta* **60** 149 (1993)
20. G J McCarthy, M T Davidson *Am. Ceram. Soc. Bull.* **54** 782 (1975)
21. A E Ringwood *Safe Disposal of High Level Nuclear Reactor Wastes: a New Strategy* (Canberra: ANU Press, 1978)
22. A E Ringwood, S E Kesson, N G Ware, W D Hibberson, A Major *Geochem. J.* **13** 141 (1979)
23. N A Toropov, V P Barzakovskii, V V Lapin, N N Kurtseva *Diagrammy Sostoyaniya Silikatnykh Sistem. Spravochnik. Dvoinye Sistemy* Vyp. 1 (Phase Diagrams of Silicate Systems. Handbook. Binary Systems, No. 1) (Leningrad: Nauka, 1969)
24. *Diagrammy Sostoyaniya Sistem Tugoplavkikh Oksidov. Spravochnik* Vyp. 5 (Phase Diagrams of Refractory Oxide Systems. Handbook, No. 5) (Leningrad: Nauka, 1991)
25. A E Ringwood, S E Kesson, K D Reeve, D M Levins, E J Ramm, in *Radioactive Waste Forms for the Future* (Eds W Lutze, R C Ewing) (Amsterdam: Elsevier, 1988) p. 233
26. W J Weber, R C Ewing, C I A Catlow, T DiazdelaRubia, L W Hobbs, C Kinoshita, H Matzke, A T Motta, M Nastasi, E K H Salje, E R Vance, S J Zinkle *J. Mater. Res.* **13** 1434 (1998)
27. S V Stefanovsky, S V Yudintsev, R Giere, G R Lumpkin, in *Energy, Waste and the Environment: a Geological Perspective* Vol.'236 (London: Geological Society, 2004) p. 37
28. G R Lumpkin *Elements* **2** 365 (2006)
29. S V Yudintsev, S V Stefanovsky, R C Ewing, in *Structural Chemistry of Inorganic Actinide Compounds* (Eds S V Krivovichev, P C Burns, I G Tananaev) (Amsterdam: Elsevier, 2007) p. 467
30. T Livshits, S Yudintsev, in *Minerals as Advanced Materials* (Ed. S V Krivovichev) (Berlin, Heidelberg: Springer, 2008)
31. D Caurant, P Loiseau, O Majérus, V Aubin-Chevaldonnet, I Bardez, A Quintas *Glasses, Glass-Ceramics and Ceramics for Immobilization of Highy Radioactive Nuclear Wastes* (New York: Nova Publishers, 2009)
32. I W Donald *Waste Immobilisation in Glass and Ceramic Based Hosts* (Chichester: Wiley, 2010)
33. B E Burakov, M Ojovan, W E Lee *Crystalline Materials for Actinide Immobilisation* (London: Imperial College Press, 2011)
34. R C Ewing, W J Weber, in *The Chemistry of the Actinide and Transactinide Elements* (Eds L R Morss, N M Edelstein, J Fuger) (Berlin, Heidelberg: Springer, 2011) p. 3813
35. *Waste Forms Technology and Performance: Final Report* (Washington, DC: Committee on Waste Forms Technology and Performance; National Research Council; The National Academies Press, 2011)
36. M I Ojovan, W E Lee *An Introduction to Nuclear Waste Immobilisation* (Amsterdam: Elsevier, 2014)
37. E R Vance, in *Comprehensive Nuclear Materials* Vol. 5 (Amsterdam: Elsevier, 2012) p. 485
38. *Nuclear Waste Materials Handbook (Test Methods)* (Washington, DC: USDOE Technical Information Center, 1981)
39. *Standard Test Methods for Determining Chemical Durability of Nuclear Waste Glasses: The Product Consistency Test (PCT). ASTM Standard C 1285-94* (Philadelphia, PA: ASTM, 1994)
40. E J Henley, E R Johnson *The Chemistry and Physics of High Energy Reactions* (University Press: Washington, DC, 1969)
41. K K Schwartz, Yu A Ekmanis *Dielektricheskie Materialy. Radiatsionnye Protsessy i Radiatsionnaya Stoikost'* (Dielectric Materials. Radiation Processes and Radiation Resistance) (Riga: Zinatne, 1989)
42. W J Weber, F P Roberts *Nucl. Technol.*, **60** 178 (1983)

43. L W Hobbs, F W Clinard Jr, S J Zinkle, R C Ewing *J. Nucl. Mater.* **216** 291 (1994)
44. R C Ewing, W J Weber, F W Clinard Jr *Prog. Nucl. Energy* **29** 63 (1995)
45. T Murakami, B C Chakoumakos, R C Ewing, G R Lumpkin, W J Weber *Am. Mineral.*, **76** 1510 (1991)
46. J F Ziegler, J P Biersack, U Littmark *The Stopping and Range of Ions in Solids* (New York: Pergamon Press, 1985)
47. K Scheffler, U Riege *Investigations on the Long-Term Radiation Stability of Borosilicate Glasses against Alpha-Emitters. Report KFK-2422, Karlsruhe, 1977*
48. R A Bonniaud, N R Jacquet-Francillon, C G Sombret, in *Scientific Basis for Nuclear Waste Management* Vol. 2 (New York, London: Plenum Press, 1980) p. 117
49. S V Stefanovsky, A G Ptashkin, S V Yudintsev, B F Myasoedov *MRS Proc.* **1444** 237 (2012)
50. S V Stefanovsky, S V Yudintsev, B F Myasoedov *Dokl. Earth Sci.* **447** 296 (2012) [*Dokl. Akad. Nauk* **447** 644 (2012)]
51. E S Prokin, V S Kuptsov, T N Ananina, E E Ermolaev, I D Kuznetsov *Radiokhimiya* **25** 530 (1983) [*Sov. Radiochem.* **25** 500 (1983)]
52. J L Woolfrey, K D Reeve, D J Cassidy *J. Nucl. Mater.* **108–109** 739 (1982)
53. E R Vance, K K S Pillay *Radiat. Effects Defects Solids* **62** 25 (1982)
54. M A Subramanian, G Aravamudan, G V S Rao *Prog. Solid State Chem.* **15** 55 (1983)
55. B C Chakoumakos, R C Ewing *MRS Proc.* **44** 641 (1985)
56. R C Ewing, W J Weber, J Lian *J. Appl. Phys.* **95** 5949 (2004)
57. V S Urusov, N I Organova, O V Karimova, S V Yudintsev, S V Stefanovsky *Dokl. Earth Sci.* **401** 319 (2005) [*Dokl. Akad. Nauk* **401** 226 (2005)]
58. S V Krivovichev, S V Yudintsev, V S Urusov, S V Stefanovsky, O V Karimova, N N Organova, in *Minerals as Advanced Materials II* (Ed. S V Krivovichev) (Heidelberg: Springer, 2011) P. 301
59. F Mazzi, R Munno *Am. Mineral.* **68** 262 (1983)
60. R Gieré, C T Williams, G R Lumpkin *Shweiz. Mineral. Petrogr. Mittelung.* **78** 433 (1998)
61. A F Wells *Structural Inorganic Chemistry* (3rd Ed.) (Oxford: Clarendon Press, 1962)
62. T Uehara, K Koto, F Kanamaru, H Horiuchi *Solid State Ionics* **22** 137 (1987)
63. T Moriga, A Yoshiasa, F Kanamaru, K Koto, M Yoshimura, S Somiya *Solid State Ionics* **31** 319 (1989)
64. P E Raison, R G Haire, T Sato, T Ogawa *MRS Proc.* **556** 3 (1998)
65. M J D Rushton, R W Grimes, C R Stanek, S Owens *J. Mater. Res.* **19** 1603 (2004)
66. R B Heimann, T T Vandergraaf *J. Mater. Sci. Lett.* **7** 583 (1988)
67. W L Gong, W Lutze, R C Ewing *MRS Proc.* **556** 63 (1999)
68. W L Gong, W Lutze, R C Ewing *J. Nucl. Mater.* **277** 239 (2000)
69. S Stefanovsky, S Dmitriev, A Zherebtsov, in *Plutonium Futures — the Science 2014, Las Vegas, NV, 2014* p. 249
70. J Lian, L M Wang, J Chen, R C Ewing, K V G Kutty *MRS Proc.* **713** 507 (2002)
71. L M Wang, S Zhu, S X Wang, R C Ewing *MRS Proc.* **663** 293 (2001)
72. T Yang, X Huang, Y Gao, C Wang, Y Zhang, J Xue, S Yan, Y Wang *J. Nucl. Mater.* **420** 430 (2012)
73. M A Pouchon, M Döbeli, C Degueldre, M Burghartz *J. Nucl. Mater.* **274** 61 (1999)
74. C Degueldre, Ch Hellwig *J. Nucl. Mater.* **320** 96 (2003)
75. C Degueldre, W Wiesenack *MRS Proc.,* **1104** (2008); DOI: http:dx.doi.org/10.1557/PROC-1104-NN03-01
76. B E Burakov, M A Yagovkina, M V Zamoryanskaya, A A Kitsay, V M Garbuzov, E B Anderson, A S Pankov *MRS Proc.* **807** 213 (2004)
77. B E Burakov, M A Yagovkina, M V Zamoryanskaya, V M Garbuzov, V A Zirlin, A A Kitsay *MRS Proc.* **1107** 381 (2008)
78. P M Martin, R C Belin, P J Valenza, A C Scheinost *J. Nucl. Mater.* **385** 126 (2009)
79. R C Belin, P M Martin, P J Valenza, A C Scheinost *Inorg. Chem.* **48** 5376 (2009)
80. K Kuramoto *8 mol.% Yttria-Stabilized Zirconia (YSZ) and Alumina-Based Ceramic Waste Forms Containing Ce and Nd. Report JAERI-M 94-027* (Tokyo: Japan Atomic Energy Research Institute, 1994)
81. H Kinoshita, K Kuramoto, M Uno, S Yamanaka, H Mitamura, T Banba *MRS Proc.* **608** 393 (2000)
82. J P Icenhower, W J Weber, N J Hess, S Thevuthasen, B D Begg, B P McGrail, E A Rodriguez, J L Steele, K N Geiszler *MRS Proc.* **757** 227 (2003)
83. P E Raison, R G Haire, Z Assefa *J. Nucl. Sci. Technol. Suppl.* **3** 725 (2002)
84. P E Raison, R G Haire *Prog. Nucl. Energy* **38** 251 (2001)
85. P E Raison, R G Haire, in *Proceedings of the GLOBAL'2001 Conference on 'Back-End of the Fuel Cycle: From Research to Solutions', Paris, France, 2001* Rep.127
86. P E Raison, R G Haire *J. Nucl. Mater.* **320** 31 (2003)
87. N P Laverov, S V Yudintsev, M P Lapina, S V Stefanovsky, S C Chae, R C Ewing *MRS Proc.* **757** 321 (2003)
88. M W A Stewart, B D Begg, E R Vance, K Finnie, H Li, G R Lumpkin, K L Smith, W J Weber, S Thevuthasan *MRS Proc.* **713** 311 (2002)
89. S V Stefanovsky, O I Kirjanova, S V Chizhevskaya, S V Yudintsev, B S Nikonov, in *Waste Management '03 Conference* (Tucson, AZ; Laser Options Inc., 2003) Rep. 365
90. O I Kir'yanova, S V Stefanovsky, S V Chizhevskaya *Fiz. Khim. Obrabotki Mater.* (2) 72 (2001)
91. W Pan, S R Phillpot, C Wan, A Chernatynskiy, Z Qu *MRS Bull.* **37** 917 (2010)
92. N P Laverov, S V Yudintsev, S V Stefanovsky, Y N Jang *Dokl. Earth Sci.* **381** 1053 (2001) [*Dokl. Akad. Nauk* **381** 399 (2001)]
93. Z G Lin, J H Ouyang, Y Zhou. *J. Mater. Sci.* **43** 2596 (1988)
94. H S Zhang, K Sun, Q Xu, F C Wang, L Liu. *J. Rare Earth* **27** 222 (2009)
95. X Wang, K Jiang, L Zhou *J. Nucl. Mater.* **458** 156 (2015)
96. R C Ewing, W J Weber, W Lutze, in *Disposal of Weapons Plutonium* (Eds E R Mertz, C E Walter) (Boston, MA: Kluwer Academic, 1996) p. 65
97. B B Ebbinghaus, R A VanKonynenburg, R J Ryerson, E R Vance, M W A Stewart, A Jostsons, J S Allender, T Rankin, J Congdon, in *Waste Management 1998 Conference, Tucson, AZ, 1998* Rep. 65-04
98. S V Stefanovsky, S V Yudintsev, B S Nikonov, B I Omelianenko, A I Gorshkov, A V Sivtsov, M I Lapina, R C Ewing *MRS Proc.* **556** 27 (1999)
99. A J Bakel, V N Zyrianov, C J Mertz, E C Buck, D B Chamberlain *MRS Proc.* **556** 181 (1999)
100. A Jostsons, E R Vance, G R Lumpkin, K P Hart, B B Ebbinghaus, in *Waste Management 2000 Conference, Tucson, AZ, 2000* Rep. 55-5
101. I A Sobolev, B F Myasoedov, S V Stefanovsky, S V Yudintsev, Yu M Kulyako *Radiochemistry* **43** 124 (2001) [*Radiokhimiya* **43** 113 (2001)]
102. N P Laverov, S V Yudintsev, S V Stefanovsky, Y N Jang, R C Ewing *MRS Proc.* **713** 337 (2002)
103. J P Icenhower, D M Strachan, B P McGrail, R D Scheele, E A Rodriguez, J L Steele, V L Legore *Am. Mineral.* **91** 39 (2006)

104. G R Lumpkin, B C Chakoumakos, R C Ewing *Am. Mineral.* **71** 569 (1986)
105. J W Wald, W J Weber, in *Advances in Ceramics. Nuclear Waste Management* Vol. 8 (Eds G G Wicks, W A Ross) (Columbus OH: The American Ceramic Society, 1984) p. 71
106. W J Weber, J W Wald, H J Matzke *Mater. Res. Soc. Symp. Proc.* **44** 679 (1985)
107. W J Weber, J W Wald, H J Matzke *J. Nucl. Mater.*, **138** 196 (1986)
108. W J Weber, H J Matzke *Radiat. Effects Defects Solids* **98** 93 (1986).
109. S V Yudintsev, A N Lukinykh, S V Tomilin, A A Lizin, S V Stefanovsky *J. Nucl. Mater.* **385** 200 (2009)
110. Yu F Volkov, S V Tomilin, A N Lukinykh, A A Lizin, A A Elesin, A G Yakovenko,V I Spiryakov, A V Bychkov, L J Jardine *Radiochemistry* **46** 351 (2004) [*Radiokhimiya* **46** 322 (2004)]
111. Yu F Volkov, S V Tomilin, A N Lukinykh, A A Lizin, A A Elesin, A G Yakovenko, V I Spiryakov, V I Konovalov, V M Chistyakov, A V Bychkov, L J Jardine *Radiochemistry,* **46** 358 (2004) [*Radiokhimiya* **46** 329 (2004)]
112. D M Strachan, R D Scheele, A E Kozelisky, R L Sell, H T Schaef, M J O'Hara, C F Brown, W C Buchmiller *MRS Proc.,* **713** 461 (2002)
113. D M Strachan, R D Scheele, E C Buck, J P Icenhower, A E Kozelisky, R L Sell, R J Elovich, W C Buchmiller *J. Nucl. Mater.* **345** 109 (2005)
114. G R Lumpkin, R C Ewing *MRS Proc.* **44** 647 (1985)
115. G R Lumpkin, R C Ewing, E M Foltyn *J. Nucl. Mater.* **139** 113 (1986)
116. G R Lumpkin, R C Ewing, in *Microbeam Analysis* (Eds A D Romig Jr, W F Chambers) (San Francisco, CA: San Francisco Press, 1986) p.145
117. R B Greegor, F W Lytle, R C Ewing, R F Haaker *MRS Proc.,* **11** 409 (1982)
118. R B Greegor, F W Lytle, R C Ewing, R F Haaker *Nucl. Instrum. Methods Phys. Res., Sect. B* **1** 587 (1984)
119. R B Greegor, F W Lytle, R C Ewing, R F Haaker, in *EXAFS and Near-Edge Structure III. Proceedings of the 3rd International EXAFS Conference* (Eds K O Hodgson, D Hedman, J E Penner-Hahn) (New York: Springer, 1984) p. 343
120. R B Greegor, F W Lytle, B C Chakoumakos, G R Lumpkin, R C Ewing *MRS Proc.* **44** 655 (1985)
121. R B Greegor, F W Lytle, B C Chakoumakos, G R Lumpkin, R C Ewing *MRS Proc.* **50** 387 (1985)
122. R B Greegor, F W Lytle, B C Chakoumakos, G R Lumpkin, R C Ewing, in *The 14th General Meeting of the International Mineralogical Association. Abstracts, Stanford, CA, 1986* p. 114
123. R B Greegor, F W Lytle, B C Chakoumakos, G R Lumpkin, R C Ewing, C Spiro, J Wong *MRS Proc.* **84** 645 (1987)
124. R B Greegor, F W Lytle, R J Livak, J W Clinard Jr *J. Nucl. Mater.* **152** 270 (1988)
125. H Yokoi, T Matsui, H Ohno, K Kobayashi *MRS Proc.* **353** 783 (1995)
126. R C Ewing, B C Chakoumakos, G R Lumpkin, T Murakami, R B Greegor, F W Lytle *Nucl. Instrum. Methods Phys. Res., Sect. B* **32** 487 (1988)
127. D D Hogarth *Am. Mineral.* **62** 403 (1977)
128. Y Eyal, A Kaufman *Nucl. Technol.* **58** 77 (1982)
129. Y Eyal, R L Fleischer *Geochim. Cosmochim. Acta* **49** 1155 (1985)
130. Y Eyal, G R Lumpkin, R C Ewing *MRS Proc.* **50** 379 (1985)
131. Y Eyal, G R Lumpkin, R C Ewing *MRS Proc.* **84** 635 (1987)
132. G R Lumpkin, Y Eyal, R C Ewing *J. Mater. Res.* **3** 357 (1988)
133. K L Smith, N J Zaluzec, G R Lumpkin *MRS Proc.* **506** 931 (1998)
134. S X Wang, B D Begg, L M Wang, R C Ewing, W J Weber, K V Govidan Kutty. *J. Mater. Res.* **14** 4470 (1999)
135. S X Wang, L M Wang, R C Ewing, G S Was, G R Lumpkin *Nucl. Instrum. Methods Phys. Res. Sect. B* **148** 704 (1999)
136. S X Wang, L M Wang, R C Ewing, K V Govidan Kutty *Nucl. Instrum. Methods Phys. Res., Sect. B* **169** 135 (2000)
137. S X Wang, L M Wang, R C Ewing *J. Non-Cryst. Solids* **274** 238 (2000)
138. G R Lumpkin, K L Smith, M G Blackford *J. Nucl. Mater.* **289** 177 (2001)
139. W J Weber, R C Ewing *MRS Proc.* **713** 443 (2002)
140. A Meldrum, C W White, V Keppens, L A Boatner, R C Ewing *Phys. Rev. B* **63** 104109 (2001)
141. B D Begg, N J Hess, D E McCready, S Thevuthasan, W J Weber *J. Nucl. Mater.* **289** 188 (2001)
142. J Lian, X T Zu, K V Govindan Kutty, J Chen, L M Wang, R C Ewing *Phys. Rev. B* **66** 054108 (2002)
143. J Lian, L M Wang, R G Haire, K B Helean, R C Ewing *Nucl. Instrum. Methods Phys. Res., Sect. B* **218** 236 (2004)
144. J Lian, J Chen, L M Wang, R C Ewing, J M Farmer, L A Boatner, K M Helean *Phys. Rev. B* **68** 134107 (2003)
145. J Lian, R C Ewing, L M Wang, K M Helean *J. Mater. Res.* **19** 1575 (2004)
146. G R Lumpkin, K R Whittle, S Rios, K Trachenko, M Pruneda, E J Harvey, S A T Redfern, K L Smith, N J Zaluzec *MRS Proc.* **932** 549 (2006)
147. J Lian, S V Yudintsev, S V Stefanovsky, L M Wang, R C Ewing *J. Alloys Compd.* **444** – **445** 429 (2007)
148. P E D Morgan, F J Ryerson *J. Mater. Sci. Lett.* **1** 351 (1982)
149. A B Harker, P E D Morgan, D R Clarke, J F Flintoff *MRS Proc.* **6** 567 (1982)
150. A B Harker, P E D Morgan, J F Flintoff, D R Clark, in *The Treatment and Handling of Radioactive Wastes* (Seattle, WA: Battelle Press, 1983) p. 325
151. P E D Morgan, A B Harker, J F Flintoff, T M Shaw, D R Clarke *Adv. Ceram.* **8** 325 (1984)
152. A B Harker, in *Radioactive Waste Forms for the Future* (Eds W Lutze, R C Ewing) (Amsterdam: Elsevier, 1988) p. 335
153. I A Sobolev, S V Stefanovsky, S V Ioudintsev, B S Nikonov, B I Omelianenko, A V Mokhov *MRS Proc.* **465** 363 (1997)
154. O A Knyazev, S V Stefanovsky, B S Nikonov, B I Omel'yanenko, S V Yudintsev *Fiz. Khim. Obrabotki Mater.* (1) 94 (1998)
155. T S Ercit, F C Hawthorne *Canad. Mineral.* **33** 1223 (1995)
156. S V Stefanovsky, S V Yudintsev, B S Nikonov, B I Omelianenko, A G Ptashkin *MRS Proc.* **556** 121 (1999)
157. I A Sobolev, S V Stefanovsky, B F Myasoedov, Y M Kulyako, S V Yudintsev, in *Plutonium Futures — The Science. Conference Transactions.*(Eds K K S Pillay, K C Kim) (Santa Fe, NM: ANS, 2000) p. 122
158. S V Stefanovsky, O I Kir'yanova, S V Yudintsev, B S Nikonov, B I Omel'yanenko *Fiz. Khim. Obrabotki Mater.* (3) 72 (2001)
159. S V Yudintsev, S V Stefanovsky, B S Nikonov, B I Omelianenko *MRS Proc.* **663** 357 (2001)
160. B S Nikonov, B I Omel'yanenko, A G Ptashkin, S V Stefanovsky, S V Yudintsev *J. Adv. Mater.* **5** 95 (2001)
161. S V Stefanovsky, V I Vlasov, A G Ptashkin, O I Kirjanova,Y M Kulyako, S A Perevalov, in *Proceedings of the GLOBAL-2001 International Conference on 'Back End of the Fuel Cycle: From Research to Solutions', Paris, France, 2001* Rep. 045
162. O V Kir'yanova, S V Stefanovsky, S V Yudintsev, B S Nikonovyu *Perspekt. Mater.* (5) 38 (2002)
163. O I Kir'yanova, S V Stefanovsky, S V Yudintsev, B S Nikonov *Perspekt. Mater.* (3) 42 (2003)

164. O I Kirjanova, S V Stefanovsky, S V Yudintsev *MRS Proc.* **757** 259 (2003)
165. V S Urusov, V S Rusakov, S V Yudintsev, S V Stefanovsky *MRS Proc.* **807** 243 (2004)
166. J Lian, L M Wang, R C Ewing, S V Yudintsev, S V Stefanovsky *J. Mater. Chem.* **15** 709 (2005)
167. O I Stefanovsky (Kirjanova), S V Stefanovsky, S V Yudintsev, B S Nikonov, in *Proceedings of the 10th International Conference on Environmental Remediation and Radioactive Waste Management ICEM'05, Glasgow, 2005* Rep. ICEM05-1220
168. S V Stefanovsky, S V Yudintsev, B S Nikonov, O I Stefanovsky *MRS Proc.* **893** 417 (2006)
169. S V Stefanovsky, S V Yudintsev, B S Nikonov, A V Mokhov, S A Perevalov, O I Stefanovsky, A G Ptashkin *MRS Proc.* **893** 429 (2006)
170. S V Stefanovsky, S V Yudintsev, B S Nikonov, O I Stefanovsky *MRS Proc.* **932** 559 (2006)
171. S V Stefanovsky, O I Stefanovsky, S V Yudintsev, B S Nikonov *MRS Proc.* **932** 599 (2006)
172. N P Laverov, S V Yudintsev, S V Stefanovsky, B I Omel'yanenko, B S Nikonov *Geol. Ore Depos.* **48** 335 (2006) [*Geolog. Rudnykh Mestorozhdenii* **48** 387 (2006)]
173. S A Perevalov, S V Stefanovsky, S V Yudintsev, A V Mokhov, A G Ptashkin *Radiochim. Acta* **94** 509 (2006)
174. S V Yudintsev, S V Stefanovsky, B S Nikonov, K I Maslakov, A G Ptashkin *J. Alloys Compd.* **444** – **445** 606 (2007)
175. S V Stefanovsky, S V Yudintsev, S A Perevalov, I V Startseva, G A Varlakova *J. Alloys Compd.* **444** – **445** 618 (2007)
176. K Maslakov, Yu Teterin, A Teterin, S Yudintsev, S Stefanovsky, in *Speciation Techniques and Facilities for Radioactive Materials at Synchrotron Light Sources. Workshop Proceedings* (Karlsruhe: Organization for Economic Cooperation and Development, 2007) p. 263
177. S V Stefanovsky, S V Yudintsev, B S Nikonov, O I Stefanovsky *Radiochemistry* **49** 346 (2007) [*Radiokhimiya* **49** 305 (2007)]
178. S V Stefanovsky, O I Stefanovskaya, S V Yudintsev, B S Nikonov *Radiochemistry* **49** 354 (2007) [*Radiokhimiya* **49** 312 (2007)]
179. S Stefanovsky, S Yudintsev, B Nikonov, O Stefanovsky *MRS Proc.* **985** 175 (2007)
180. S V Stefanovsky, A G Ptashkin, O A Knyazev, S V Yudintsev, B S Nikonov, M I Lapina *Fiz. Khim. Obrabotki Mater.* (4) 68 (2007)
181. S V Stefanovsky, A G Ptashkin, O A Knyazev, S V Yudintsev, B S Nikonov, M I Lapina, O I Stefanovskaya *Fiz. Khim. Obrabotki Mater.* (5) 42 (2007)
182. S V Stefanovsky, O I Stefanovskaya, S V Yudintsev, B S Nikonov *Voprosy Radiats. Bezopasnosti* (4) 3 (2007)
183. O I Stefanovskaya, S V Stefanovsky, S V Yudintsev, B S Nikonov *Voprosy Radiats. Bezopasnosti* (1) 16 (2008)
184. A Merkushkin, A Ochkin, S Stefanovsky, O Stefanovsky, in *38emes Journees des Actinides* (Poland: Wroclaw, 2008) p. 88
185. S V Stefanovsky, A V Ochkin, A O Merkushkin, O I Stefanovsky, in *Plutonium Future — The Science 2008. A Topical Conference on Plutonium and the Actinides, Dijon, France, 2008* p. 116
186. A N Lukinykh, S V Tomilin, A A Lizin, S V Yudintsev, S V Stefanovsky *Radiochemistry* **50** 541 (2008) [*Radiokhimiya* **50** 469 (2008)]
187. S V Stefanovsky, G A Varlakova, I V Startseva, S V Yudintsev, B S Nikonov, M I Lapina *Radiochim. Acta* **97** 17 (2009)
188. V Yarmolyuk *Vestn. RFFI* **1** 59 (2012)
189. S V Stefanovsky, S V Yudintsev, T S Livshits, in *Actinides 2009: IOP Conference Series: Mater. Sci. Eng.* **9** 012001 (2009)
190. S V Krivovichev, S V Yudintsev, S V Stefanovsky, N I Organova, O V Karimova, V S Urusov *Angew. Chem. Int., Ed.* **49** 9982 (2010)
191. N P Laverov, S V Yudintsev, S V Stefanovsky, B I Omelianenko, B S Nikonov *Radiochemistry* **53** 229 (2011) [*Radiokhimiya* **53** 196 (2011)]
192. N P Laverov, V S Urusov, S V Krivovichev, A S Pakhomova, S V Stefanovsky, S V Yudintsev *Radiochemistry* **53** 273 (2011) [*Radiokhimiya* **53** 307 (2011)]
193. K I Maslakov, A Yu Teterin, Yu A Teterin, K E Ivanov, S V Yudintsev, S V Stefanovsky *Radiochemistry* **54** 115 (2012) [*Radiokhimiya* **54** 107 (2012)]
194. N P Laverov, S V Yudintsev, S V Stefanovsky, R C Ewing *Dokl. Earth Sci.* **443** 526 (2012) [*Dokl. Akad. Nauk* **443** 726 (2012)]
195. N P Laverov, S V Yudintsev, S V Krivovichev, S V Stefanovsky, B I Omel'yanenko, B S Nikonov, T S Livshits, in *Fundamental'nye Osnovy Formirovaniya Resursnoi Bazy Strategicheskogo Syr'ya (Au, Ag, Pt, Cu, Redkie Elementy i Metally)* [The Fundamentals for the Formation of the Resource Base of Strategic Raw Materials (Au, Ag, Pt, Cu, Rare Earth Elements and Metals)] (Moscow; GEOS, 2012) p. 275
196. S V Yudintsev, S V Stefanovsky, O I Kir'yanova, J Lian, R Yuing *Fiz. Khim. Pbrabotki Mater. (1) 44 (2001)*
197. N P Laverov, S V Yudintsev, S V Stefanovsky, J Lian, R C Ewing *Dokl. Earth Sci.* **377** 175 (2001) [*Dokl. AN* **376** 665 (2001)]
198. S V Yudintsev, S V Stefanovsky, O I Kir'yanova, J Lian, R Ewing *Atom. Energy* **90** 487 (2001) [*Atom. Energ.* **90** 467 (2001)]
199. J Lian, R C Ewing, S V Yudintsev, S V Stefanovsky in *Proceedings of the 8th International Conference on Environmental Management. ICEM '01* (Bruges: ASME, 2001) Rep. 34
200. J Lian, S V Yudintsev, S V Stefanovsky, O I Kirjanova, R C Ewing *MRS Proc.* **713** 455 (2002)
201. N P Laverov, S V Yudintsev, T S Yudintseva, S V Stefanovsky, R C Ewing, J Lian, S Utsonomiya, L M Wang *Geol. Ore Depos.* **45** 423 (2003) [*Geolog. Rudnykh Mestorozhdenii* **45** 483 (2003)]
202. J Lian, L M Wang, R C Ewing, S V Yudintsev, S V Stefanovsky *MRS Proc.* **807** 225 (2004)
203. J Lian, L M Wang, R C Ewing, S V Yudintsev, S V Stefanovsky *J. Appl. Phys.* **97** 113536 (2005)
204. S V Stefanovsky, A N Lukinykh, S V Tomilin, A A Lizin, S V Yudintsev *Fiz. Khim. Obrabotki Mater.* (6) 32 (2007)
205. S V Stefanovsky, A N Lukinykh, S V Tomilin, A A Lizin, S V Yudintsev *MRS Proc.* **1107** 389 (2008)
206. D Lattard *Contrib. Mineral. Petrol.* **97** 264 (1987)
207. A A Voronkov, N G Shumyatskaya, Yu A Pyatenko *Kristallokhimiya Mineralov Tsirkoniya i ikh Iskusstvennykh Analogov (Crystal Chemistry of Zirconium Minerals and Their Synthetic Analogues)* (Moscow: Nauka, 1978)
208. B M Gatehouse, I E Grey, R J Hill, H J Rossel *Acta Crystallogr., Sect. B* **37** 306 (1981)
209. T J White *Am. Mineral.* **69** 1156 (1984)
210. P Bayliss, F Mazzi, R Munno, T J White *Mineral. Mag.* **53** 565 (1989)
211. A A Coelho, R W Cheary, K L Smith. *J. Solid State Chem.,* **129** 346 (1997)
212. K L Smith, G R Lumpkin, in *Defects and Processes in the Solid State: Geoscience Applications* (Eds J N Boland, J D Fitz Gerald) (Amsterdam: Elsevier, 1993) p. 401
213. S E Kesson,W J Sinclair, A E Ringwood *Nucl. Chem. Waste. Manag.* **4** 259 (1983)
214. A Jostsons, E R Vance, D J Mercer, V M Oversby *MRS Proc.* **353** 775 (1995)

215. E R Vance, M L Carter, B D Begg, R A Day, H F Leung *MRS Proc.* **608** 431 (2000)
216. H Xu, Y Wang, P Zhao, W L Borcier, R Van Konynenburg, H F Shaw *MRS Proc.* **757** 235 (2003)
217. E R Vance, B D Begg, R A Day, C J Ball *MRS Proc.* **353** 767 (1995)
218. B D Begg, E R Vance, R A Day, M Hambley, S D Conradson *MRS Proc.* **465** 325 (1997)
219. B D Begg, E R Vance, G R Lumpkin *MRS Proc.* **506** 79 (1998)
220. K P Hart, E R Vance, M W A Stewart, J Weir, M L Carter, M Hambley, A Brownscombe, R A Day, S Leung, C J Ball, B B Ebbinghaus, L Gray, T Kan *MRS Proc.* **506** 161 (1998)
221. K P Hart, Y Zhang, E Loi, Z Aly, M W A Stewart, A Brownscombe, B B Ebbinghaus, W Bourcier *MRS Proc.* **608** 353 (2000)
222. J Malmström, E Reusser, R Giere, G R Lumpkin, M Duggelin, D Mathys, R Guggenheim *MRS Proc.* **556** 165 (1999)
223. E W Heinrich *Mineralogy and Geology of Radioactive Raw Materials* (New York: McGraw-Hill 1958)
224. S V Stefanovsky, S V Yudintsev, B S Nikonov, A V Ochkin, S V Chizhevskaya, N E Cherniavskaya *MRS Proc.* **608** 407 (2000)
225. N S Mikhailenko, A V Ochkin, S V Stefanovsky, O I Kirjanova *MRS Proc.* **807** 327 (2004)
226. N Mikhailenko, S Stefanovsky, A Ochkin *MRS Proc.* **985** 211 (2007)
227. W C Mosley *J. Am. Ceram. Soc.* **54** 475 (1971)
228. H Mitamura, S Matsumoto, T Tusboi, E R Vance, B D Begg, K P Hart *MRS Proc.* **353** 1405 (1995)
229. A E Ringwood, V M Oversby, W Sinclair, in *Scientific Basis for Nuclear Waste Management* Vol. 2 (Ed. C J M Northrup Jr) (New York, London: Plenum Press, 1980) p. 273
230. G R Lumpkin, M Colella, K L Smith, R H Mitchell, A O Larsen *MRS Proc.* **506** 207 (1998)
231. T S Livshits, A A Lizin, S V Tomilin *Geolog. Rudnykh Mestorozhdenii* **56** 497 (2014)
232. K D Reeve, J L Woolfrey *J. Austral. Ceram. Soc.* **16** 10 (1980)
233. J P Evans, K A Boult, E L Paige, J A C Marples *The Preparation of Fully Active Synroc and its Radiation Stability — Progress. Report AERE-G4010* (Harwell, UK: Harwell Laboratory, 1986)
234. K L Smith, M G Blackford, G R Lumpkin *MRS Proc.* **506** 929 (1998)
235. A Meldrum, L A Boatner, R C Ewing *MRS Proc.* **481** 401 (1998)
236. F G Karioris, K Appaji Gowda, L Cartz, J C Labbe *J. Nucl. Mater.* **108 – 109** 748 (1982)
237. K L Smith, G R Lumpkin, M G Blackford, E R Vance *MRS Proc.* **556** 1185 (1999)
238. K R Whittle, M G Blackford, G R Lumpkin, K L Smith, N J Zaluzec *MRS Proc.* **1193** 55 (2009)
239. K R Whittle, M G Blackford, R D Aughterson, G R Lumpkin, K L Smith, N J Zaluzec *MRS Proc.* **1265** 157 (2010)
240. A V Ochkin, S V Chizhevskaya, N E Archakova (Cherniavskaya), A O Merkushkin, I A Petukhova, N S Mikhailenko, S V Stefanovsky *MRS Proc.* **757** 303 (2003)
241. S V Chizhevskaya, N E Cherniavskaya, A V Ochkin, A M Chekmarev, S V Stefanovsky *MRS Proc.* **663** 367 (2001)
242. In *Geologicheskii Slovar'* (Dictionary of Geological Terms) (Moscow: Nedra, 1978) Vol. 1, p. 187
243. D Elwell *Man-Made Gemstones* (New York: Wiley, 1980)
244. I O Galuskina, E V Galuskin, T Armbruster, B Lazic, J Kusz, P Dzieranowski, V M Gazeev, N N Pertsev, K Prusik, A E Zadov, A Winiarski, R Wrzalik, A G Gurbanov *Am. Mineral.* **95** 1172 (2010)
245. B E Burakov, B E Anderson, D A Knecht, M A Zamoryanskaya, E E Strykanova, M A Yagovkina *MRS Proc.* **556** 55 (1999).
246. B E Burakov, E B Anderson, in *Plutonium Futures — The Science 2000. Conference Transactions* (Eds K K S Pillay, K C Kim) (Santa Fe, NM: ANS ,2000) p. 159
247. B E Burakov, E B Anderson, M A Zamoryanskaya, M A Petrova *MRS Proc.* **608** 419 (2000)
248. S V Yudintsev, A A Osherova,A V Dubinin, A V Zotov, S V Stefanovsky *MRS Proc.* **824** 287 (2004)
249. Zs Rak, R C Ewing, U Becker *Phys. Rev. B* **83** 155123 (2011)
250. Zs Rak, R C Ewing, U Becker *Phys. Rev. B* **84** 155128 (2011)
251. Zs Rak, R C Ewing, U Becker *J. Nucl. Mater.* **436** 1 (2013)
252. J Zhang, T S Livshits, A A Lizin, Q Hu, R C Ewing *J. Nucl. Mater.* **407** 137 (2010)
253. S Utsonomiya, S Yudintsev, R C Ewing *J. Nucl. Mater.* **336** 251 (2005)
254. S Utsonomiya, L M Wang, S V Yudintsev, R C Ewing *J. Nucl. Mater.* **303** 177 (2002)
255. T S Livshits, A A Lizin *Vestn. Otd. Nauk o Zemle RAN* (1) 2009 http:www.scgis.ru/russian/cp1251/h_dgggms/1-2009/informbul-1_2009/geoecol-8.pdf
256. J T Szymansky, J D Scott *Canad. Mineral.* **20** 271 (1982)
257. R D Shannon *Acta Crystallogr., Sect. A* **32** 751 (1976)
258. E R Vance, J N Watson, M I Carter, R A Day, B D Begg *J. Am. Ceram. Soc.* **84** 141 (2001)
259. S V Stefanovsky, S V Yudintsev, A A Shiryaev, V Y Murzin *J. Eur. Ceram. Soc.* (in the press)
260. E R Vance, M L Carter, M W A Stewart, R A Day, B D Begg, C J Ball *MRS Proc.* **713** 319 (2002)
261. M James, J N Watson *J. Solid State Chem.* **165** 261 (2002)
262. M James, M L Carter, J N Watson *J. Solid State Chem.* **174** 329 (2003)
263. K S Finnie, Z Zhang, E R Vance, M L Carter *J. Nucl. Mater.* **317** 46 (2003)
264. M Colella, G R Lumpkin, Z Inc Zhang, E C Buck, K L Smith *Phys. Chem. Mineral.* **32** 52 (2005)
265. S E Kesson, A E Ringwood *Radiat. Waste Manag. Nucl. Fuel Cycle* **4** 159 (1983)
266. A G Solomah, T S Sridhar, S C Jones *Adv. Ceram.* **20** 259 (1986)
267. S G Cochran, W H Dunlop, T A Edmunds, L M MacLean, T H Gould *Fissile Material Disposition Program Final Immobilization Form Assessment and Recommendation. UCRL-ID-128705* (Livermore, CA: Lawrence Livermore National Laboratory, 1997)
268. S V Stefanovsky, O A Knyazev, D B Lopukh, S V Ioudintsev, in *Proceedings of the International Conference on Incineration and Thermal Treatment Technologies, Salt Lake City, UT, 1998* p. 155
269. S V Stefanovsky, S V Yudintsev, B S Nikonov, M I Lapina, A S Aloy *MRS Proc.* **663** 315 (2001)
270. M W A Stewart, E R Vance, A Jostsons, K Finnie, R A Day, B B Ebbinghaus *MRS Proc.*, **713** 381 (2002)
271. S V Yudintsev, S V Stefanovsky, M Yu Kalenova, B S Nikonov, M S Nikol'sky, A M Koscheev, A S Schepin *Radiochemistry* **57** 321 (2015) [*Radiokhimiya* **57** 272 (2015)]
272. S V Yudintsev, S V Stefanovsky, O I Stefanovskaya, B S Novikov, M S Nikol'skii *Radiochemistry* **57** 640 (2015) [*Radiokhimiya* **57** 547 (2015)]
273. W J Weber, A Navrotsky, S Stefanovsky, E R Vance, E Vernaz *MRS Bull.,* **34** 46 (2009)
274. Y Zhang, K P Hart, W L Bourcier *J. Nucl. Mater.* **289** 254 (2001)

275. Y Zhang, K P Hart, B S Thomas, Z Aly, H Li, M Carter *MRS Proc*. **663** 341 (2001)
276. Y Zhang, K P Hart, B D Begg, E A Keegan, R A Day, A Brownscombe, M W A Stewart *MRS Proc*. **713** 389 (2002)
277. Y Zhang, B S Thomas, G R Lumpkin *J. Nucl. Mater*. **321** 1 (2003)
278. B S Thomas, Y Zhang *Radiochim. Acta* **91** 463 (2003)
279. Y Zhang, G R Lumpkin, H Li, M G Blackford, M Colella, M L Carter, E R Vance *J. Nucl. Mater*. **350** 293 (2006)
280. M L Carter, H Li, Y Zhang, A L Gillen, E R Vance *MRS Proc*. **1124** 195 (2009)
281. F X Zhang, M Lang, L Zhenxian, R C Ewing *J. Solid State Chem*. **184** 2834 (2011)
282. Y Zhang, D J Gregg, G R Lumpkin, B D Begg, M Jovanovic *J. Alloys Compd*. **581** 665 (2013)
283. G R Lumpkin, Y Gao, R Giere, T Williams, N Mariano, T Geisler *Mineral. Mag*. **78** 1071 (2014)
284. S V Stefanovsky, S V Yudintsev, O I Kir'yanova *Fiz. Khim. Obrabotki Mater. (5) 90 (2001)*
285. J Lian, L M Wang, G R Lumpkin, R C Ewing *Nucl. Instrum. Methods Phys. Res. Sect. B* **191** 565 (2002)
286. D M Strachan, R D Scheele, J P Icenhower, E C Buck, A E Kozelisky, R L Sell, R J Elovich, W C Buckmiller *Radiation Damage Effects in Candidate Ceramics for Plutonium Immobilization: Final Report. PNNL-14588* (Richland, WA: Pacific Northwest National Laboratory, 2004)
287. W A Deer, R A Howie, J. Zussman *Rock-Forming Minerals. Ortho- and Ring Silicates* Vol 1 (London: Longmans, 1962)
288. A V Milovskii, O V Kononov *Mineralogiya* (Mineralogy) (Moscow: Moscow State University, 1982)
289. G M Bancroft, J B Metson, N S McIntyre *Adv. Ceram*. **8** 282 (1984)
290. S V Stefanovsky, S V Yudintsev, B S Nikonov, B I Omelianenko, M I Lapina *MRS Proc*. **608** 455 (2000)
291. P J Hayward, in *Radioactive Waste Forms for the Future* (Eds W Lutze, R C Ewing) (Amsterdam: Elsevier, 1988) p. 427
292. T N Lashtchenova, S V Stefanovsky, in *Proceedings of the XVIII International Congress on Glass, San-Francisco, CA, 1998* Rep. ICG 666-P02-033
293. E R Vance, J B Metson *Phys. Chem. Mineral*. **12** 255 (1985)
294. F C Hawthorne, L A Groat, M Raudsepp, N A Ball, M Kimata, F D Spike, R Gaba, N M Halden, G R Lumpkin, R C Ewing, R B Greegor, F W Lytle, T S Ercit, G R Rossman, F J Wicks, R A Ramik, B L Sherriff, M F Fleet, C McCammon *Am. Mineral*. **76** 370 (1991)
295. E R Vance, F G Kariorus, L Cartz, M S Wong *Adv. Ceram*. **8** 62 (1984)
296. E R Vance, C D Cann, P G Richardson *Radiat. Eff*. **98** 71 (1986)
297. D V Stevanovic, D A Thompson, E R Vance *J. Nucl. Mater*. **161** 169 (1989)
298. S V Ioudintsev, B S Nikonov, B I Omelianenko, S V Stefanovsky, T N Lashtchenova, in *Proceedings of the Sixth International Conference on Radioactive Waste Management and Environmental Restoration. ICEM'97* (Singapore: ASME, 1997) p. 323
299. S V Stefanovsky, S V Ioudintsev, B S Nikonov, B I Omelianenko, T N Lashtchenova *MRS Proc*. **506** 269 (1998)
300. T N Lashchenova, S V Stefanovsky, B S Nikonov, B I Omel'yanenko, S V Yudintsev *Perspekt. Mater*. (2) 67 (1998)
301. J Ito. *Am. Mineral*. **52** 1094 (1967)
302. J Ito *Am. Mineral*. **53** 890 (1968)
303. S Utsonomiya, S Yudintsev, L M Wang, R C Ewing *J. Nucl. Mater*. **322** 180 (2003)
304. M P Mefod'eva, N N Krot *Soedineniya Transuranovykh Elementov* (Compounds of Transuranic Elements) (Moscow: Atomizdat, 1987)
305. S V Stefanovsky, F A Lifanov *Neorg. Mater*. **25** 502 (1989)
306. F A Lifanov, S V Stefanovsky, I A Sobolev, in *Glass 89. The XVth International Congress on Glass* Vol. 3b (Leningrad: Nauka, 1989) p. 202
307. F A Lifanov, S V Stefanovsky *Radiokhimiya* **32** 166 (1990) [*Sov. Radiochem*. **32** 291 (1990)]
308. F A Lifanov, S V Stefanovsky, O N Tsveshko, T N Lashchenova *Fiz. Khim. Stekla* **17** 810 (1991)
309. S V Stefanovsky, I A Ivanov, A N Gulin *Zh. Prikl. Spektrosk*. **57** 67 (1992)
310. S V Stefanovsky, O A Trul' *Zh. Prikl. Spektrosk*. **57** 322 (1992)
311. S Stefanovsky, F Lifanov, I Ivanov, in *Proceedings of the XVIth International Congress on Glass, Madrid, 1992* Vol.3, p. 209
312. S V Stefanovsky *Zh. Prikl. Spektrosk*. **62** 150 (1995)
313. A S Aloy, B S Kuznetsov, T I Kolycheva, S A Dmitriev, S V Stefanovsky, in *Proceedings of the Fifth International Conference on Radioactive Waste Management and Environmental Remediation. ICEM'95, Berlin, 1995* p. 1117
314. T N Lashtchenova, S V Stefanovsky, F A Lifanov, in *Waste Management 97 Conference, Tucson, AZ, 1997* Rep. 13-17
315. A S Aloi, S A Dmitriev, S V Stefanovsky *Fiz. Khim. Obrabotki Mater*. (1) 83 (1997)
316. G A Malinina, O I Stefanovsky, S V Stefanovsky *J. Nucl. Mater*. **416** 230 (2011)
317. G A Malinina, O I Stefanovsky, S V Stefanovsky *Glass Phys. Chem*. **38** 280 (2012) [*Fiz. Khim. Stekla* **38** 347 (2012)]
318. G Nagelschmidt *J. Chem. Soc*. 865 (1937)
319. E R Segnit *Mineral. Mag*. **29** 173 (1950)
320. S Gross *The Mineralogy of the Hatrurim Formation, Israel* (Geological Survey of Israel Bull. No. 70, 1977)
321. M Fleischer, L J Carbi, G Y Chao, A Pabst *Am. Mineral*. **63** 424 (1978)
322. K Sugiyama, Y Kato, T Mikouchi, in *20th General Meeting of the International Mineralogical Association. Budapest, Hungary, 2010* p. 725
323. N N Shvetsova, N N Bushuev, S I Vol'fkovich, R G Atsiev *Vestn. MGU. Ser. 2. Khimiya* **22** 110 (1981)
324. G Celotti, E Landi *J. Eur. Ceram. Soc*. **23** 851 (2003)
325. W Brammond, G Armantrout, in *Waste Management 1998 Conference, Tucson, AZ, 1998* Rep. 65-05
326. E R Vance, M W A Stewart, S A Moricca *J. Austral. Ceram. Soc*. **50** 38 (2014)
327. M W A Stewart, E R Vance, S A Moricca, D R Brew, C Cheung, T Eddowes, W Bermudez *Sci. Technol. Nucl. Install*. Art.ID 926026 (2013)
328. M Suárez, A Fernández, J L Menéndez, R Torresillas, H U Kessel, J Hennicke, R Kirchner, T Kessel, in *Sintering Applications* (Istambul: In Tech, 2012) p. 319
329. M Tokita *Jpn. J. Soc. Powder. Technol*. **30** 790 (1993)
330. L Gao, H Z Wang, J S Hong, H Miyamoto, K Miyamoto, Y Nishikawa, S D D L Torre *J. Eur. Ceram. Soc*. **19** 609 (1999)
331. Z M Xie, R Liu, Q F Fang, Y Zhou, X P Wang, C S Liu *J. Nucl. Mater*. **444** 175 (2014)
332. L S Golovkina, A I Orlova, A V Nokhrin, M S Boldin, V V Sakharov *Adv. Ceram. Sci. Eng*. **2** 161 (2013)
333. B M Clark, P Tumurugoti, S K Sandaram, J W Amoroso, J C Marra, K S Brinkman *Microsc. Microanal*. **20** (Suppl. 3) 1932 (2014)
334. B M Clark, S K Sundaram, K S Brinkman, K M Fox, J M Amoroso, in *Advances in Materials Science for Environmental and Energy Technologies III* (Eds T Ohji, J Matáš, J Manjooran, G Pickrell, A Jitianu) (Wiley, 2014) p. 127

335. B M Clark, P Tumurugoti, S K Sandaram, J W Amoroso, J C Marra, K S Brinkman *Metal. Mater. Trans., E* **1** 341 (2014)
336. T Yao, F Lu, H Sun, J Wang, R C Ewing, J Lian *J. Am. Ceram. Soc.* **97** 2409 (2014)
337. W Lutze, in *Radioactive Waste Forms for the Future* (Eds W Lutze, R C Ewing) (Amsterdam: Elsevier, 1988) p. 1
338. H Pentinghaus, in *Proceedings International Seminar on Chemistry and Process Engineering for High Level Liquid Waste Solidification* (Jülich: KfK, 1981) p. 713
339. I A Sobolev, C V Stefanovsky, F A Lifanov *Radiokhimiya* **35** 99 (1993)
340. I A Sobolev, S V Stefanovsky, F A Lifanov *MRS Proc.* **353** 833 (1995)
341. V I Aleksandrov, V V Osiko, A M Prokhorov, V M Tatarintsev *Russ. Chem. Rev.* **47** 213 (1978)
342. Yu B Petrov *Induktsionnaya Plavka Okislov* (Induction Melting of Oxides) (Moscow: Energoatomizdat, 1991)
343. Yu S Kuz'minov, V V Osiko *Fianity* (Fianites) (Moscow: Nauka, 2001)
344. Yu S Kuz'minov, E E Lomonova, V V Osiko *Tugoplavkie Materialy iz Kholodnogo Tiglya* (Refractory Materials from Cold Crucible) (Moscow: Nauka, 2004)
345. S Naline, F Gouyaud, V Robineau, C Girold, B Carpentier, in *Waste Management 2010 Conference, Phoenix, AZ, 2010* Rep. 10382
346. R Didierlaurent, E Chauvin, J F Hollebecque, J Lacombe, C Mesnil, C Veyer, O Pinet, in *Waste Management 2014 Conference, Phoenix, AZ, 2014* Rep. 14035
347. D B Lopukh *Voprosy Radiats. Bezopasnosti* (2) 26 (2009)
348. V V Lebedev, S V Stefanovsky *Voprosy Radiats. Bezopasnosti* (2) 16 (2011)
349. O A Knyazev, S V Stefanovsky, S V Ioudintsev, B S Nikonov, B I Omelianenko, A V Mokhov, A I Yakushev *MRS Proc.* **465** 401 (1997)
350. S V Stefanovsky, B S Nikonov, B I Omel'yanenko, S V Yudintsev, A I Yakushev *Fiz. Khim. Obrabotki Mater.* (6) 111 (1997)
351. S V Stefanovsky, O I Kirjanova, S V Yudintsev, O A Knyazev In *Waste Management 2001 Conference* (Tucson, AZ: Laser Options Inc., 2001) Rep. 324
352. S V Stefanovsky, A G Ptashkin, O A Knyazev, S A Dmitriev, S V Yudintsev, B S Nikonov *J. Alloys Compd.* **444 – 445** 438 (2007)
353. O A Knyazev, A G Ptashkin, S V Stefanovsky, M S Zen'ovskaya, S V Yudintsev, B S Nikonov, O I Stefanovsky, in *Proceedings of the 11th International Conference on Environmental Remediation and Radioactive Waste Management. ICEM-07* (Bruges: ASME, 2007) Rep. ICEM07-7126
354. S V Stefanovsky, A G Ptashkin, O A Knyazev, M S Zen'kovskaya, O I Stefanovskaya, G A Varlakova, O A Burlaka, S V Yudintsev, B S Nikonov *Fiz khim. Obrabotki Mater.* (4) 60 (2008)
355. A Mühlbauer, in *International Scientific Colloquium Modelling for Material Processing, Riga, 2006* p. 13
356. C C Herrick, R A Penneman *Nucl. Technol.*, **60** 253 (1983)
357. V I Vlasov, O L Kedrovskii, A S Nikiforov, A S Polyakov, I Yu Shishtcits, in *Back End of the Nuclear Fuel Cycle* (Vienna: IAEA, 1987) p. 109
358. I A Sobolev, S V Stefanovsky, F A Lifanov, V I Vlasov, S A Dmitriev, I A Ivanov *Fiz. Khim. Obrabotki Mater.* (4 – 5) 150 (1994)
359. I A Sobolev, F A Lifanov, S V Stefanovsky, S A Dmitriev, in *Waste Management 1995 Conference, Tucson, AZ, 1995* p. 17-11
360. T Advocat, C Fillet, J Marillet, G Leturcq, J M Boubals, A Bonnetier *MRS Proc.* **506** 55 (1998)
361. V V Kushnikov, Yu I Matyunin, T V Smelova, A V Demin *MRS Proc.* **465** 55 (1997)
362. P Loiseau, D Caurant, N Baffier, C Fillet *MRS Proc.* **663** 169 (2001)
363. A V Demine, N V Krylova, P P Poluektov, I N Shestoperov, T V Smelova, V F Gorn, G M Medvedev *MRS Proc.* **663** 27 (2001)
364. J Crum, V Maio, J McCloy, C Scott, BRiley, B Benefiel, J Vienna, K Archibald, C Rodriguez, V Rutledge, Z Zhu, J Ryan, M Olszta *J. Nucl. Mater.* **444**481 (2014)
365. P J McGlinn, T Advocat, E Loi, G Leturcq, J P Mestre *MRS Proc.* **663** 249 (2001)
366. T Advocat, P J McGlinn, C Fillet, G Leturcq, S Schuller, A Bonnetier, K P Hart *MRS Proc.* **663** 277 (2001)
367. P Loiseau, D Caurant, I Bardez, O Majerus, N Baffer, C Fillet *MRS Proc.* **757** 281 (2003)
368. R A Day, J Ferenczy, E Drabarek, T Advocat, C Fillet, J Lacombe, C Ladirat, C Veyer, R Do Quang, J Thomasson, in *Waste Management 2003 Conference, Tucson, AZ, 2003* Rep. 2604
369. T V Smelova, N V Krylova, S V Yudintsev, B S Nikonov *Dokl. Earth Sci.* **374** 1149 (2000) [*Dokl. Akad. Nauk* **374** 242 (2000)]
370. S Stefanovsky, A Ptashkin, O Knyazev, S Yudintsev, B Nikonov *37iemes Journees des Actinides, Sesimbra, Portugal, 2007 p. 135*
371. S V Stefanovsky, S V Yudintsev, B S Nikonov, B I Omel'yanenko *Geoekologiya* (4) 58 (1996)
372. N V Laverov, B I Omelynenko, S V Yudintsev, B S Nikonov, I A Sobolev, S V Stefanovsky *Geol. Ore Depos.* **39** 179 (1997) [*Geolog. Rudnykh Mestorozhdenii* **39** 211 (1997)]
373. S V Stefanovsky, A G Ptashkin, O A Knyazev, M S Zen'kovskaya, O I Stefanovsky, S V Yudintsev, B S Nikonov, M I Lapina, in *Waste Management 2008 Conference, Phoenix, AZ, 2008* Rep. 8036
374. S V Stefanovsky, G A Varlakova, O A Burlaka, O I Stefanovsky, B S Nikonov, S V Yudintsev, in *Waste Management 2009 Conference, Phoenix, AZ, 2009* Rep. 9299
375. S V Stefanovsky, V V Lebedev, A G Ptashkin, S A Dmitriev, J C Marra *Adv. Sci. Technol.* **73** 183 (2010)
376. S V Yudintsev, A A Lizin, T S Livshits, S V Stefanovsky, S V Tomilin, R C Ewing *J. Mater. Res.* **30** 1516 (2015)
377. S V Stefanovsky, I A Knyazev, B F Myasoedov, B S Nikonov, S V Yudintsev *Fiz. Khim. Obrabotki Materialov* (3) 70 (2013)
378. S V Yudintsev, S V Stefanovsky, B S Nikonov *Dokl. Earth Sci.* **454** 54 (2014) [*Dokl. Akad. Nauk* **454** 211 (2014)]
379. N P Laverov, V I Velichkin, B I Omel'yanenko, S V Yudintsev, V A Petrov, A V Bychkov *Izolyatsiya Otrabotavshikh Yadernykh Materialov* (Isolation of Spent Nuclear Materials) (Moscow: IFZ RAN, 2008)
380. S V Yudintsev, S V Stefanovsky, B S Nikonov, M S Nikol'skii, T S Livshits *Radiochemistry* **57** 187 (2015) [*Radiokhimiya* **57** 161 (2015)]
381. F Komatsu, Y Sawada, K Ohtsuka, J Ohuchi, in *Management of Alpha-Contaminated Wastes* (Vienna: IAEA, 1981) p. 325
382. F Komatsu, A Takusagawa, T Masaki *Kobe Steel Eng. Rep.* **33** 1074 (1984)
383. W H Hardwick, R Gayler, V Murphy, in *International Seminar on Chemistry and Process Engineering for High-Level Waste Solidification* (Jülich: KfK, 1981)
384. M S Morrell, V Murphy, M Smith *An Active Pilot Plant Demonstration of the Microwave Vitrification Process, AERE-R 10474, Harwell, UK, 1983*
385. M S Stennett, N C Hyatt *MRS Proc.* **1124** 147 (2009)

386. A A Kurkumeli, M I Molokhov, O D Sadkovskaya, V I Kononov, G B Borisov, V F Savel'ev, A I Kachurin *Atom. Energy* **73** 730 (1992) [*Atom. Energ.* **73** 210 (1992)]
387. G B Borisov, A V Nazarov, V I Komarov, M N Molokhov, A A Sorokin *Tekhnol. Mashinostroeniya* (3) 47 (2001)
388. M N Molokhov, A A Sorokin, V G Osipov *Novye Prom. Tekhnol.* (2) 49 (2007)
389. A S Aloi, E Yu Ivanov, B S Kuznetsov, G Sh Batorshin, S N Elsukov, A I Bobylev, A V Ryakov, I I Morozov *Voprosy Radiats. Bezopasnosti* (3) 48 (2010)
390. S E Vinokurov, Yu M Kulyako, B F Myasoedov in *Rossiiskaya Konferentsiya 'Fundamental'nye Aspekty Bezopasnogo Zakhoroneniya RAO v Geologicheskikh Formatsiyakh'* (Russian Conference 'Fundamental Aspects of the Safe Disposal of Radioactive Waste in Geological Formations', Moscow, 2013) p. 22
391. M S Denton, in *Waste Management 2010 Conference, Phoenix, AZ, 2010* p. 10279
392. V V Bysyuk, S A Dmitriev, I A Sobolev, S V Stefanovsky, in *Plazmennye Protsessy i Apparaty* (Plasma Processes and Apparatus) (Minsk: Lykov ITMO, 1984) p. 60
393. I A Sobolev, S A Dmitriev, S V Stefanovsky, S M Lashchenov, F A Lifanov, I A Knyazev, A L Mosse, in *Plazmennye Protsessy i Apparaty* (Plasma Processes and Apparatus) (Minsk: Lykov ITMO, 1984) p. 67
394. S V Stefanovsky, I A Knyazev, S A Dmitriev *Phys. Chem. Mater. Treat.* **25** 386 (1991) [*Fiz. Khim. Obrabotki Mater.* (4) 72 (1991)]
395. R J Munz, G Q Chen. *J. Nucl. Mater.* **161** 140 (1989).
396. M W Shuey, P P Ottmer, in *Waste Management 2006 Conference, Tucson, AZ, 2006* Rep. 6460
397. M Nikashima, T Fukui, N Nakashio, M Osobe, A Ohtake, T Wakui, T Hirabayashi *J. Nucl. Sci. Technol.* **39** 687 (2002)
398. J K Wittle, R A Hamilton, P J Wilver, J C Kidd, in *Proceedings of the International Conference on Incineration and Thermal Treatment Technologies, Salt Lake City, UT, 1998* p. 305
399. I A Sobolev, S A Dmitriev, F A Lifanov, A P Kobelev, V N Popkov, M A Polkanov, A E Savkin, A P Varlakov, S V Karlin, S V Stefanovsky, O K Karlina, K N Semenov, in *Waste Management 2003 Conference, Tucson, AZ, 2003* p. 366
400. K Yamate, H Ikenoya, M Murata, A Umemera, D Sakarai, in *Waste Management 1996 Conference*, Tucson, AZ, 1996 Rep. 38-18
401. I A Sobolev, S A Dmitriev, F A Lifanov, A P Kobelev, S V Stefanovsky, in *Waste Management 2004 Conference, Tucson AZ, 2004* Rep. 4300
402. F Lemont, P Charvin, A Russello, K Poizot *Adv. Sci. Technol.* **73** 148 (2010)
403. A G Merzhanov *Russ. Chem. Rev.* **72** 289 (2003)
404. V G Vereskunov, K P Zakharova, V V Kulichenko, P Zimakov *Atom. Energy* **20** 314 (1966) [*Atom. Energ.* **20** 277 (1966)]
405. K P Zakharova, G M Ivanov, V V Kulichenko, N V Krylova, Yu V Sorokin, M I Fedorova *Atom. Energy* **24** 588 (1968) [*Atom. Eenerg.* **24** 475 (1968)]
406. E E Konovalov, O V Starkov, M P Myshkovskii, L S Gudkov *Izv. Vyssh. Uchebn. Zaved., Yadernaya Energetika* (3) 36 (1997)
407. E M Glagovskii, A V Kuprin, L P Pelevin, E E Konovalov, O V Starkov, E V Levakov, A Yu Postnikov, F D Lisitsa *Atom. Energy* **87** 514 (1999) [*Atom. Energ.* **87** 57 (1999)]
408. E M Glagovsky, A V Kouprin, L P Pelevin, S V Yudintsev, E E Konovalov, in *Proceedings of the Conference Global-2001 on 'Back-End of the Fuel Cycle: From Research to Solutions', Paris, France, 2001* Rep. 0.39
409. G A Petrov, S V Stefanovsky, M I Ozhovan, B S Nikonov *Fiz. Khim. Obrabotki Mater.* (6) 78 (1998)
410. E M Glagovskii, S V Yudintsev, A V Kuprin, L P Pelevin, E E Konovalov, V I Velichkin, B F Myasoedov *Radiochemistry* **43** 632 (2001) [*Radiokhimiya* **43** 557 (2001)]
411. S V Yudintsev, T S Ioudintseva, A V Mokhov, E E Konovalov, S A Perevalov, S V Stefanovsky, A G Ptashkin *MRS Proc.* **807** 273 (2004)
412. T V Barinova, I P Borovinskaya, V I Ratnikov, T I Ignat'eva *Radiochemistry* **50** 316 (2008) [*Radiokhimiya* **50** 274 (2008)]
413. E M Glagovsky, A V Kuprin, A I Bogdanov, S V Yudintsev, B S Nikonov, E E Konovalov, in *Proceedings of the International Conference Global 2009, Paris, France, 2009* p. 412
414. N P Laverov, S V Yudintsev, Yu I Korneiko, E E Konovalov, T O Mishevets, B S Nikonov, B I Omel'yanenko *Dokl. Chem.* **434** 214 (2010) [*Dokl. Akad. Nauk* **434** 60 (2010)]
415. T V Barinova, I P Borovinskaya, V I Ratnikov, T I Ignat'eva, A F Belikova, N V Skachkova, N Yu Khomenko *Int. J. Self-Prop. High-Temp. Synth.* **20** 67 (2011)
416. N P Laverov, S V Yudintsev, E E Konovalov, M S Nikol'skii, T O Mishevets, B S Nikonov, B I Omel'yanenko *Radiochemistry* **54** 511 (2012) [*Radiokhimiya* **54** 472 (2012)]
417. T V Barinova, I P Borovinskaya, V I Ratnikov, T I Ignat'eva, A F Belikova *Radiochemistry* **55** 629 (2013) [*Radiokhimiya* **55** 539 (2013)]
418. G A Petrov, I A Sobolev, S A Dmitriev, E M Timofeev, S V Stefanovsky, A G Petrov *Poroshkoobraznye Metallizirovannye Topliva dlya Tekhnologii Pererabotki Radioaktivnykh Otkhodov* (Powdered Metallized Fuels for Radioactive Waste Processing Technologies) (Moscow: Nauka, 2003)
419. M I Ojovan, W E Lee *Glass Technol.* **44** 218 (2003)
420. M I Ojovan, W E Lee, I A Sobolev, S A Dmitriev, O K Karlina, V L Klimov, G A Petrov, K N Semenov *Proc. Inst. Mech. Eng.* **218** 261 (2004)
421. X Mao, Z Qin, X Yuan, C Wang, X Cai , W Zhao, K Zhao *J. Nucl. Mater.* **443** 428 (2013)
422. A V Kuprin, A I Lastov, A I Bogdanov, V V Shapovalov, N A Nerozin, E E Konovalov, in *7-ya Rossiiskaya Konferentsiya po Radiokhimii 'Radiokhimiya 2012'* (The Second Russian Conference on Radiochemistry 'Radiochemistry 2012', Dimitrovgrad, 2012) p. 245
423. S Stefanovsky, E R Vance, R A Day, B D Begg, in *Proceedings of the Second International Meeting of Pacific Rim Ceramic Societies, Cairns, Australia, 1996* (Eds P Walls, C Sorrell, A Ruys) Rep. 505